AIX-MARSEILLE UNIVERSITÉ

ED 251 – Sciences de l'Environnement

UMR 7334 - CEREGE

Thèse présentée pour obtenir le grade universitaire de Docteur de l'Université d'Aix-Marseille.

Aurore HÜTZLER

The flux of meteorites on Earth: Contribution of measuring the concentration of multiple cosmogenic nuclides, and collections in arid areas.

Le flux de météorites sur Terre: apport de la mesure de multiples nucléides cosmogéniques, et collectes en milieu désertique.

Soutenue le 30/01/2015 devant le jury :

Ingo LEYA	University of Bern	Rapporteur
Kees WELTEN	University of California	Rapporteur
Brigitte ZANDA	MNHN, Paris	Examinateur
Jérôme GATTACCECA	CEREGE/CNRS	Examinateur
Didier BOURLES	CEREGE	Directeur de thèse
Pierre ROCHETTE	CEREGE	Directeur de thèse

RESUMÉ

Le flux de météorites vers la Terre peut être déterminé en observant des bolides, ou en étudiant des collections de météorites. Pour estimer l'intensité et la composition du flux, nous avons collecté et classifié une collection de 213 météorites issues du désert de l'Atacama (Chili). Nous avons développé un modèle mathématique pour faciliter l'appariement des météorites, et ainsi avoir un nombre fiable de chutes par unité de surface. Nous avons développé un protocole chimique afin d'extraire des nucléides cosmogéniques (^{10}Be, ^{26}Al, ^{36}Cl and ^{41}Ca) de chondrites ordinaires. La fraction métallique est d'abord séparée de la météorite. Les échantillons sont ensuite dissouts dans l'acide, et les éléments utiles sont extraits et purifiés grâce à des résines échangeuses d'ions et des précipitations contrôlées. Après la mesure par Spectroscopie de Masse à Accélération (SMA), les concentrations de nucléides cosmogéniques nous permettent de calculer l'âge terrestre, le rayon pré-atmosphérique et la profondeur dans le météoroide, en utilisant l'approche développée par Leya & Masarik (2009). En combinant le nombre de météorites par unité de surface et les spectres d'âge terrestre, nous pouvons déterminer un flux de 218 météorites>10g/Ma/km^2 sur une période de 700 ka avec la méthode ^{41}Ca.

On applique la même procédure à une sélection de météorites de fer. Dans le cadre d'une collaboration avec l'Université de Bern (Suisse), nous avons aussi mesuré les concentrations en gaz rares (isotopes de l'He, Ne et Ar) dans certaines de ces météorites. Les concentrations en gaz rares et en nucléides radiogéniques ont ensuite été étudiées avec le modèle développé par Ammon et al. (2009), afin de déterminer le temps d'exposition dans l'espace, l'âge terrestre, le rayon pré-atmosphérique et la profondeur dans le météoroide. Ces résultats nous ont permis d'évaluer la probabilité de trouver d'autres pièces de certaines météorites, ou encore de discuter de l'histoire des cratères associés à certaines météorites.

Mots-clés : nucléides cosmogéniques ; météorites chiliennes ; flux de météorites ; datation.

ABSTRACT

Meteorite flux to the Earth can be determined using observations of fireballs or studying meteorites collections. To estimate the intensity and the composition of the flux, we collected and classified a 213 samples collection from the Atacama desert (Chile). We developed a mathematical model to help pairing of meteorites, and hence get a reliable number of falls per unit of surface. A chemical procedure to extract the cosmogenic nuclides ^{10}Be, ^{26}Al, ^{36}Cl and ^{41}Ca from ordinary chondrites was developed. The metallic fraction was extracted from the bulk meteorite. Samples were dissolved into acid and the elements of interest were extracted and purified using ion-exchange resins and pH controlled precipitation. After measurements using the Accelerator Mass Spectrometry (AMS) technique, the cosmogenic nuclides concentrations enable us to calculate terrestrial age, pre-atmospheric radius and shielding depth, using the Leya & Masarik (2009) model. Combining the number of meteorites per km^2 and the terrestrial ages spectrum, we determine a flux of 218 meteorites > 10g/Ma/km^2 over 700 ka with the ^{41}Ca calculation method.

Applying the same procedure as described above, we studied a selection of iron meteorites in which noble gases (He, Ne and Ar isotopes) concentrations were measured in collaboration with the University of Bern (Switzerland). Stable and radiogenic nuclides concentration results were then used according to the Ammon et al. (2009) model to determine Cosmic Ray Exposure (CRE) ages, terrestrial ages, pre-atmospheric radii and shielding depths. These results allowed us to evaluate the probability of finding additional remains of meteorites, or to discuss the history of craters associated with some of these meteorites.

Keywords: cosmogenic nuclides; Chilean meteorites; meteorite flux; dating.

REMERCIEMENTS

Les 4 années de thèse qui viennent de s'écouler ont été riches d'enseignements, d'évolutions et d'expériences. Je vais sûrement oublier des personnes, je m'en excuse par avance.

Je voudrais d'abord remercier Pierre Rochette et Jérôme Gattacceca, mes directeurs de thèse, l'un officiel, l'autre officieux, mais qui m'ont suivie, soutenue, aidée dans ma thèse. Vous avez cru en mon travail beaucoup plus que moi-même (ou alors, vous cachiez bien votre jeu !). Je remercie aussi vivement Didier Bourlès, mon deuxième directeur de thèse officiel, pour m'avoir laissé une très grande liberté dans ma recherche.

Dans la foulée, il me faut remercier François Demory, qui gère le chalet de main de maître. Merci pour le côté science, et merci pour les discussions animées ! Un grand merci à la « team ASTER », Georges, Maurice, Fred et Karim, pour leur disponibilité et leur gentillesse.

Merci à Lucilla et Valéry, pour leurs conseils et leur aide pratique sur le ^{36}Cl.

Un immense merci à Silke Merchel, sans qui rien n'aurait été possible...Silke m'a apporté une rigueur, une envie de perfection dans les manips que je n'avais pas. C'est grâce à elle que j'ai pu monter mon propre laboratoire, sans trop faire de bêtises (j'espère !).

A huge thanks to Ingo Leya and Kees Welten, for their thoughtful comments on the manuscript.

Merci à Bertrand et Arthur, mes jeunes mathématiciens qui écrivent en Scilab et Matlab plus vite que leur ombre.

Merci à Isabelle Hammad, qui m'a patiemment rappelé chaque année les démarches administratives nécessaires pour l'Ecole Doctorale.

Carole et Cécile, vous avez été indispensables à ces années. Sans vous, rien n'aurait été pareil. Une pensée aussi pour les stagiaires, doctorants, et post-doctorants que j'ai pu brièvement croiser au CEREGE. Millarca, Natalia, Agata, Sandy (alors, ce saut en parachute?), Marcela, Eddi-Valdo et plus récemment William, vous m'avez beaucoup marquée.

Merci à Bertrand Devouard, qui est arrivé bien tard au CEREGE, mais qui anime tout stage de terrain ou toute conférence, aussi bien d'un point de vue scientifique que dans l'exploration des lieux malfamés locaux.

Merci à Martine Ruzzier et à l'équipe des Doctoriales 2013 et 2014. Ces deux éditions des Doctoriales, aussi bien en tant que doctorante qu'en tant qu'organisatrice, ont été une épiphanie. J'ai une vision de moi et de mon futur bien plus claire, et c'est grâce à vous.

Merci à Carole Dumas, puis à Amandine Delus pour m'avoir accueillie pendant ma thèse. Merci à Benjamin d'avoir partagé du thé et des réflexions pendant une grosse année. Ma vaisselle s'en ressent encore, mais c'était une belle période.

Merci à l'Association des Elèves et Anciens Elèves des ENS de Lyon, Fontenay-aux-Roses et Saint-Cloud, qui m'a permis de découvrir de nombreux centres d'intérêt, et de faire ce que j'aime.

A warm thank to Daniele, who has been here for me for many things, including proof-reading this work.

Merci à Alexandre, pour avoir été à mes côtés une bonne moitié de ma thèse.

Merci à mes parents, qui ont patiemment aidé pour les déménagements, les chagrins, les ras-le-bol... Je sais que j'ai un nid à la maison pour toujours.

Merci à mon étalon Palladir d'avoir supporté tous les 6 mois une tornade de douches, de sport, d'excitation...avant de retrouver la douce torpeur de son pré.

Merci à mes collocs, qui se sont tellement bien occupés de moi pendant la rédaction, à coup de repas, de coinche et d'aide mathématique...

Merci encore à Bertrand...

Merci enfin à l'atmosphère, qui nous protège du rayonnement cosmique !

“But carbon dating puts it at 65 million years B.C. !”

Darcy, in Transformers: Age of Extinction.

TABLE OF CONTENTS

RESUMÉ **3**

ABSTRACT **4**

REMERCIEMENTS **5**

TABLE OF CONTENTS **9**

Chapter 1: Theoretical approach, basic notions and previous work. **13**

1.1 Flux intensity, or What are the chances to find a meteorite in your garden? **15**

1.1.1 Previous studies. 15

1.1.1.a Geographical inhomogeneity, or Do I have the same chances as my neighbor of finding a meteorite? 15

1.1.1.b The current flux 15

1.1.1.c The ancient fluxes 16

1.1.2 How to collect a proper meteorite collection. 17

1.1.3 What if two different stones were actually from the same fall? The unavoidable pairing step. 18

1.1.4 How to date a meteorite : terrestrial ages from cosmogenic nuclides. 18

1.1.4.a Cosmogenic nuclides production. 18

1.1.4.b Basic principles 23

1.2 Flux composition, or did the dinosaurs see the same kind of meteorites I see today? **24**

1.2.1 Meteorites zoology. 24

1.2.2 Previous work. 25

Chapter 2: Meteorite Flux over the last million years. **29**

2.1 Atacama: a preferential location for meteorite hunting. **31**

2.2 Description of a very dense meteorite collection area in western Atacama: insight into the long-term composition of the meteorite flux to Earth using a new pairing method. **33**

Abstract 33

Introduction 34

Methods 36

Geology and Geomorphology 37

Characteristics of Studied collections 40

Pairing 42

Statistics of Chilean collections 45

Meteorite Concentration 53

Conclusions 54

Acknowledgments: 56

References 57

Chapter 3: Chemistry 75

3.1 Chemical extraction 77

3.1.1 Isotope carriers 78

3.1.2 Sample dissolution 78

3.1.3 First Chlorine precipitation 79

3.1.4 Removal of sulfur 79

3.1.5 Second precipitation of AgCl 80

3.1.6 Removal of silver 80

3.1.7 Aliquot for elementary concentrations 81

3.1.8 Removal of iron 81

3.1.9 Anion exchange column 81

3.1.10 Hydroxide precipitation 81

3.1.11 Cation exchange column 82

3.1.12 Aluminium and Beryllium target precipitation 82

3.1.13 Manganese precipitation 82

3.1.14 Nickel precipitation 83

3.1.15 Calcium target precipitation 83

3.1.16 Iron fraction extraction 84

3.1.17 Useful tips. 84

3.2 ICP-MS (SARM) 85

3.3 Sample pressing 85

3.4 Chemistry blank 86

3.5 Replica and validation of measurements 86

3.6 Result treatments 88

3.6.1 Carrier weights 88

3.6.2 Elemental concentrations 88

3.7 ASTER AMS measurements and activities calculations 89

3.8 Uncertainties on cosmogenic activities 89

3.8.1 Chemistry procedure uncertainties 90

3.8.2 AMS and global uncertainties 91

3.9 Model calculations 92

3.9.1 Iron meteorites 92

3.9.1.a Lavielle *et al.* (1999) 92

3.9.1.b Ammon *et al.* (2009) 94

3.9.2 Chondrites and other stony meteorites (Leya & Masarik 2009). 97

3.10 Fixed point 99

3.11 Uncertainties on model calculations 99

3.12 Conclusion 101

Chapter 4: Cosmogenic results and interpretation 103

4.1 Samples and results 105

4.1.1 Iron 105

4.1.1.a Choice of the samples 105

4.1.1.b Cosmogenic nuclides activities. 106

4.1.1.c Calculations of CRE ages, terrestrial ages and physical parameters. 107

4.1.2 Chilean chondrites (Hutzler, 2014) 108

4.1.2.a Choice of the samples 108

4.1.2.b Radionuclides results 109

4.1.2.c Terrestrial ages 109

4.2 Interpretation 111

4.2.1 Iron results 111

4.2.1.a Gebel Kamil (Egypt) 111

4.2.1.b La Caille (France) 112

4.2.1.c Mont Dieu (France) 112

4.2.1.d Saint-Aubin (France) 113

4.2.1.e Agoudal (Morocco) 113

4.2.1.f Tamentit (Algeria) 114

4.2.1.g Morasko (Poland) 114

4.2.1.h Cerro del Inca (Chile) 115

4.2.1.i Dolores (Chile) 116

4.2.1.j Guanaco (Chile) 116

4.2.1.k Cuenca del Tiburon (Chile) 116

4.2.2 Iron age spectra 116

4.2.3 Chondrites 117

Conclusions and outlooks 123

Conclusions et perspectives 129

REFERENCES 135

APPENDIX 143

APPENDIX A : Kohout et al. (2014) 144

APPENDIX B: Pairing meteorites (Matlab). 158

APPENDIX C: Calculations of CRE ages, terrestrial age and pre-atmospheric size (Scilab).. 164

APPENDIX D: El Médano collection meteorites: a selection. 194

Chapter 1: Theoretical approach, basic notions and previous work.

1.1 Flux intensity, or What are the chances to find a meteorite in your garden?

1.1.1 Previous studies.

It has taken a long time for scientists from the past to acknowledge the extra-terrestrial origin of meteorites. Now that it is fully understood, the question is no longer "Where does that stone come from", but "How many more could arrive from space?" and many scientist have dedicated their work to study meteorite flux.

There are two ways to study meteorite flux. You can observe the sky, and record observation of bright fireballs. You can also go to the field, and collect meteorites. We describe both methods in the following.

1.1.1.a Geographical inhomogeneity, or Do I have the same chances as my neighbor of finding a meteorite?

When I explain what I do for a living to random people, they usually assume I am going to places such as Chili, or Sahara because more meteorites **fall** in these places. I then have to explain that I have the very same chance of being hit by a meteorite in Atacama, Chile, than they have in their backyard.

A study by (Halliday 1964) actually proves this statement is wrong. Halliday models the rate of fall for various meteorites velocities, and as a function of both ecliptic and geographical latitude. The results show that in polar regions, the rate of impact represents only 50-60% of the impact rate at the equator. You should better live in Tromsø than in Quito if you are afraid the sky could be falling on you.

1.1.1.b The current flux

Camera networks have been used to watch the sky for several decades now. Though some are now shut down (MORP network in Canada, Prairie network in the United States) after giving useful information, some remain in activity, such as the European Fireball Network, the Desert Fireball Network (DFN) (Bland *et al.* 2014), and more recently, the French FRIPON project (ongoing installation). Some recent projects plan on working with weather radar

networks, which have the advantage of being worldwide and already installed (Fries *et al.* 2014).

This kind of project usually involves the local population to help with the observations and the recovering of potential meteorites.

The observations can be realized only in clear-sky conditions, and usually at night. The results have to be corrected for this bias, along with a correction for latitude (Halliday 1964).

The observed events also have to be separated into two types: fireballs that may or may not have deposited meteorites.

From the data from MORP, (Halliday *et al.* 1989) Halliday and co-authors develop a model linking number of fireballs N and estimated mass m of the largest surviving fragment:

For masses under 1030 g:

$$\log N = -0.49log(m) + 2.41$$

For masses greater than 1030 g:

$$\log N = -0.82log(m) + 3.40$$

Following the model, one can predict a flux of 83 meteorites over 10 g per year per 10^6 km^2. The same results are presented by (Oberst *et al.* 1998) using the European Fireball Network. Uncertainties still reside in deriving a dynamical mass from a fireball image; an error of a factor 2 can be envisioned (Halliday *et al.* 1991).

1.1.1.c The ancient fluxes

Flux calculated from collections covers different time scales, depending on the collection. For example, a flux from an Antarctic collection could cover the last hundred thousand years, a hot desert collection the last dozen thousand years, and the Ordovician fossil meteorites from Sweden provide us with a glimpse of what the flux was 480 Ma ago (Schmitz *et al.* 2001).

This method allows us to estimate potential temporal variations in flux, and tackle intriguing problems such as meteoroid delivery mechanism.

Zolensky *et al.* (1990) using the Roosevelt County collection in SW USA found an accumulation of 115 events over 10g/km^2/Ma; Nullarbor Region in

Australia yields 36 meteorites over 10g/km^2/Ma and the Sahara (Acfer dense collection area) yields 95 meteorites over 10g/km^2/Ma. From Antarctic meteorites, Huss (1990) develops an approach using cumulated mass rather than number of meteorites, leading to 105 kg/km^2/Ma.

Some authors conclude to a recent change in the number of events (Gattacceca *et al.* 2011), while others consider the flux as stable on the last 50 ka (Bland *et al.* 2000). Still, the Ordovician flux was at least 25 times higher than today (Schmitz *et al.* 2001).

1.1.2 How to collect a proper meteorite collection.

To get a proper quantitative flux, it is vital to have a statistically reliable collection. The collection must be composed of a sufficiently large amount of meteorites, ideally several hundreds, to have a reliable number of rare meteorites (accounting for a few % of falls). Then, the collection field must be devoid of any concentrating mechanism, or if such a mechanism exists, it must be thoroughly quantified. Finally, the collection must be exhaustive, on a known surface. The best way to collect almost every single stone is by foot, slowly following a grid of parallel lines. This method allows recovering of very small stones, but restricts the searched area. It is particularly efficient in very dense collection areas. For less dense collection areas, a search by car allows more ground to be covered.

As presented in §2 *Meteorite Flux over the last million years*, we chose to search our study area by foot.

We obtain a recovery density, i.e. the number of meteorites you can recover from a given surface. Due to weathering, burial and removal rates, meteorites disappear with time. Once the collection duration, or more precisely the probability function to recover a meteorite versus the time of fall, we can calculate an estimate of the number of meteorites that fell on Earth on the same given surface and on a given period of time (Zolensky *et al.* 2006) (Bland *et al.* 2000). Collection duration can be estimated using geomorphological criteria (age of the surface), models of removal rate (Zolensky *et al.* 1990), or direct measurement of the terrestrial age of the meteorite (i.e. time since fall). In our study, we work in the measurement of terrestrial age of the meteorites.

1.1.3 What if two different stones were actually from the same fall? The unavoidable pairing step.

A crucial step to get a reliable collection is pairing. When a meteoroid falls on Earth, it usually breaks apart during passage in the atmosphere. It results in several pieces on the ground all from the same fall. Also, meteorites can be fragmented during terrestrial history. Since we are interested in calculating a number of falls per unit of time and surface, it is very important to distinguish in the meteorite collection which stones are from the same fall.

To do so, we compare different properties (mineral abundances, petrographic type, weathering grade, geographic proximity…) of the stones.

Pairing is a non-trivial problem (Benoit *et al.* 2000). Even if two meteorites have very similar properties, the pairing always involves some degree of uncertainty. It is easier to refute a pairing (a single different property is enough to do so) than to prove one.

We developed a mathematical model comparing several parameters for pairs of meteorites. For more details, see §2.2.

1.1.4 How to date a meteorite : terrestrial ages from cosmogenic nuclides.

1.1.4.a Cosmogenic nuclides production.

Cosmogenic isotopes are formed by nuclear reactions between high-energy particles from cosmic rays (both galactic and solar) and atoms. In the case of extra-terrestrial matter, the production happens mainly while in space, since the galactic cosmic-rays (GCR) and the solar cosmic-rays (SCR) are filtered by the atmosphere and the magnetic field. SCR penetrate only a few millimeters into the meteoroid, and produce no significant secondary particles (because of the low energy level of SCR). The few millimeters showing the influence of SCR are lost by abrasion while entering the atmosphere: only cosmogenic isotopes produces by GCR interactions can be measured.

There are two types of cosmogenic nuclides: stable nuclides and radioactive nuclides. As for radionuclides with a very long half-life ($>10^9$yrs), they can be considered as stable in the following.

Stable isotopes studied in extra-terrestrial matter all belong to noble gases, such as ^{3}He, ^{4}He, ^{36}Ar, ^{38}Ar or ^{20}Ne, ^{21}Ne and ^{22}Ne (plus Kr et Xe). As long as the meteorite is in space, the stable isotopes are constantly produced. When on Earth, there is no more production, but the concentration of stable isotopes remains constant.

Radionuclides, on the other hand, are produced in space, but they are also decaying. While in space, the production and the decaying are happening, to reach after approximately $t=10*t_{1/2}$ an equilibrium, when the radionuclide concentration remains constant. It is said the meteorite is at saturation. When on Earth, the production of radionuclide is not happening anymore, hence only the decaying leads to a decrease of radionuclide concentration. Useful cosmogenic radionuclides belong to five different element categories: alkali earth metal (^{10}Be, ^{41}Ca), transition elements (^{53}Mn), halogens (^{36}Cl), other metals (^{26}Al) and non-metal (^{14}C).

Both behaviors are summarized in figure 1 and figure 2.

From figure 2 we see that the concentration of cosmogenic nuclides we can measure in a given sample depends on the time the meteoroid spent in space (cosmic ray exposure age or CRE age) and on the time the meteorite spent on earth (terrestrial age).

The production of cosmogenic nuclides is not homogenous inside extraterrestrial matter, since the penetration into matter is conditioned by the energy of the incident particle. Hence, the concentration of a cosmogenic nuclide depends on the pre-atmospheric size of the meteoroid, and of the sample location within the investigated object, known as shielding depth. The production rate also depends on the shape of the meteoroid; for convenience, models calculating production rates assume meteoroids are spheres, though promising studies are trying to model the effect of meteoroid shape on cosmogenic production rates (Prettyman *et al.* 2014).

Production rate also depends on the target elements, thus the need to measure the composition of the analysed meteorite.

When studying a meteorite, we want to find out several unknowns: the length of time the meteoroid stayed in space, how big it was, where the sample was inside the meteoroid, and how long the meteorite spent on Earth.

To solve such an equation system, we need several different inputs, hence several different cosmogenic elements.

I describe here how isotopes are created in space. I focus on the isotopes I use in my study. Half-lives are listed in table 1, major target elements in table 2.

The four radionuclides (^{10}Be, ^{26}Al, ^{36}Cl and ^{41}Ca) we focus on are the one we are able to measure at CEREGE. They are a very good start to calculate what we want to know about the meteorites we studied. For a full study, we measure the noble gases we cite in table 1 and table 2.

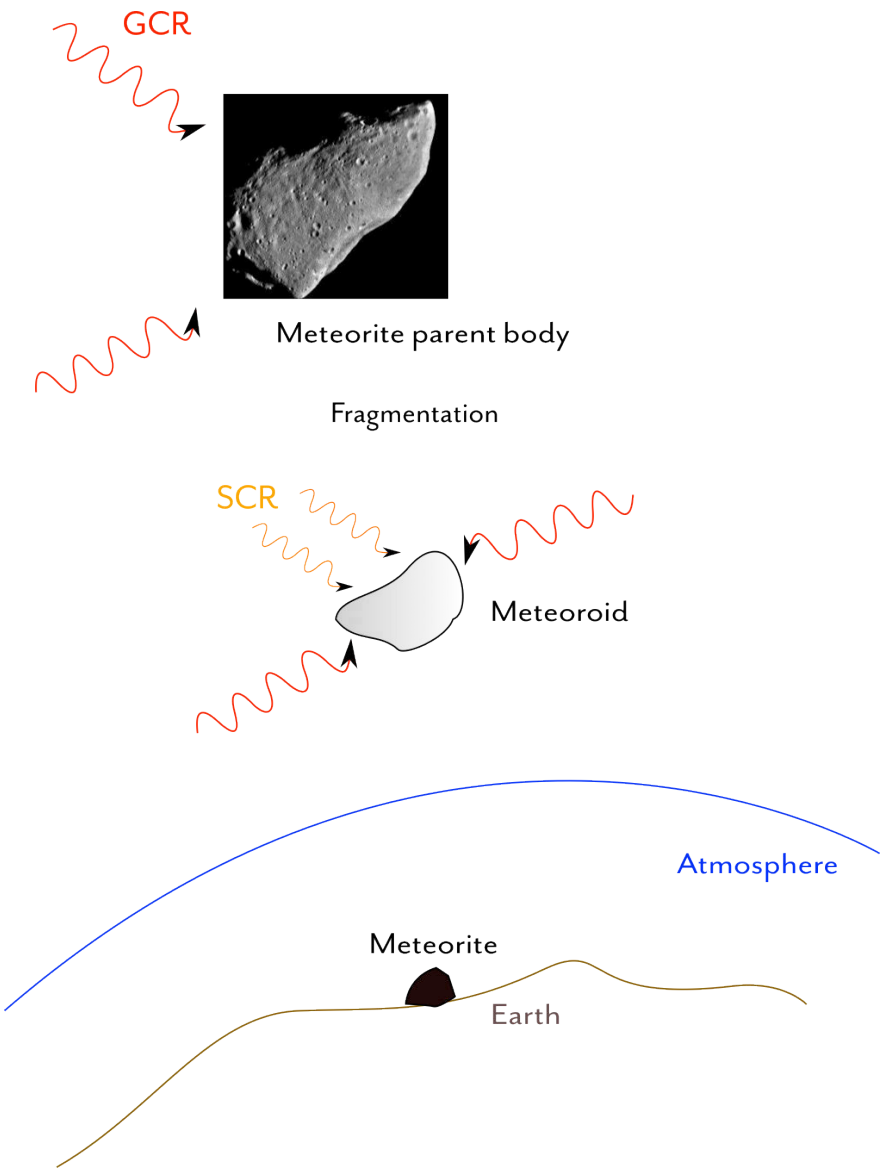

Figure 1: Exposition of extra-terrestrial matter to high energy cosmic rays.

Table 1: Cosmogenic nuclides in meteorites (extracted and measured in this work).	
Nuclide	Half-life (Myr)
^{3}He, ^{4}He	S
^{20}Ne, ^{21}Ne, ^{22}Ne	S
^{36}Ar, ^{38}Ar	S
^{41}Ca	0.104 ± 0.004 (Kutschera *et al.* 1992)
^{36}Cl	0.301 ± 0.002 (Nishiizumi *et al.* 1997)
^{26}Al	0.708 ± 0.017 (Nishiizumi 2004)
^{10}Be	1.36 ± 0.07 (Nishiizumi *et al.* 2007)
S means the element is stable. Adapted from (Eugster *et al.* 2006).	

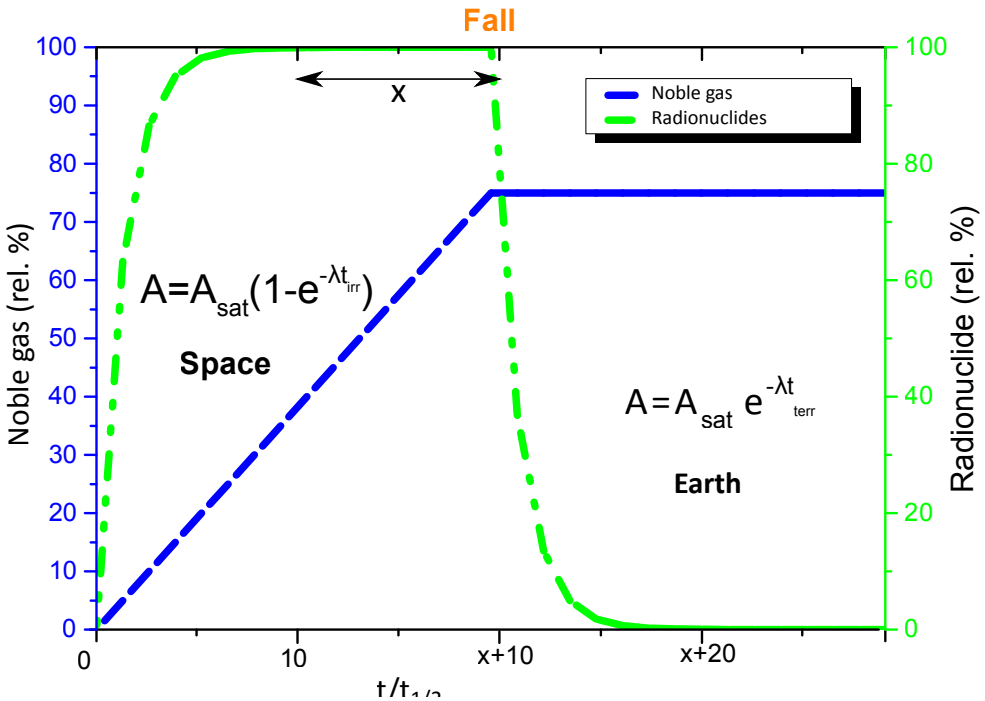

Figure 2: Levels of cosmogenic nuclides, both radiogenic (green) and stable (blue) in extra-terrestrial matter, in space and on the earth.

Table 2: Main target elements for cosmogenic nuclides production		
Nuclide	Main target element	Neutron reaction pathways
^{3}He, ^{4}He	O, Mg, Si, Fe, Ni,	
^{20}Ne, ^{21}Ne, ^{22}Ne	Mg, Al, Si, Fe	$^{24}Mg(n,\alpha)^{21}Ne$
^{36}Ar, ^{38}Ar	Fe, Ca, K	
^{41}Ca	Ca, Ti, Fe, Ni	$^{40}Ca(n,\gamma)^{41}Ca$
^{36}Cl	Cl, K, Ca, Ti, Fe, Ni	$^{35}Cl(n,\gamma)^{36}Cl(\beta^{-})^{36}Ar$
^{26}Al	Si, Al, Fe	
^{10}Be	O, Mg, Si, Fe, Ni	

i Cosmogenic beryllium (^{10}Be)

Beryllium has one stable nuclide and two cosmogenic radionuclides, ^{10}Be and ^{7}Be. ^{7}Be has a half-life too short (53 days) to be used in meteorite research field. ^{10}Be is mainly produced by spallation reaction on oxygen. In iron meteorites or metallic fractions, ^{10}Be is produced by spallation from iron and other heavy element, including the trace elements phosphorus and sulfur (Ammon *et al.* 2009). The production from these two last elements has to be carefully taken into account.

ii Cosmogenic aluminium (^{26}Al)

Aluminium has one stable nuclide, ^{27}Al and one radiogenic nuclide, ^{26}Al. ^{26}Al is produced by transfer reactions from silicium and aluminium, and by spallation on calcium and heavier elements. Note the spallation production from sulfur and phosphorus, also to be considered carefully.

iii Cosmogenic chlorine (^{36}Cl)

Chlorine has two stable nuclides (^{37}Cl and ^{37}Cl) and one radiogenic nuclide, ^{36}Cl.

^{36}Cl has three reaction pathways: transfer reaction from calcium, spallation on iron and other heavy nuclides, and low-energy thermal neutron reaction from ^{35}Cl. This last reaction depends on the content on chlorine, which can be very variable within a meteorite, and between different types of meteorites. The advantage of using cosmogenic nuclides in the metal fraction is that we don't take into account the neutron reaction. Doing so, the comparison with theoretical production rates can be only with high energy production rates which are better constrained.

Contrary to the other radiogenic nuclides, Cl is highly sensitive to contamination issues, and has to be extracted with great care in a dedicated room.

iv Cosmogenic calcium (^{41}Ca)

Calcium has five stable nuclides, ^{40}Ca, ^{42}Ca, ^{43}Ca, ^{44}Ca and ^{46}Ca, and one radionuclide, ^{41}Ca. ^{41}Ca is formed by spallation in the metal phase, and as a product of low-energy nuclear reaction from ^{40}Ca. In large meteoroids, the neutron flux is a function of meteoroid size and of the shielding depth. Because it this, ^{41}Ca from the silicate phase is a good indicator for shielding depth (Eugster *et al.* 2006).

^{41}Ca is also really interesting because of its half-life, which is between ^{14}C and ^{36}Cl. It is ideal for determining terrestrial ages of most of meteorites.

The AMS measurement is not yet a routine measurement in CEREGE, and has to be done with great care.

1.1.4.b Basic principles

As for any other radioactive nuclides, cosmogenic nuclides decay following the equation

$$t = -\frac{1}{\lambda} ln\left(\frac{N}{N_0}\right)$$

N_0 being the initial number of atoms, N the remaining number of atoms, and λ the decay constant (Jull 2006).

As seen in the previous paragraph, radionuclides are produced in space; they can also be produced to a far lesser extent on Earth, for samples exposed a few kilometers a.s.l. (above sea level). After the fall of the meteorite, the equation for the concentration of radionuclides would be, if we define N_0 as $\frac{P_s}{\lambda}$.

$$N = \frac{P_s}{\lambda} e^{-\lambda t} + \frac{P_t}{\lambda}(1 - e^{-\lambda t})$$

with P_s and P_t the production rates in space and on earth respectively. Except for peculiar samples, with long terrestrial ages or high altitude exposure, we consider $P_t = 0$.

N_0 or P_s are dependent on the chemical composition, the size, the depth of the sample and the CRE age. N_0 can be modeled considering a long enough CRE age to reach saturation state. Since the chemical composition is easy to measure, the only unknowns are pre-atmospheric size and shielding depth.

In some case, we can avoid the shielding dependence by using the ratio of two radionuclides with different half-lives

$$\frac{N_1}{N_2} = \frac{P_1\lambda_2}{P_2\lambda_1} e^{(\lambda_2-\lambda_1)t} \Leftrightarrow t = \frac{1}{(\lambda_2-\lambda_1)}\left(ln\left(\frac{N_1}{N_2}\right) - ln\left(\frac{N_1}{N_2}\right)_0\right)$$

We will go through the mainly used pairs in §3.9 *Model calculations*.

We now theoretically know how to collect meteorites and how to get rid of the problem of multiple stones for one fall to get a reliable number of meteorites per unit of surface. Knowing terrestrial ages spectrum of our collection, we can calculate a quantitative meteorite flux.

What about different types of meteorites? Can we study if the flux has qualitatively changed over time?

1.2 Flux composition, or did the dinosaurs see the same kind of meteorites I see today?

1.2.1 Meteorites zoology.

Meteorites originated in space. Several parent bodies can be responsible for the origin of meteorites, leading to a large diversity of meteorites.

To help the scientific community to communicate easily, meteorites are classified in different groups. Meteorites can be separated using different parameters.

The meteorite classification system currently used is based on the works of Prior (1920) and Mason (1966) with some recent modifications. The first dichotomy arises between chondrites (undifferentiated meteorites) and achondrites (differentiated meteorites).

Chondrites have solar-like composition and are from asteroids that did not experience planetary differentiation. Chondrites from the same class share the same mineral assemblage and whole-rock chemical composition. We define three **classes** of chondrites, carbonaceous (C) chondrites, ordinary (O)

chondrites and enstatite (E) chondrites (Weisberg *et al.* 2006). A **group** of meteorites indicates that the meteorites originated from the same parent body. A **clan** of meteorite is a rather new term for groups of chondrites sharing a particularity, such as isotopic anomaly, petrographic texture or similar refractory elements abundances.

Inside chondrites groups, we define petrographic types (Van Schmus & Wood 1967), showing different degrees of metamorphism and equilibrium. Types are labeled from 1 to 6, type 3 being unequilibrated, type 4 deriving from type 3 by in-situ metamorphism, and types 5 and 6 showing higher related degrees of metamorphism. For a finer classification of types 3, we use the work of (Bunch *et al.* 2012) and (Grossman & Brearley 2005) based on Cr content in ferroan olivine.

We also define the weathering grade, based on the percentage of oxidation of metal and troilite (W0 to W4) then on the alteration of silicates (W5 and W6) (Wlotzka 1993).

The shock grade is also a tool for differentiating meteorites, see Stöffler *et al.* (1991) for OC, Rubin *et al.* (1997) for EC and Scott *et al.* (1992) for CC.

A rather new tool for classifying meteorite is magnetism. It has been demonstrated that magnetic susceptibility can be used to characterize and classify ordinary chondrites (Rochette *et al.* 2003), non-ordinary chondrites (Rochette *et al.* 2008) or stony achondrites (Rochette *et al.* 2009). Magnetic susceptibility is a quick and non-destructive method, available on the field and in the laboratory. It also preserves the natural remanent magnetization, which can bring valuable scientific information. This is why testing meteorites with a magnet must be discouraged.

1.2.2 Previous work.

After classification, we can compare different collections. We can in particular compare the finds (any collection from meteorites which fall has not been observed, generally from hot deserts and Antarctica), and the falls collection.

We can see several common patterns between finds and falls: ordinary chondrites are the most represented. Within the H and L groups, H5 and L6 types are the most common. We can also see differences between both types of

collections: within ordinary chondrites, H chondrites are more abundant than L chondrites in finds collections, whereas L chondrites are more abundant than H chondrites in falls collection. Other types of meteorites' abundances are variable within the collections. The purpose of any serious study of qualitative flux is first to present a statistically reliable collection, and then to consider if the differences between the studied collection and the falls come from a genuine flux difference, or from terrestrial mechanisms and way of recovery.

We also have to be conscious that the falls collection, now accounting for over 1,200 meteorites, is biased toward high masses, because or the higher probability of large falls observation and recovery. Hence, the falls abundance doesn't really represent what is currently arriving on earth. An H chondrites study in Antarctica by Benoit & Sears (1996) shows that the abundance of H chondrites, and hence, of other types of meteorites depends on stochastic events, and is not independent of time.

More recently, Gattacceca *et al.* (2011) found discrepancies that cannot all be explained by terrestrial weathering or selective picking between a large chilean collection and the falls collection. Our work (see §2 *Meteorite flux over the last million years*) supports this hypothesis with a larger collection.

We now have an introduction of what the extraterrestrial matter flux is. We know how to determine a "quantitative" flux – how many meteorites are falling on Earth, and a "qualitative" flux - the abundances of different types of meteorites. We have notions of dating using radionuclides, and we have seen how these cosmogenic isotopes are produced.

Chapter 2 "Meteorite Flux over the last million years." is about the composition of a chilean collection. I explain why we chose Chile as a preferred field of research, and then describe the collection.

Chapter 3 "Chemistry" describes in details how to extract cosmogenic nuclides of interest, how to measure isotopic ratios on ASTERisques AMS facility, and how to interpret the data.

Chapter 4 "Cosmogenic results and interpretation." presents the results for two types of samples. First, large iron meteorites, and then, a subsample of the Chilean collection described in chapter 2. Results on large iron meteorites are presented as new insights into these iron meteorites histories. Results on the Chilean collection enable us to calculate a flux of meteorites over 10g.

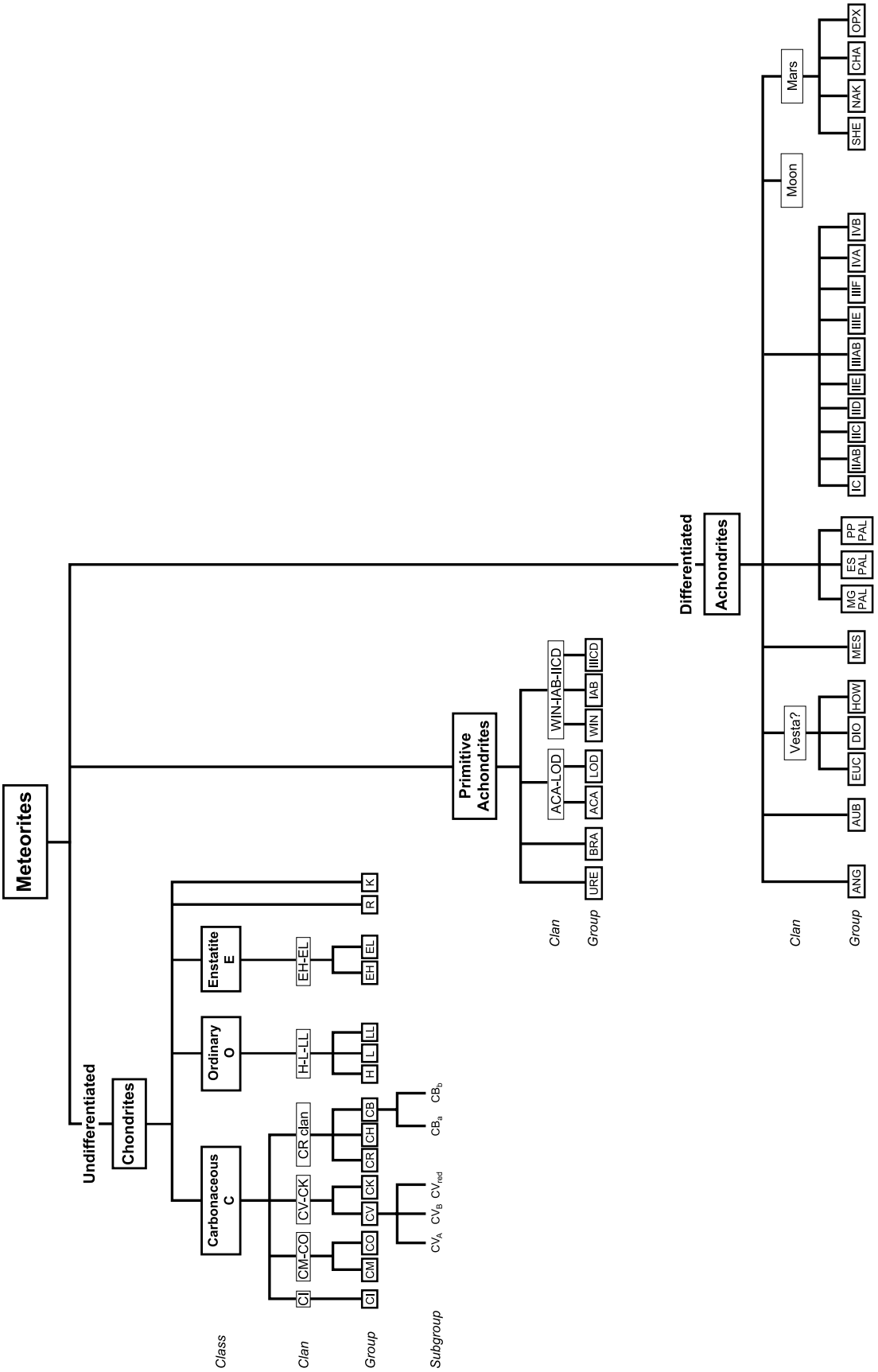

URE=Ureilite; ACA=Acapulcoite; LOD=Lodranite; ANG=Angrite; AUB=Aubrite; BRA=Brachinite; WIN=Winonaite; HED=Howardite-Eucrite-Diogenite; MES=Mesosiderite; MG PAL=Main-Group Pallasite; ES PAL=Eagle Station Pallasite; PP PAL=Pyroxene Pallasite; SHE=Shergottite; NAK=Nakhlite; CHA=Chassignite; OPX=Orthopyroxenite.

Figure 3: Systematics of meteorite classification. Main divisions (classes, clans, groups) and relationships amonst meteorite groups. From Weisberg et al. (2006).

Chapter 2: Meteorite Flux over the last million years.

We present here a collection from the Atacama desert, in Chile. In this chapter, I explain why we chose Atacama as a preferential recovery field and how we found dense collections areas using micrometeorites. I then describe the obtained collection in a submitted article (MAPS, 2014).

2.1 Atacama: a preferential location for meteorite hunting.

Private hunters and research missions have roamed Atacama for a few years now, and over 500 meteorites have been declared to the Meteoritical Society (http://www.lpi.usra.edu/meteor/index.php).

In the following, we show that the long-standing aridity (Clarke 2006) of Atacama desert makes it a good location for conservation of meteorites and hence recovery of large and old collections.

The Chile desert is also easily accessible, in a time when a lot of destinations are not recommended.

CEREGE has developed a partnership with the University of Chile (Santiago): all recovered meteorites are brought back to CEREGE for study, but remain property of Chile, and will be eventually shipped back.

To find dense collection areas in the rather large Atacama desert, we chose the field exclusively in the Central Depression, away from any water source that could enhance weathering. We also looked for microspherules by collecting and sorting sand. The idea was that if an area is favorable for micrometeorites preservation, it should also be for meteorites preservation. We went then to some of the rich microspherules sites. In all but one site (MM9, probably because of a large abundance of ubiquitous dark terrestrial rocks), we found a high number of meteorites. We present in table 3 four micrometeorites sites we searched for meteorites. The local meteorite recovery density represents the number of recovered meteorites less than a few hundred meters from the micrometeorite site.

Table 3: Micrometeorites recovery density and linked meteorite density.

Site name	DCA	Micrometeorites density (>200μm/m^2)	Local meteorite recovery density
MM9	Palestina	5000	0
MM10	Caleta el Cobre	10359	180
MM16	San Juan	2681	36
MM18	El Medano	n.d.	50

Note that in the §2.2 , figures and tables are numbered as they are in the submitted article

.

2.2 Description of a very dense meteorite collection area in western Atacama: insight into the long-term composition of the meteorite flux to Earth using a new pairing method.

Aurore HUTZLER[1]*, Jérôme GATTACCECA[1,2], Pierre ROCHETTE[1], Régis BRAUCHER[1], Bertrand CARRO[1,3], Eric J. CHRISTENSEN[4], Cécile COURNEDE[1], Matthieu GOUNELLE[5], Nejia LARIDHI OUAZAA[6], Rodrigo MARTINEZ[7], Millarca VALENZUELA[8], Michael WARNER[9], Didier BOURLES[1].

[1]Aix-Marseille Université, CNRS-IRD-Collège de France, UM 34 CEREGE, Technopôle de l'Environnement Arbois-Méditerranée, BP80, 13545 Aix-en-Provence, France.

[2]Department of Earth, Atmospheric, and Planetary Sciences, Massachusetts Institute of Technology, 77 Massachusetts Avenue, Cambridge, MA 02139, USA.

[3]Ecole Normale Supérieure de Lyon, Lyon, France.

[4] Lunar and Planetary Laboratory, University of Arizona,Tucson, Arizona, USA.

[5]Institut de minéralogie, de physique des matériaux et de cosmochimie - UMR7590, Muséum National d'Histoire Naturelle, 57 rue Cuvier, 75 231 Paris, France.

[6]Université de Tunis El Manar, Faculté des Sciences, Unité de Recherche, Pétrologie Cristalline et Sédimentaire, Département de Géologie, Campus Universitaire, 2092 Manar II, Tunis, Tunisia.

[7]Museo del Meteorito, San Pedro de Atacama Chile.

[8]Instituto de Astrofísica, Pontificia Universidad Católica de Chile, Vicuña Mackena 4860, Macul, Santiago.

[9]CTIO-NOAO, Chile.

*corresponding author. E-mail : hutzler@cerege.fr.

Abstract

We describe the geological, morphological and climatic settings of two new meteorite collections from Atacama (Chile). The "El Médano collection" was recovered by systematic on-foot search in El Médano and Caleta el Cobre Dense Collection Areas, and is composed of 213 meteorites before pairing, 142 after pairing. The "private

collection" has been recovered by car by three private hunters, and consists of 189 meteorites. As for other hot desert finds, and contrary to the falls and Antarctica finds, both collections show an overabundance of H chondrites. A recovery density can be calculated only for the "El Médano collection", and gives 251 and 168 meteorites (larger than 10 g) per km^2 before and after pairing respectively. It is by far the densest collection area described in hot deserts. The Atacama desert is known to have been hyper-arid for a long period of time, and, based on cosmic ray exposure ages on the order of 1-10 Ma, to have been very stable. Such a high meteorite concentration might be explained invoking either a yet unclear concentration mechanism (possibly related to downslope creeping), or a previously underestimated meteorite flux in previous studies, or an average terrestrial age over 2 Myr. This last hypothesis is supported by the high weathering grade of meteorites, and by a long-term fragmentation of the meteorites.

Introduction

Deserts experience semiarid to hyper-arid climates which allow preservation and accumulation of meteorites. In hot deserts the lack of vegetation and the favorable geomorphologic features simplify the search for meteorites. They are easier to reach than Antarctica where the surfaces with the highest meteorite density have been found so far, with more than 30 met/km^2 in some areas (Huss 1990). 28% of the meteorites in collections come from hot deserts, compared to 67% from Antarctica (after Meteoritical Bulletin Database).

The Atacama desert is the oldest continuously arid region on Earth (Clarke 2006), affected since at least 25 Ma by very low denudation rates (Dunai *et al.* 2005). Compared to the thoroughly searched deserts of Sahara, Arabia (mostly Oman), SW USA and Australia, relatively few meteorites have been recovered in the Atacama desert so far (see review of (Muñoz *et al.* 2007)). However, as shown in (Gattacceca *et al.* 2011), it is a very promising place for meteorite recovery, with a high meteorite concentration estimated to 14 unpaired stones/km^2 in the San Juan dense collection area (DCA). This density is at least one order of magnitude larger than the one estimated in Oman or Libya, for example (Schlüter *et al.* 2002, Hezel *et al.* 2011). In fact, as for meteorite recovery rate, Atacama recently ranked among the major deserts apart the Sahara from which most meteorites are usually collected without geographic information, at the same level as Oman and an order of magnitude over Australia and SW USA (Fig.1).

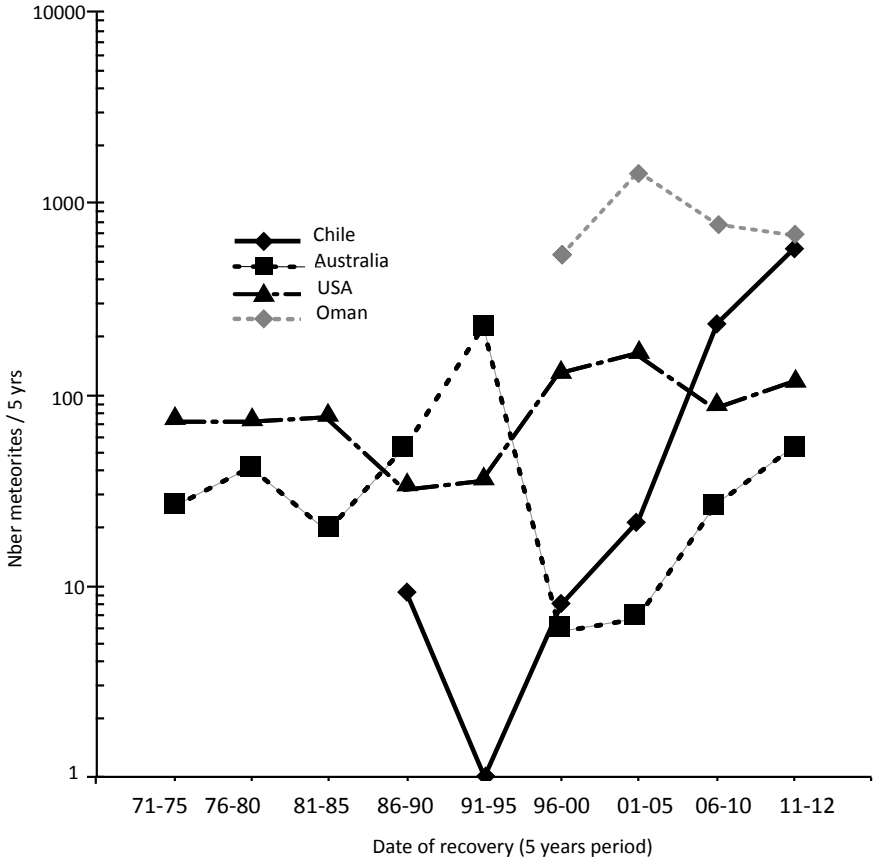

Figure 1: Number of meteorites recovered per period of 5 years in various deserts: since 1971 in Australia and SW USA, 1986 in Chile, 1996 in Oman. For the last period only the 2011-2012 years are counted (and adjusted to a five-year period by multiplying by 2.5). From the MetBull database in April 2014.

In this paper, we present the outcomes of recent meteorite recovery expeditions we organized in two contiguous DCAs in the Atacama desert, Caleta El Cobre and El Médano. We also present the analysis of a collection of 189 Chilean meteorites collected in Los Vientos, Catalina, Paposo and El Médano DCAs by three independent private meteorite hunters. We describe the geology, geomorphology and climate of the area, and the statistics of both collections which are compared to the other well documented chilean DCAs, San Juan and Pampa de Mejillones (including la Yesera and Pampa meteorites). The seven above-mentioned DCAs concentrate most meteorites finds in Chile since 1986 (489 out of 510 meteorites), when extensive dedicated search started. The 21 finds from other DCA since 1986 are fortuitous rather than the result of systematic search and show a dominance of iron meteorites (11 over 21). Previous finds (essentially during the 19th century and up to 1967) were made occasionally by geologists and mining prospectors, who concentrated on iron meteorites (31 over a total of 39 finds).

Methods

Meteorite classification

Classification was performed at CEREGE. Petrographic type (Van Schmus & Wood 1967) and weathering grade (Wlotzka 1993) were determined on polished sections using a Leica DM polarizing microscope. Microscope observations were realized independently by two of the authors (J. Gattacecca, A. Hûtzler) to ensure maximum reliability. Electron microprobes analyses were performed at Camparis facility (Université Paris 6), using a Cameca SX100 or a Cameca SX Five or at the MIT microprobe facility (Cambridge, Massachusetts) using a JEOL-JXA-8200 microprobe. Each probe was calibrated with natural standards. SEM imaging was performed on a Hitachi S-3000N microscope at CEREGE. Magnetic susceptibility was measured at CEREGE using a KLY2 instrument from Agico equipped with both a large (65cm^3) and a small (10cm^3) coil. For samples too large to fit inside the coil, a SM30 contact probe was used using the calibration of (Gattacceca *et al.* 2004)

Surface ages

The in situ-produced ^{10}Be cosmogenic nuclide concentrations were measured within quartz pebbles collected at the surface of the desert to estimate the surface ages. Samples were massive vein quartzes, rarely scattered on the surface of the desert.

The chemical treatment of all samples and all AMS measurements were carried out at the Centre Européen de Recherche et d'Enseignement des Géosciences de l'Environnement (CEREGE), Aix-en-Provence. Samples were prepared for ^{10}Be concentration measurements following chemical procedures of (Brown *et al.* 1991) and (Merchel & Herpers 1999). Pure quartz was obtained by repeated H_2SiF_6–HCl etching. Atmospheric ^{10}Be was subsequently eliminated by sequential dissolutions with diluted HF. ~100 µl of an in-house 3×10^{-3} g g^{-1} ^{9}Be carrier solution, prepared from deep-mined phenakite (Merchel *et al.* 2008), was added to each sample, and residual grains were dissolved in a strong HF solution. After the obtained solutions were evaporated to dryness and the residues were dissolved in hydrochloric acid, beryllium was separated by anion and cation exchange columns. After reduction of the solution volumes by heating, the beryllium hydroxides precipitated using NH_{3aq} were dried and finally ignited at 900°C to BeO. BeO targets were prepared for measurement at the French National Accelerator Mass Spectrometry facility (ASTER), in CEREGE, Aix-en-Provence. The obtained $^{10}Be/^{9}Be$ ratios were corrected for procedural blanks and calibrated against the National Institute of Standards and Technology standard reference material 4325 by

using an assigned value of $2.79\pm0.03\times10^{-11}$ and a ^{10}Be half-life of $1.387\pm0.012\times10^{6}$ years (Korschinek *et al.* 2010, Chmeleff *et al.* 2010). Analytical uncertainties (reported as 1σ) include uncertainties associated with AMS counting statistics, chemical blank measurements and AMS internal error (0.5%). Long-term AMS measurements of procedural blanks yield a background ratio of $3.0\pm1.5\times10^{-15}$ for ^{10}Be/^{9}Be (Arnold *et al.* 2010). A sea level, high-latitude (SLHL) spallation production of 4.49 at g^{-1} yr^{-1} was used and scaled for latitude (Stone 2000) and elevation. All obtained ^{10}Be data are reported in Table 1.

Geology and Geomorphology

The Atacama desert is located between the western central Andes and the Pacific ocean, and extends from Southern Peru (18°S) to Copiapo, Chile (30°S) (Muñoz *et al.* 2007). The two investigated contiguous DCAs we have investigated, El Médano and Caleta el Cobre, are located between 24°S and 26°S latitude, and centered on 70°W longitude (Fig. 2). They overlap two morphotectonic units: the Coastal Range and the Central Depression. The Coastal Range is influenced by a coastal fog, and thus is only semi-arid, whereas the Central Depression is hyper-arid, being protected from the coastal fog influences by the western margin (<1000m) and from the seasonal rainfall in the Andes (>2800m) (Muñoz *et al.* 2007). The search concentrated only on the hyper-arid part of these DCAs, i.e. the Central Depression. El Médano and Caleta el Cobre productive search areas are bordered to the west by the Atacama Fault (Fig.2).

El Médano and Caleta el Cobre DCAs are composed of two main geological formations: Jurassic-Cretaceous intrusive igneous rocks (granodiorites, diorites and gabbros) and Tertiary and Quaternary alluvium and colluvium.

The investigated area is a set of approximately 30 small areas (see fig 2), for a total of 1.5 km^2 that were searched systematically on foot. They spread over a total surface of approximately 200 km^2, ensuring a smaller probability of pairing with respect to a single rectangle of 1.5 km^2. El Médano and Caleta el Cobre DCAs are different from San Juan DCA in that the favorable places for meteorite search are less extended because of more pronounced topography. Relatively flat surfaces, in an altitude range from 1950 m to 2400 m a.s.l (above sea level) were searched., Most of the investigated surfaces present a gentle average slope below 3° (at a few hundred meters scale), with a few larger sloped exceptions (6° maximum). Surfaces with a slope higher than 6° were not investigated as meteorites may not be stable in the long term on such slopes.

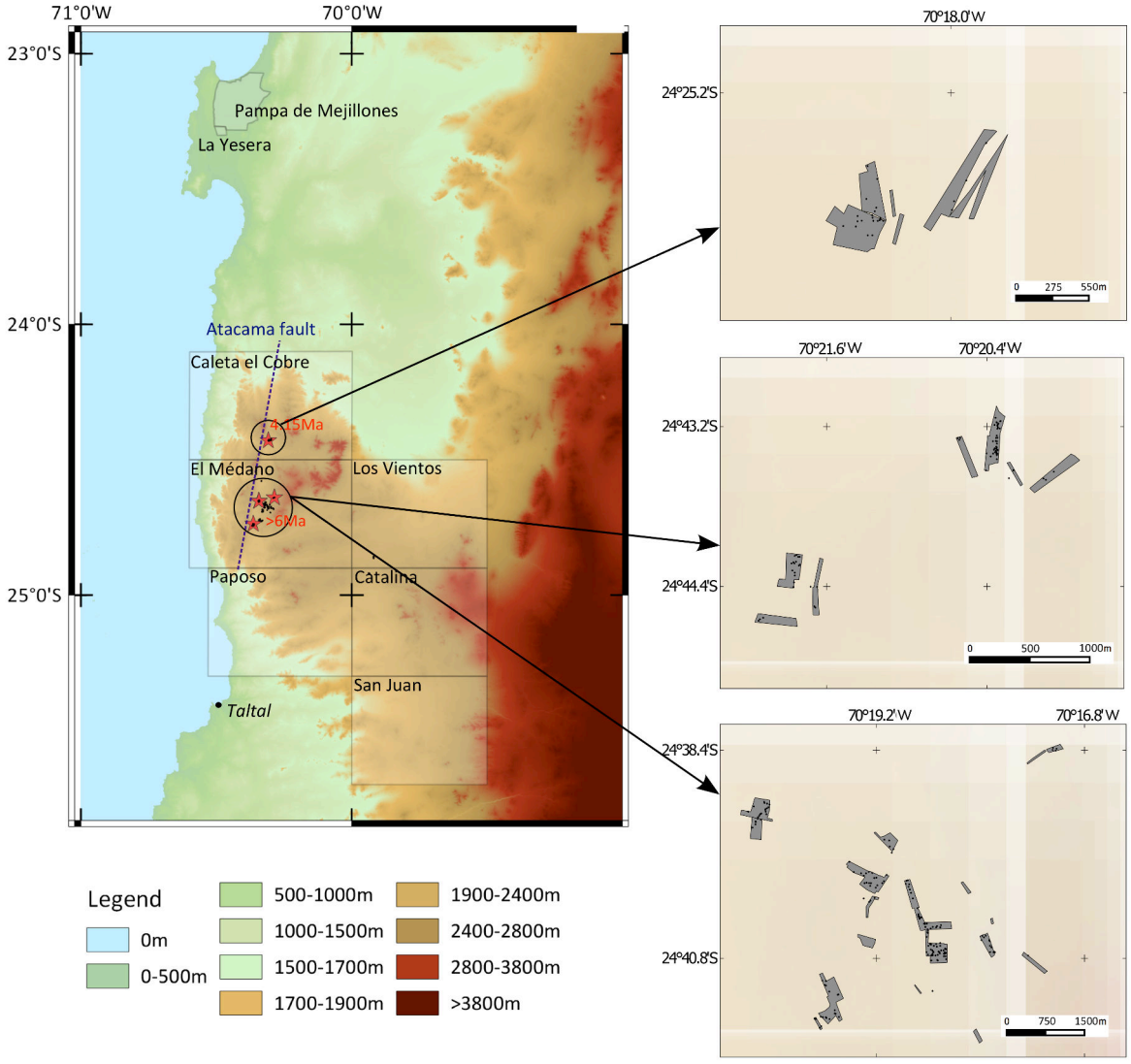

Figure 2: Map of Chilean DCAs, and explored areas in the Caleta el Cobre DCA and the El Médano DCA. Dated quartzes are represented by red stars. Meteorites are represented by black dots. The Atacama fault is indicated on the large map. The data were obtained through the online Data Pool at the NASA Land Processes Distributed Active Archive Center (LP DAAC). ASTER GDEM is a product of METI and NASA.

The other DCAs included in this study, Paposo, Los Vientos, Catalina, and San Juan were non-systematically searched by three of the authors (R. Martinez, E.J. Christensen, M. Warner). They also searched in El Médano (18 meteorites recovered). While the Paposo search zone is the southern prolongation of El Médano, the Los Vientos and Catalina search areas are located further East in the central depression, north of the San Juan DCA (fig. 2).

Surface ages estimated from the cosmic-ray exposure (CRE) ages of surface quartz pebbles are given in Table 1.

Table 1: Exposure ages for five quartz pebbles collected In Caleta el Cobre and El Médano DCAs. Samples were about 5cm thick. A density of 2500 kg.m^3 was used. Topographic shielding factor was 1.

Sample name	Altitude (m)	Latitude/Longitude	[^{10}Be] (Matoms.g^{-1})	Minimum exposure age (Ma)	Max.erosion rate (cm/Ma)
Q1	1953	-24.429050° ; -70.308110°	23.84 ± 0.55	4.15 ± 0.1	2.8
Q2	2082	-24.737374° ; -70.363476°	16.31 ± 0.41	1.59 ± 0.04	2.7
Q3	2305	-24.639760° ; -70.285610°	37.89 ± 1.1	impossible	2.8
Q4a	2089	-24.652550° ; -70.343340°	29.46 ± 0.69	impossible	2.8
Q4b	2076	-24.652883° ; -70.342745°	29.19 ± 0.42	impossible	2.8

The in situ-produced ^{10}Be is a cosmogenic nuclide that accumulates within rock minerals, mainly quartz, while they are exposed to energetic cosmic ray derived particles at or close to the Earth's surface. Its concentration depends on the geomorphological stability of the sampled surfaces. Indeed, it results from both the gain accumulated during the exposure duration within the first meters of earth surface, and from losses due to radioactive decay and to the denudation (both chemical weathering and physical erosion) affecting the sampled surface. Measuring only one cosmogenic nuclide concentration, it is not possible to determine both parameters (exposure duration and denudation rate). We may either determine a minimum exposure duration assuming no denudation or a maximum denudation rate assuming infinite exposure duration.

Because denudation rates may be considered negligible in the Atacama desert (<3cm.Ma^{-1},(Dunai *et al.* 2005)), minimum exposure duration was estimated.

However, the in situ-produced ^{10}Be concentration measured in three pebbles out of five are out of the theoretical maximum ^{10}Be range, i.e. even an infinite exposure duration with no denudation cannot account for the measured ^{10}Be. The only probable explanation for such an observation is that the considered samples have accumulated their ^{10}Be concentration at a higher altitude and have then crept down the slope to reach the current sampling altitude. In Table 2, the altitudes where the quartz pebbles should have been exposed were calculated for three arbitrary-chosen exposure durations (1.8Ma, 4Ma and >6Ma). Considering the surrounding altitudes, and the local

(a hundreds of meters) slopes, we can evaluate if such an altitude change is reasonable. Q4a and Q4b are at the bottom of circa 200 m high hills, with an average slope of 5.8°. Hence, it is likely that the quartzes have crept down the hills to account for the limited altitude difference needed to fit the data with an exposure duration >4 Ma. As for Q3, it lies on a surface with a gentle slope of 3.7°, and with no high hills in the vicinity (in a radius of 2 km, maximum altitude is 2430 m a.s.l.).

Table 2: Differential between current altitude and required altitude for three different exposure ages for quartz pebbles (table 1). (Δ=required altitude-current altitude).

Sample name	Sample altitude (m)	Δ if T_{age} = 1.8 Ma (m)	Δ if T_{age} = 4 Ma (m)	Δ if T_{age} = 6 Ma (m)
Q3	2305	+969	+339	+187
Q4a	2089	+759	+154	+8
Q4b	2076	+783	+153	+31

Even accounting for the uncertainty of a change of altitude, it is clear that our quartz samples studied were exposed for more than 1.5 Ma and up to >6 Ma. Therefore, the El Médano and Caleta el Cobre DCAs have older surface exposure ages than the San Juan DCA (where exposure durations determined with the same methodology yield consistent minimum exposure durations of 1.5 Ma). A more detailed study of exposure history, including noble gases data will be performed in the future.

Characteristics of Studied collections

We present here two distinct Chilean meteorite collections.

The first collection was recovered during two search campaigns organized by CEREGE and the University of Chile in 2010 and 2011. The search was conducted by foot alongside a grid of parallel lines, less than 10 m distant from each other. The investigated areas are spread across the El Médano DCA and the Caleta el Cobre DCA (Fig. 2). Since all the investigated areas are part of the same geomorphological unit, all results are presented together and this collection will be referred to in the rest of the text as the “El Médano collection”, or the “ElM collection”.

281 stones were recovered over a cumulated surface of 1.5 km^2. Meteorites with a mass lower than 10g were not studied, except for the ones that seemed unusual (22 stones). 213 were classified and declared to the Meteorite Nomenclature Committee. Except for the mass distribution which considers all

meteorites, in the following, the results regarding the 213 classified meteorites are discussed.

Meteorites were mostly of brownish color, due to weathering (Fig. 3 – for more pictures, see Appendix…). About 30% of the meteorites over 200g are still covered by fusion crust on more than half their surface. Meteorites are slightly buried, the burial height ranging from a few millimeters to 5 cm, the larger stones being more buried in absolute terms. Most meteorites show a whitish deposit of caliche on the buried side.

Figure 3: Photographs of meteorites from the El Médano DCA. (a) ElM 133, an LL6 ordinary chondrite (84mm x 32mm). (d), (e) and (f) Elm 101 (circa 25 x25 mm). (b) and (c) ElM 078 ((b) : 110 x 70mm).(g) ElM 185 several pieces of a more typical meteorite from the Atacama (largest piece = 44 x 33mm). Note the brownish color and the rather flat shape of the pieces.

The second collection amounts to 189 meteorites. It was recovered since 2009 by three of the authors (R. Martinez, E.J. Christensen, M. Warner) and their team, searching mostly by car in the central depression. All but four meteorites were classified at CEREGE. Note that the meteorites composing the private collection are only a part of the vast meteorite collections of the hunters. The stones were sometimes chosen on an unusual aspect or an unusual magnetic susceptibility, artificially enhancing the abundance of rare meteorites. The meteorites in this collection come from different DCAs: Los Vientos (58 meteorites), Catalina (83 meteorites), El Médano (24 meteorites), Paposo (16 meteorites), and San Juan (8 meteorites). We combine the results for all these areas. This collection will be referred in the rest of the text as the “private collection”. Exact locations of finds inside the DCA are temporarily undisclosed. Note that among the 67 San Juan meteorites present in the Meteoritical Society Database, 8 are part of the private collection, the rest being reported in (Gattacceca *et al.* 2011).

The aspect of the stones in the private collection is roughly the same as in the ElM collection. The private collection meteorites display more fusion crust than the ElM collection, with 45% showing more than half of fusion crust left.

Meteorites from both collections were reported in the Meteoritical Bulletins No. 89 (Russell *et al.* 2005), 100, 101, 102 and 103 (Ruzicka *et al.* 2014). Details are given in the Appendix A (El Médano collection) and B (private collection).

Each meteorite numbered in the field may correspond to several fragments collected over a few meters distance (31% of meteorites with more than one fragment for the ElM collection). In zones of very high meteorite density the choice to group fragments under the same name or to generate a new name was arbitrary. A systematic study was conducted through visual inspection and measurement of magnetic susceptibility, sometimes leading to the separation of the initial group into several smaller groups and the generation of new names.

Pairing

Pairing is a crucial step in any study willing to accurately investigate abundances of types of meteorites, and meteorite concentration. We present a mathematical model we designed and used for a quick pairing of a large number of meteorites.

To help with the pairing of hundreds of stones, we used a model predicting the possibility of pairing between 2 stones. The model calculates P, a factor transcribing the probability of two meteorites being paired, following the formula:

$$P = \left(\prod_i p_i^{w_i}\right)^{1/\sum w_i}$$

with p_i the probability of pairing for two meteorites for the i criterion, and w_i the weight given to the i criterion. Note that P is not mathematically speaking a probability, since the function's integral is not equal to one. We will use the term "factor" instead.

Since a pairing can be invalidated by a single criterion we chose to calculate pairing probability using geometric mean (based on the product of the values) and not arithmetic mean (based on the sum of the values), which would hide non-conclusive criteria.

Although we reference (Benoit *et al.* 2000) for insight into which criteria are useful, we develop a different approach. First, Benoit et al. used preset abundances from falls to find a pairing probability: this method does not allow us to study the possible variations in the composition of the flux of meteorite over time. Moreover, they

calculate the product of the probabilities for each criterion, instead of the geometric mean: their results are not mathematically homogenous.

We used the model we developed exclusively for equilibrated ordinary chondrites. Other types of meteorites are rare enough in our collection to evaluate pairing directly, without using a pairing model.

For ordinary chondrites we separated H, L and LL groups: two meteorites from two different groups cannot be paired.

Amongst all the criteria that can be used for pairing (Benoit *et al.* 2000), we chose the meteorite petrographic type, weathering grade, shock grade, fayalite and ferrosillite content, magnetic susceptibility and distance between stones. For each criterion, a probability function was chosen.

Weathering grade, shock grade, fayalite and ferrosillite contents, and magnetic susceptibility probability functions were modeled as Gaussian functions of the difference between the values of the criterion $p = e^{-\frac{c_A - c_B}{2\sigma^2}}$, c_A and c_B being the criterion of both meteorites, and σ a parameter set for each criterion (see Table 3). We needed a function giving values close to 1 when c_A-c_B was not too far from 0, and quickly decreasing after a given threshold. The gaussian function is a good fit. σ was calibrated by using an already paired Chilean collection (San Juan DCA, in (Gattacceca *et al.* 2011).

A discrete function was applied to distances (Table 3). We consider that fragments separated by more than 50km are very unlikely to be paired. The probability function might be dependent on the area, and thus must be adapted to each environment. For example, in the Allan Hills region of Antarctica, paired fragments were only a few kilometers apart (Benoit *et al.* 1993), whereas in the Elephant Moraine area fragments were more widely dispersed (Benoit et al. 2004).

Petrographic type was also represented by a discrete function. We consider that type 3 chondrites cannot be paired with other types. Probabilities used are shown in Table 3. An improvement to the pairing model would be to differentiate the probability depending on the petrographic type, and not only on the difference between both meteorites, as we do now.

Then, we assigned a weight to each criterion: some criteria are more robust than some others, and thus were given a higher weight. Distance is usually only supportive of pairing: thus, we used a weight of 0.5. Also, since the search areas are rather disseminated, distance is not really statistically reliable.

Pairing criteria listed in (Benoit *et al.* 2000) as primary were given a weight of 2: shock grade, magnetic susceptibility, fayalite and ferrosillite content, except for the weathering grade, which may be variable within a meteorite. Other criteria were given a weight of 1. Missing data were given a weight of zero. Thus, all our pairing factors are mathematically homogenous.

After running the code, we obtain a symmetric matrix showing pairing factors. All pairs showing a factor higher than 0.9 were then checked "manually" by comparing the textures using a petrographic microscope. More than half of the pairs detected by the program were false (meteorites were not paired). This may be improved by using additional criteria (such as porosity, polycrystallinity of troilite…), but the manual checking step cannot be avoided to get an accurate pairing.

The code was designed using Matlab language, and is available on request

Table 3: Parameters used in the pairing model for ElM collection.

Criterion	Distribution	Parameters	Weight
Weathering grade	Gaussian	1.3	1
Shock grade	Gaussian	1.3	2
Fayalite content	Gaussian	0.7	2
Ferrosillite content	Gaussian	0.7	2
Magnetic susceptibilty	Gaussian	0.7	2
Petrographic type	Discrete	p=1 if Δ = 0	1
		p=0.75 if Δ = 1	
		p=0.1 if Δ >1	
Distance	Discrete	p = 1 si d<10m	0.5
		p = 0.85 si d<10km	
		p = 0.83 if d<20km	
		p = 0.8 if d<30km	
		p = 0.75 if d<40km	
		p = 0.3 if d<50km	
		p = 0 if d>50km	

Statistics of Chilean collections

Mass distribution

All 281 meteorites of the ElM collection were taken into account. Meteorites masses range from 1.1 g to 2220 g, with 90% below 160 g and 28% under 10 g. The mass distribution (Fig. 4) is broadly similar to that of the Nullarbor Plain, San Juan and Roosevelt County areas where systematic search on foot was performed, with a large population of meteorites having a mass lower than 40 g. Due to the relative abundance of meteorite-looking rocks, the search team would be keeping a slow pace and is thus more able to spot small pieces of meteorite. Providing that enough time and attention was spent on the field, it is assumed that other collections could show a similar percentage of small meteorites. However, the fact is that the aspect of the field is indeed very decisive for meteorite recovery: in the San Juan DCA for instance, the high abundance of meteorite-colored terrestrial rocks in the cm size can clearly prevent efficient detection of smaller meteorites (Gattacceca *et al.* 2011).

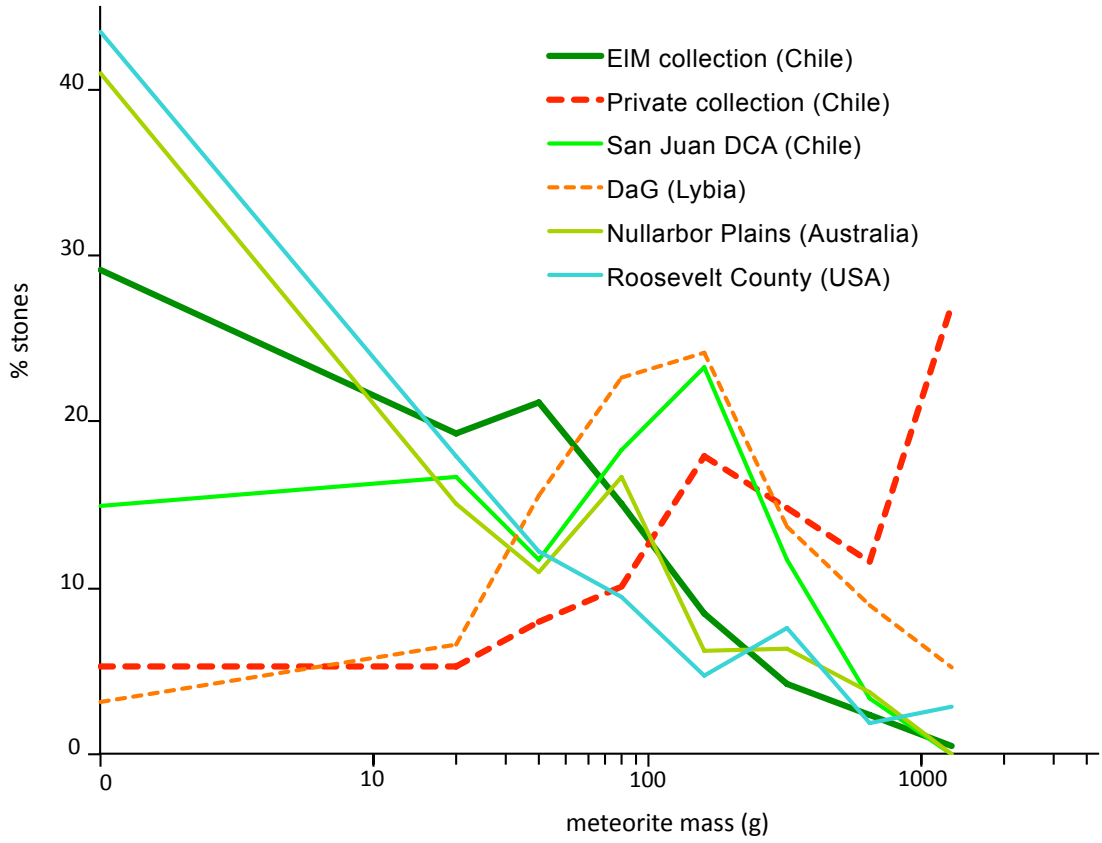

Figure 4: Distribution of meteorites masses for hot deserts meteorites. San Juan data are from Gattacceca et al. (2011), other deserts data are from Koblitz (2005). Dhofar (Oman), Acfer (Algeria), NWA (Sahara) and HaH (Lybia) have mass distributions similar to DaG.

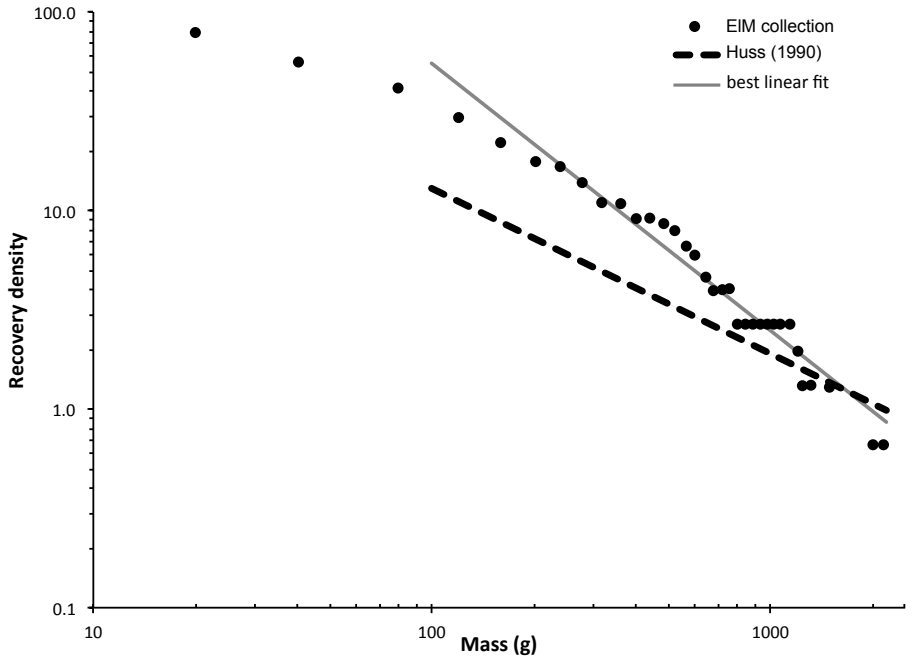

Figure 5: Cumulative recovery density as a function of mass. Best linear fit is shown (R^2=0.9567 on the range 120-2200g), and Huss distribution (s = -0.83) is displayed (dotted line).

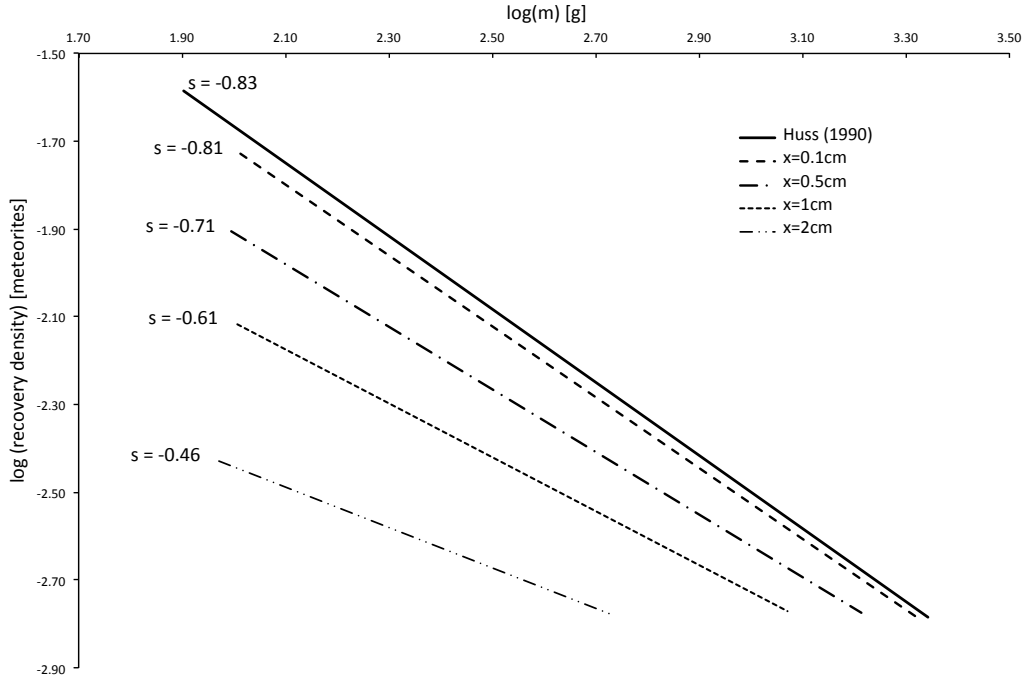

Figure 6: Results obtained eroding the original distribution proposed by (Huss 1990), with x (cm) the thickness of meteorite eroded, considering meteorites are spheres with a density of 3.5.

An observation reported by (Gattacceca *et al.* 2011) highlights that the meteorites from the San Juan DCA are subject to aeolian erosion. The small pieces would then disappear faster in the San Juan DCA than in the El Médano and Caleta el Cobre DCAs, since the aeolian erosion appears to be less potent in the last two DCAs (ventifacts are more present in the San Juan area than in the El Médano and Caleta and Cobre areas.).

Meteorites falling on Earth are found to follow a power-law mass distribution with a slope of -0.83 (Huss 1990). Figure 5 present the data for the ElM collection, and the regression for masses larger than 100g. The slope is -1.35, steeper than the theoretical distribution (also shown on Fig. 5). Simple aeolian erosion cannot explain such a steep slope – on the contrary, the slope would decrease with increasing aeolian erosion (Fig. 6). Aeolian erosion cannot explain the slope we calculate for ElM collection.

Another explanation would be a higher fragmentation of meteorites in the ElM DCA, enabled by an older age of the population. When big meteorites are fragmented, the mass distribution tends toward small masses and the slope increases.

The ElM, San Juan DCA and Nullarbor Plains collections show a lack of meteorites heavier than 1kg. We believe the searched area was not large enough to get a statistically reliable number of large meteorites.

Since the stones were recovered by car, the mass distribution of the private collection shows a totally different pattern than the collection described above. Meteorite masses range from 1.9 g up to 30.8 kg, with 30% over 1 kg. Mass distribution shows roughly the same pattern as in Dar al Gani DCA for low masses, with an overabundance of stones above 1 kg. The same pattern is found in Dhofar (Oman), Acfer (Algeria), NWA (Sahara) and HaH (Lybia) (Fig. 4).

Weathering grade

Compared to the San Juan DCA, as well as to the private Chilean collection, the ElM collection shows more weathered meteorites, with 52 % W3 and over and no W0 (Fig. 7).

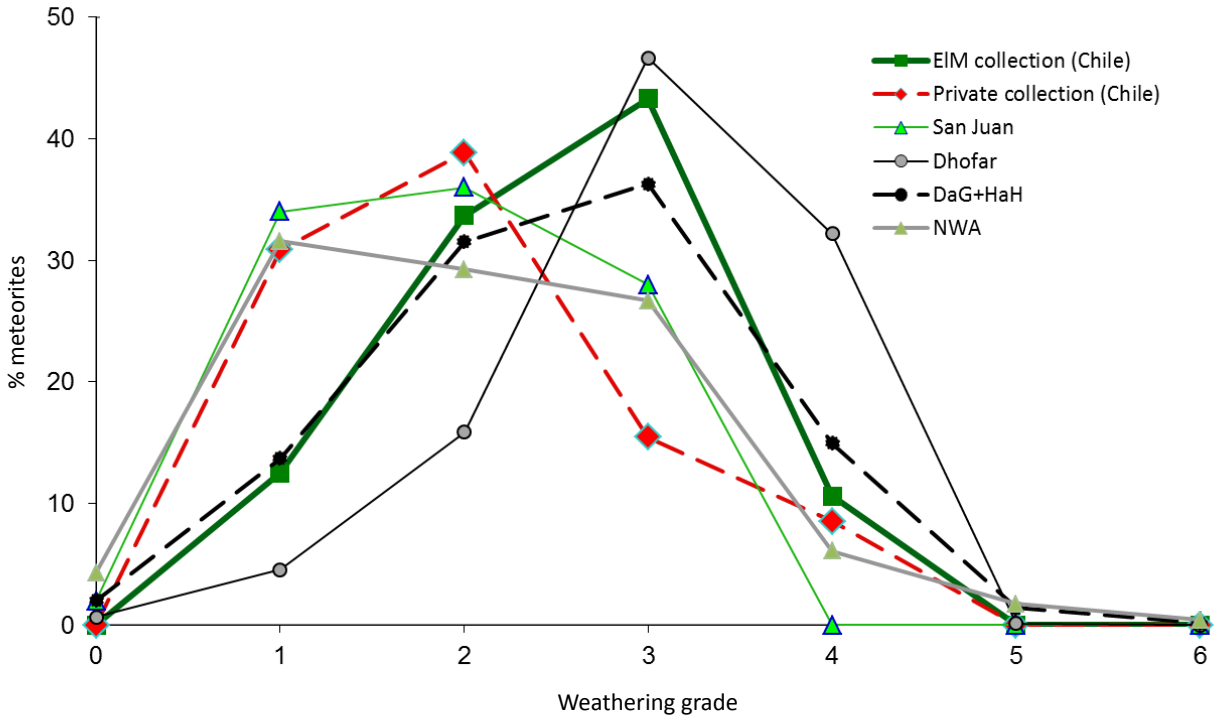

Figure 7: Distribution of meteorites weathering grade for hot deserts meteorites. San Juan data are from (Gattacceca *et al.* 2011) Gattacceca et al. (2011), other deserts data are from Koblitz (2005).

The private collection shows less weathered meteorites, with 70% below W3.

To test the hypothesis that the bigger meteorites get less weathered, we plotted the percentage of meteorites showing a weathering grade higher than W2 for the ElM collection before pairing and for the private collection (fig. 8).

In both collections, we note that this percentage decreases with increasing mass, indicating that the larger meteorites are indeed less weathered on average.

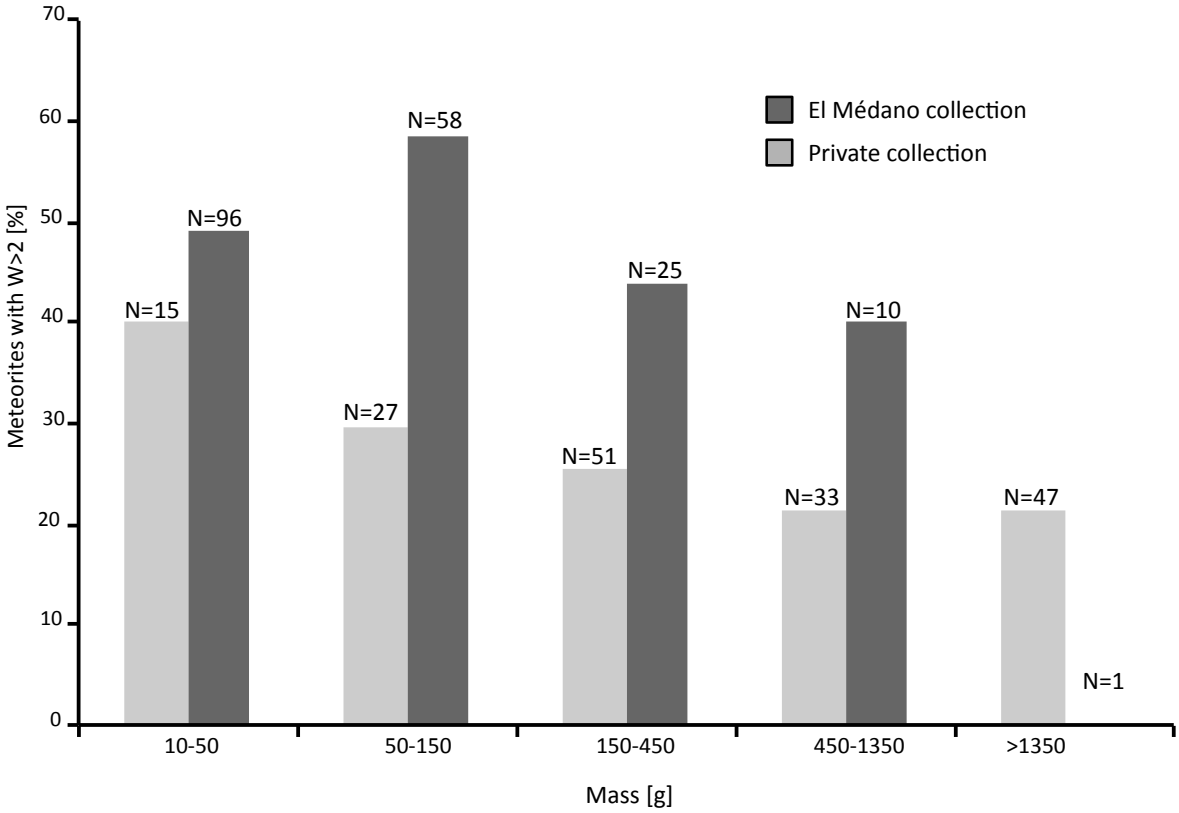

Figure 8: Percentage of meteorites with a weathering grade higher than 2 for both collections.

Relative abundances: group and type

We present the statistical properties of several collections in Table 4: ElM and private collection, falls, Antarctica finds and hot desert finds (including Dhofar, Acfer and Dar al Gani collections). The comparison with other collections enables us to consider a possible qualitative change in meteorite flux, if we consider the period of accumulation of the different collections. Antarctica has concentrated meteorites for up to several 100 ka in some places (Huss, 1990); terrestrial ages up to 1 Ma have been reported (Nishiizumi, 1989). In hot deserts, the age spectrum covers a few dozen kyr (Jull 2006). Falls cover the last 200 years.

Table 4. Relative abundances by groups and types from ElM collection, private collection, falls, Antarctica finds and hot desert finds.

	ElM collection			Private collection [a]		Falls [d]	Antarctic finds [d,c]	Hot desert finds [d,e]
Classification	**Number[a]**	**Abundance[b] (%)**	**Abundance after max pairing [b] (%)**	**Number**	**Abundance[b] (%)**	**Abundance[b,c] (%)**	**Abundance (%)**	**Abundance (%)**
H	**134 (82)**	**62.9**	**57.7**	**98.0**	**52.1**	**41.1/28.3**	**40.4**	**54.7**
H3	5 (3)	3.7	3.7	7.0	7.1	4.5	3.7	5.0
H4	29 (14)	21.6	17.1	21.0	21.4	17.0	27.7	19.4
H5	62 (38)	46.3	46.3	41.0	41.8	48.0	41.3	33.3
H5/6	4 (2)	3.0	2.4	4.0	4.1	0.0		11.2
H6	29 (21)	21.6	25.6	22.0	22.4	25.7	26.4	23.8
H3-5	1 (1)	0.7	1.2	3.0	3.1			0.6
H4-6	1 (1)	0.7	1.2	0.0	0.0			
H4/5	3 (2)	2.2	2.4	0.0	0.0			
H/L	**1 (1)**	**0.5**	**0.7**	**0.0**	**0.0**	**0.2**	**0.0**	**0.0**
L	**63 (47)**	**29.6**	**33.1**	**63.0**	**33.5**	**46.7/32.1**	**35.2**	**37.9**
L3	1 (1)	1.6	2.1	4.0	6.3	3.2	4.8	3.1
L4	9 (7)	14.3	14.9	2.0	3.2	6.7	6.2	8.8
L5	4 (3)	6.3	6.4	3.0	4.8	20.9	34.4	24.5
L5-6	2 (2)	3.2	4.3	1.0	1.6	0.0		
L6	47 (34)	74.6	72.3	53.0	84.1 (78.7)	66.7	54.0	57.4
L/LL	**0 (0)**	**0.0**	**0.0**	**1.0**	**0.5**	0.9	**0.1**	
LL	**10 (7)**	**4.7**	**4.9**	**12.0**	**6.4**	**11.0/7.6**	**16.3**	**7.4**
LL3	1 (1)	10.0	14.3	2.0	16.7	13.5	3.2	
LL5	1 (1)	10.0	14.3	6.0	50.0	22.9	51.5	
LL6	8 (5)	80.0	71.4	4.0	33.3	49.0	37.0	
iron	**0 (0)**	**0.0**	**0.0**	**0**	**0**	**3.9**	**0.4**	
C	**4 (4)**	**1.9**	**2.8**	**8.0**	**4.2**	**3.5**	**3.2**	**4.1**
HED	**0 (0)**	**0.0**	**0.0**	**2.0**	**1.1**	**4.8**	**2.1**	
others	**1 (1)**	**0.5**	**0.7**	**5.0**	**2.6**		**0.8**	
Total number	213 (142)			189.0				
H/L ratio	**2.13**		**1.74**	**1.60**		0.88	**1.15**	**1.44**

[a]after maximum pairing between parenthesis
[b]for petrographic types, abundance is within the group
[c]abundance within ordinary chondrites/resp. within total meteorites.
[d]data from Meteoritical Bulletin Database (http://www.lpi.usra.edu/meteor/), as of May 2014.
[e]includes Dar al Gani, Dhofar and Acfer collections.

H chondrites are overabundant (compared to falls and Antarctica) in the ElM collection and the private collection. Pairing in the ElM collection lowers the H/L ratio (2.1 before pairing, 1.7 after). ElM and private collection's H/L ratios, as well as San Juan's ratio (2 according to (Gattacceca *et al.* 2011)) are like other hot desert finds ratio (1.4), and significantly higher than falls ratio (0.9), suggesting that the present-day composition of the meteorite flux is not representative of the long term one. Antarctica shows a ratio (H/L = 1.15) closer to the falls than to the hot deserts ones. An adhoc scenario is to imagine a complex qualitative change in flux such as the ratio was around 1 before the hot deserts age spectrum (Antarctic signal), then tended toward 2, then back to a flux with a ratio close to 1. Another possible explanation for why Antarctica has such a low ratio is that pairing is impossible because of the transport into ice, with a specific fragmentation process that may affect H and L differently.

Although H/L ratios are close in the ElM collection, private collection and hot desert finds, the distribution of petrographic types is very different: ElM and private collections show a higher percentage of the most common types (46% and 42% respectively H5 among all H chondrites and 72% and 84% respectively L6 among all L chondrites), while other hot deserts finds show a much lower percentage (33% H5 and 57% L6). An explanation would be that meteorites classified as H5/6 in hot desert collections have been classified as H5 in our collections: if we add the abundances of H5 and H5/6 for hot deserts collections, we obtain 44.5%, which is very close to our observations.

The L6 abundance is reduced to 78.7% in the private collection after pairing of the only obvious case in this collection, a large L6 shower. The result is still above other hot deserts finds. Hypothetically we missed another L6 shower in both collections. Another explanation is that the flux changed qualitatively over time.

We notice in the ElM collection a deficit of LL chondrites (abundances of 4.7% before pairing, 4.9% after), compared with the fall statistics (11.0%). The private collection shows a smaller deficit (6.4%), maybe explained by the fact that LL chondrites have a low magnetic susceptibility, and hence were preferentially chosen when the private collection was gathered. The deficit in the ElM collection (already noted in the San Juan DCA on a smaller database) can be explained by the fact that LL chondrites contain less FeNi metal than other ordinary chondrites, and thus are harder to spot on the field. As already raised by several authors (Harvey & Cassidy 1989, Benoit & Sears 1996, Gattacceca *et al.* 2011), another hypothesis is that the flux of meteorites changed qualitatively over the falls time scale (a few hundred years).

An overabundance of type 3 ordinary chondrites was observed in the San Juan DCA based on the study of 48 meteorites (Gattacceca *et al.* 2011). This is not observed anymore for the ElM and private collection, based on 213 and 189 meteorites, respectively. We may conclude the San Juan collection was not large enough.

No iron meteorite was found in our systematic search, and only a single one was found in the private collection's searching area (Catalina 003, found by the hunter L. Labenne), leading to abundance on the order of 0.5%. This is at odds with the fall and the pre-1986 abundances: 3.8% and 79%, respectively. However, the same deficit of irons is observed in Sahara, Oman, Antarctica. In deserts experiencing a long human occupation (Sahara, Oman, Chile), iron meteorites might have been collected in pre-historical and historical times as a source of iron. However, this does not explain the case of Antarctica: we prefer the hypothesis of the deficit being explained by the mass distribution of the various collections. Iron meteorites are indeed usually of large mass, e.g. among the 43 irons from Chile only 4 are below 1 kg, with a minimum of 260 g. If we consider the abundance of iron meteorites among the systematically searched >1kg meteorites, we obtained 1.6% (1 over 60) for the private collection, and 0 over 3 for the ElM collection. On the contrary, iron meteorites are artificially overabundant in falls, since the mass distribution is biased toward high masses (the median being at 1.8kg for 1201 samples), due to the higher probability of large falls recovery. It is also possible that the flux changed over time, with a recent increase in proportion of iron meteorites.

HED meteorites, the most abundant achondrite group apart from iron, yield an abundance of 0% for the ElM collection and 1.1% for the private collection, again lower than falls (4.8%). We interpret this as due to the color effect described below in §Meteorite Concentration.

To calculate an accurate abundance of carbonaceous chondrites for the ElM collection, we need to take into account the fact that the carbonaceous chondrites we classified are lighter than 10g. We then calculate the abundance using the total number of meteorites, not only the classified meteorites. We obtain an abundance of 1.4% before pairing, and 1.9% after pairing, which is low compared to the other collections. Carbonaceous chondrites are also more difficult to spot on the ground, the metal content being lower than in ordinary chondrites. The private collection abundance (4.2%) is higher than the falls one (3.5%), maybe because of the bias toward the choice of unusual stones in this collection.

The abundances distribution is conditioned by several factors: the way of collecting meteorites (by car or by foot), the aspect of the ground (color, sand or

stones…), the alteration processes (affecting which type of meteorite will weather faster), and the possible qualitative changes in the flux of meteorites with time.

Meteorite Concentration

In this part, only the ElM collection is considered, since the private collection does not result from a systematic recovery, making a discussion in terms of density of meteorites impossible. To calculate an accurate meteorite concentration on the ground from the recovery density, we need to correct for two biases. Most of Atacama arid surface is scattered with dark magmatic rocks, or with rocks made darker by desert varnish (Goldsmith *et al.* 2014). However, compared to the San Juan area (Gattacceca *et al.* 2011), the new DCAs reported here are characterized by a rather light cream-colored main lithology (upper Cretaceous acid volcanic or intrusive rocks) with little amount of darker material. Meteorites were identified in the field mostly by their brownish color, due to weathering of metal or sulfides, although a few fresh fusion-crusted and black-colored meteorites were found. Therefore meteorites with low metal or sulfide content are more difficult to spot. HED meteorites, Martian and lunar meteorites, and aubrites (amounting to about 8% of meteorites based on fall statistics) have a metal plus sulfide content one order of magnitude lower than LL chondrites (e.g., (Rochette *et al.* 2003, Rochette *et al.* 2008, Rochette *et al.* 2009), and as such are almost unrecognizable in the field if they do not possess the remains of a fusion crust. To take into account this bias, we increase the total number of meteorites by 8%.

Although search on foot allows a better recovery of meteorites, hunters were obliged to keep a certain distance between them, to cover more ground. The distance usually used was 10m. If we plot the number of meteorites found against the distance to the walking line, we noticed that there was a deficit of meteorites found in the 2-5m range, with 68% found within 2m of the hunter. Following the same reasoning as in Gattacceca et al (2011), we calculate that about 69% of the meteorites located more than 2m away from the walking grid were not collected.

With 191 meteorites (not considering the 22 unusual stones under 10 g) heavier than 10 g collected on 1.5 km^2, the recovery density is of 127 meteorites above 10g per km^2 (after pairing, 86 meteorites>10g.km^{-2}). Taking into account the two biases described above, we obtain a meteorite density of 225 (resp. 152) meteorites above 10g per km^2 before (respectively after) pairing. This is by far the densest meteorite collection area in the world, even compared to Antarctica, and even considering a uncertainty of about 20% on the concentration (uncertainty derived from the localization of the GPS

points, and on the determination of both bias described before). A few hypotheses can be considered to explain such a high concentration of meteorites.

Individual search areas are rather small (less than one twentieth of km²) compared to strewn fields of a given fall (up to a few dozen km^2 (Gnos et al., 2009)). As explained in (Halliday *et al.* 1989), each area could show more falls than are representative of the surface itself. Following this reasoning, the concentration would be slightly overestimated, though quantification of this overestimate is difficult.

Contrary to the situation in Antarctica, there are no obvious concentration mechanisms, although we may take into account that some meteorites creep slowly down the slopes, as the quartz pebbles may have done (§Geology and Geomorphology). We also observe that fragments of the same meteorite are very often distributed along the slope, with smaller fragments laying downslope. During such long term creeping, concentration could occur on lower slope areas.

Assuming Halliday et al. (1989) modeled an accurate flux (83 meteorites above 10g per million km^2 per year), we would have a meteorite accumulation over the last 2 Ma at El Médano, a surprisingly long duration for hot deserts, although meteorites may have indeed accumulated for such along time, according to the old surface age and long-standing hyper-aridity in this area (Dunai *et al.* 2005). It is also possible that Halliday's model is inaccurate for low masses. Measurements of the cosmogenic nuclides content of the meteorites are in progress to eventually obtain a terrestrial age distribution for the ElM collection. Also, even if the correlation is not clearly established yet, the high weathering grade of the ElM collection is a hint toward old ages.

We also have to consider the lack of permanent human occupation in the Atacama desert, compared to other hot deserts. In the Atacama desert, meteorites have not been collected over the last thousand years (except for a few iron meteorites), and meteorite strewn fields have not been disturbed (except for the areas near the mines), allowing meteorites to stay for a long time in this desert.

Conclusions

We classified 213 meteorites, including 191 meteorites larger than 10g, recovered by systematic search on foot over a surface of $1.5km^2$ in El Médano and Caleta el Cobre DCAs. After maximum pairing, this corresponds to 142 different falls. We

completed this systematic collection with 189 meteorites from private hunters from several Chilean DCAs.

The El Médano collection shows a mass distribution typical of areas searched on foot (high abundance of small masses), whereas the private collection is typical of areas searched by car (overabundance of meteorites above 1kg).

The El Médano collection shows weathered meteorites, with 52% over W2, whereas the private collection has better preserved meteorites (70% of W2 or lower). Both collections show a correlation between mass and weathering, the larger stones being less weathered.

We notice an overabundance of H chondrites compared to L chondrites in both collections with respect to the falls statistics, in line with results from other hot and cold deserts. We feel that the case for a large change of H/L ratio over time is more and more robust.

There is a lack of iron meteorites (0% for the ElM collection, 0.5% for the private collection) compared to falls (3.5%), though if we take into account the fact that iron meteorites are usually over 1kg, we obtain an abundance of iron meteorites of 1.6% for the private collection in that mass range. One need to take into account that falls mass distribution is biased toward high masses, hence that iron abundance is artificially overestimated. Again, these anomalous ratios show that a qualitative change in meteorite flux has occurred recently.

The Central Depression of Atacama was already shown to be an exceptional field for recovery of meteorites, and the results of the present study show an exceptional meteorite concentration comprised between 152 and 225 meteorites over 10g per km^2. Although these numbers should be slightly reduced by the effect of the size of the search areas compared to the size of a typical strewn field, we expect the collection to have accumulated over a long time span. The high age of the population is also supported by the fragmentation of meteorites over time (see §Mass distribution) and the alteration of the meteorites, with 52% over W2.

The Atacama desert has been hyper-arid for several Ma and the El Médano and Caleta el Cobre DCAs experienced a negligible denudation rate, which allows the meteorites to be preserved over a long time span. In addition, the lack of human occupation also allowed their preservation over a longer time period in this desert comparatively to the Sahara and Arabia deserts.

Acknowledgments:

M. Arnold, G. Aumaître and K. Keddadouche are thanked for the ^{10}Be measurements at the ASTER AMS national facility (CEREGE, Aix-en-Provence, France), which is supported by the INSU/CNRS, the ANR through the "Projets thématiques d'excellence" program for the "Equipements d'excellence" ASTER-CEREGE action, IRD and CEA. The ASTER GDEM data product was obtained through the online Data Pool at the NASA Land Processes Distributed Active Archive Center (LP DAAC), USGS/Earth Resources Observation and Science (EROS) Center, Sioux Falls, South Dakota (https://lpdaac.usgs.gov/data_access). D. Gaetano is thanked for proofreading the language. Financial support was provided by INSU and CNES through the Programme National de Planétologie.

References

Arnold M., Merchel S., Bourlès D. L., Braucher R., Benedetti L., Finkel R. C., Aumaître G., Gottdang A., and Klein M. 2010. The French accelerator mass spectrometry facility ASTER: Improved performance and developments. Nuclear Instruments and Methods in Physics Research B 268:1954– 1959.

Benoit P. H. and Sears D. W. G. 1996. Rapid changes in the nature of the H chondrites falling to Earth. Meteoritics & Planetary Science 31:81–86.

Benoit P. H., Sears D. W. G., Akridge J. M. C., Bland P. A., Berry P. A., and Pillinger C. T. 2000. The non-trivial problem of meteorite pairing. Meteoritics & Planetary Science 35:393–417.

Brown E. T., Edmond J. M., Raisbeck G. M., Yiou F., Kurz M. D., and Brook E. J. 1991. Examination of surface exposure ages of Antarctic moraines using in situ produced ^{10}Be and ^{26}Al. Geochimica et Cosmochimica Acta 55:2269–2283.

Chmeleff, J., von Blanckenburg, F., Kossert, K., Jakob, J, 2010. Determination of the ^{10}Be half-life by multicollector ICP-MS and liquid scintillation counting. Nuclear Instruments and Methods in Physics Research B 268, 192- 199.

Clarke J. D. A. 2006. Antiquity of aridity in the Chilean Atacama Desert. Geomorphology 73:101–114.

Dunai T. J., Gonzalez Lopez G. A., and Juez-Larré J. 2005. Oligocene-Miocene age of aridity in the Atacama Desert revealed by exposure dating of erosion-sensitive landforms. Geology 33:321–324.

Gattacceca J., Eisenlohr P., and Rochette P. 2004. Calibration of in situ magnetic susceptibility measurements. Geophysical Journal International 158:42–49.

Gattacceca J., Valenzuela M., Uehara M., Jull A. J. T., Giscard M., Rochette P., Braucher R., Suavet C., Gounelle M., Morata D., Munayco P., Bourot-Denise M., Bourles D., and Demory F. 2011. The densest meteorite collection area in hot deserts : The San Juan meteorite field (Atacama Desert, Chile). Meteoritics & Planetary Science 46:1276–1287.

Gnos E., Lorenzetti S., Eugster O., Jull A. J. T. , Hofmann B. A., Al-Kathiri A. and Eggimann M. 2009. The Jiddat al Harasis 073 strewn field, Sultanate of Oman. Meteoritics & Planetary Science 44:375-387.

Goldsmith Y., Stein M., Enzel Y. 2013. From dust to varnish : Geochemical constraints on rock varnish formation in the Negev Desert, Israel. Geochimica et Cosmochimica Acta 126 :97-111.

Halliday I., Blackwell A. T., and Griffin A. A. 1989. The flux of meteorites on the Earth's surface. Meteoritics 24:173– 178.

Harvey R. P. and Cassidy W. A. 1989. A statistical comparison of Antarctic finds and modern falls: Mass frequency distributions and relative abundance by type. Meteoritics 14:9–14.

Hezel D.C., Schlüter J., Kallweit H., Jull A. J. T., Al Fakeer O. Y., Al Shamsi M., Strekopytov S. 2011. Meteorites from the United Arab Emirates: Description, weathering, and terrestrial ages. Meteoritics & Planetary Science 46:327-336.

Huss G.R. 1990. Meteorite infall as a function of mass: Implications for the accumulation of meteorites on Antarctic ice. Meteoritics & Planetary Science 25:41-56.

Koblitz J. 2005. MetBase—Meteorite data retrieval software, version 7.1. Bremen, Germany. CD-ROM.

Korschinek, G., Bergmaier, A., Faestermann, T., Gerstmann, U.C., Knie, K., Rugel, G.,Wallner, A., Dillmann, I., Dollinger, G., von Gostomski, Lierse Ch., Kossert, K., Maitia,M., Poutivtsev, M., Remmert, A., 2010. A new value for the half-life of ^{10}Be by Heavy-Ion Elastic Recoil Detection and liquid scintillation counting. Nuclear Instruments and Methods in Physics Research B. 268, 187-191.

Jull A.J.T. 2006. Terrestrial Ages of Meteorites. Meteorites and the Early Solar System II 889-905.

Merchel S. and Herpers U. 1999. An update on radiochemical separation techniques for the determination of long-lived radionuclides via accelerator mass spectrometry. Radiochimica Acta 84:215–219.

Merchel S., Arnold M., Aumaître G., Benedetti L., Bourlès D. L., Braucher R., Alfimov V., Freeman S. P. H. T., Steier P., and Wallner A. 2008. Towards more precise ^{10}Be and ^{36}Cl data from measurements at the 10–14 level: Influence of sample preparation. Nuclear Instruments and Methods in Physics Research B 266:4921–4926.

Nishiizumi K., Elmore D., Kubik P.W. 1989. Update on terrestrial ages of Antarctic meteorites. Earth and Planetary Science Letters 93:299-313.

Munoz C., Guerra N., Martinez-Fris J., Lunar C., and Cerda J. 2007. The Atacama Desert: A preferential arid region for the recovery of meteorites—Find location features and strewfield distribution patterns. Journal of Arid Environments 71:188-200.

Schlüter J., Schultz L., Thiedig F., Al-Mahdi B. O., and Abu Aghreb A. E. 2002. The Dar al Gani meteorite field (Libyan Sahara): Geological setting, pairing of meteorites, and recovery density. Meteoritics & Planetary Science 37:1079-1093.

Stone J. O. 2000. Air pressure and cosmogenic isotope production. Journal of Geophysical Research 105:23753–-23759.

Van Schmus W. R. and Wood J. A. 1967. A chemical petrologic classification for the chondritic meteorites. Geochimica et Cosmochimica Acta 81:747-765.

Wlotzka F. 1993. A weathering scale for the ordinary chondrites (abstract). Meteoritics 28:460.

Brown E. T., Edmond J. M., Raisbeck G. M., Yiou F., Kurz M. D., and Brook E. J. 1991. Examination of surface exposure ages of Antarctic moraines using in situ produced ^{10}Be and ^{26}Al. Geochimica et Cosmochimica Acta 55:2269–2283.

Rochette P., Sagnotti L., Bourot-Denise M., Consolmagno G., Folco L., Gattacceca J., Osete M. L., and Pesonen L. 2003. Magnetic classification of stony meteorites: 1. Ordinary chondrites. Meteoritics & Planetary Sciences 38:251–258.

Rochette P., Gattacceca J., Bourot-Denise M., Consolmagno G., Folco L., Kohout T., Pesonen L., and Sagnotti L. 2009. Magnetic classification of stony meteorites: 3. Achondrites. Meteoritics & Planetary Science 44:405–427.

Russel S., Zolensky M., Righter K., Folco L., Jones R., Connolly H.C. Jr, Grady M., Grossman J.N. 2005. The Meteoritical Bulletin, No. 89. Meteoritics & Planetary Science 40:A201–A263.

Appendix (A). Classification, physical properties and pairing of meteorites from the El Médano collection.

Official name	TKW (g)	Number of stones	Classification	W	Fa (%)	PMD Fa (%)	Magnetic susceptibility	Pairing group	Latitude S	Longitude W	Met Bull
Caleta El Cobre 001	9	1	H6	4					24.26604177	70.03337458	100
Caleta El Cobre 002	18	1	H6	3	19.1		4.55	C002	24.42980454	70.30541796	100
Caleta El Cobre 003	338	4	H5	2	18.5		5.08	C003	24.42876745	70.30491983	100
Caleta El Cobre 004	254	1	H5	2	18.1		5.25		24.42880676	70.30467155	100
Caleta El Cobre 005	193	10	H5	2	18.6		5.04	C003	24.42881623	70.30505125	100
Caleta El Cobre 006	179	1	L6	3	25.4		4.53	C006	24.4234467	70.2975772	100
Caleta El Cobre 007	24	1	L6	3	23.0		4.52		24.42746046	70.29978549	100
Caleta El Cobre 008	15	1	H6	3	19.6		4.62		24.42917000	70.30742000	100
Caleta El Cobre 009	95	1	L4	1	22.7		4.77	C009	24.42884000	70.30644000	100
Caleta El Cobre 010	47	1	L4	1	23.0		4.90	C009	24.42848000	70.30643000	100
Caleta El Cobre 011	32	1	L6	4	25.1		4.39		24.4288000	70.30615000	100
Caleta El Cobre 012	17	1	L4	1	22.9		4.81	C009	24.4292000	70.30655000	100
Caleta El Cobre 013	105	1	L4	3	23.0		4.73		24.42859000	70.30540000	100
Caleta El Cobre 014	20	1	H4	2	18.8		4.82		24.42842000	70.30543000	100
Caleta El Cobre 015	115	1	L6	3	25.4		4.34	C006	24.42881000	70.30535000	100
Caleta El Cobre 016	34	5	H5	2	18.6		4.83	C003	24.42861000	70.30487000	100
Caleta El Cobre 017	41	4	H5	2	19.4		4.95	C003	24.42869000	70.30485000	100
Caleta El Cobre 018	6	1	H5	4	18.1		4.47		24.42980706	70.30573589	100
Caleta El Cobre 019	1.1	1	H6	3	18.8		4.62	C002	24.42805767	70.29992765	100
Caleta El Cobre 020	633	1	H5	3	18.7		4.73		24.42503549	70.30574410	102
Caleta El Cobre 021	37.3	1	L4	3	23.3		4.91		24.42814900	70.30525400	102
El Médano 001	10	1	H6	2	18.6		4.98	E001	24.64006200	70.28554200	100
El Médano 002	12	5	L6	3	25.2		4.58		24.63950000	70.28605000	100
El Médano 003	11	1	H5	2	18.6		4.99		24.63992000	70.28614000	100
El Médano 004	151	1	H4	1	17.4		5.32	E004	24.63970000	70.28536000	100
El Médano 005	582	5	L6	2	24.6		4.59	E005	24.65288300	70.34274500	100
El Médano 006	55	1	LL6	4	28.7		3.85	E006	24.65180800	70.34462300	100
El Médano 007	31	1	LL6	4	28.3		3.46	E006	24.65080200	70.34355900	100
El Médano 008	33	1	L6	3	25.6		4.31		24.65259600	70.34251200	100
El Médano 009	65	1	L6	3	24.9		4.61	E009	24.65131400	70.34128400	100

W = weathering grade (Wlotzka, 1993); magnetic susceptibility is given in log χ, with χ in 10-9 $m^3.kg$-1. Possible pairing groups are indicated. PMD = percentage mean deviation (for type 3 only).

Appendix (A). Classification, physical properties and pairing of meteorites from the El Médano collection.

Official name	TKW (g)	Number of stones	Classification	W	Fa (%)	PMD Fa (%)	Magnetic susceptibility	Pairing group	Latitude S	Longitude W	Met Bull
El Médano 010	7	1	H4	4	17.3		4.57	E010	24.651445	70.341340	100
El Médano 011	87	1	H6	3	17.9		4.81	E011	24.651792	70.341264	100
El Médano 012	54	2	H6	3	18.4		4.79	E011	24.652038	70.341185	100
El Médano 013	5.2		CO3		16.6	16.41	4.37		24.652290	70.341136	100
El Médano 014	54		H4	2	16.8		4.95	E010	24.652309	70.342333	100
El Médano 015	98		H4	3	17.4		4.73	E015	24.652150	70.342100	100
El Médano 016	57		L6	4	24.7		4.01		24.649940	70.341570	100
El Médano 017	156		L6	3	25.0		4.03		24.650130	70.341480	100
El Médano 018	15		H4	3	16.7		4.77	E015	24.651150	70.341010	100
El Médano 019	11		H3	3	18.3	5.69	4.48	E019	24.650950	70.340730	100
El Médano 020	102		L6	3	24.6		4.28		24.742470	70.361550	100
El Médano 021	50		H6	3	18.3		4.78	E021	24.742620	70.361430	100
El Médano 022	47		H6	3	18.5		4.87	E021	24.739470	70.364090	100
El Médano 023	115		L6	3	24.0		4.37		24.740060	70.364150	100
El Médano 024	9		H5	3	18.6		4.47	E024	24.744260	70.368520	100
El Médano 025	132		H6	3	18.4		4.91	E021	24.744080	70.368360	100
El Médano 026	154		L6	3	25.2		4.71		24.743890	70.367940	100
El Médano 027	46	1	H5	3	19.2		4.93	E027	24.737374	70.363476	100
El Médano 028	141	3	L5	1	24.2		4.76	E028	24.736280	70.363569	100
El Médano 029	392	15	L5	1	24.0		4.90	E028	24.736282	70.363382	100
El Médano 030	32	2	H6	3	19.2		4.45	E030	24.737247	70.363371	100
El Médano 031	35	1	H5	2	19.9		4.90		24.738617	70.363996	100
El Médano 032	28	1	H6	2	18.9		4.73	E001	24.736889	70.363841	100
El Médano 033	45	1	H5	4	19.0		4.48	E024	24.736148	70.364001	100
El Médano 034	10	1	H6	3	19.1		4.61	E030	24.736965	70.364166	100
El Médano 035	72	1	H5	2	19.3		4.93	E027	24.737991	70.364293	100
El Médano 036	54	1	H5	3	18.5		4.77	E021	24.737100	70.364405	100
El Médano 037	111	1	L6	3	24.7		4.54		24.736066	70.363789	100
El Médano 038	3.8	1	H6	3	18.2		4.66	E038	24.650440	70.340530	100
El Médano 039	3.1	1	H5	3	16.9		4.64		24.650261	70.340990	100

W = weathering grade (Wlotzka, 1993); magnetic susceptibility is given in log χ, with χ in 10-9 m3.kg-1. Possible pairing groups are indicated. PMD = percentage mean deviation (for type 3 only).

Appendix (A): Classification, physical properties and pairing of meteorites from the El Médano collection.

Official name	TKW (g)	Number of stones	Classification	W	Fa (%)	PMD Fa (%)	Magnetic susceptibility	Pairing group	Latitude S	Longitude W	Met Bull
El Médano 040	3.6	1	H6	4	19.3		4.62		24.740017	70.361216	100
El Médano 041	1.9	1	H5	3	18.4		4.53		24.737102	70.364040	100
El Médano 042	22.6	1	L6	3	25.3		4.35		24.689990	70.327992	101
El Médano 043	24.8	1	H4	2	18.7		5.11	E043	24.678454	70.309249	101
El Médano 044	44.4	2	L6	3	25.7		4.32	E044	24.678800	70.309023	101
El Médano 045	319	2	H5	2	19.0		5.18	E045	24.679150	70.306986	101
El Médano 046	40.1	1	H4	2	17.4		4.92		24.679402	70.309413	101
El Médano 047	57.9	1	H4	1	18.5		5.18		24.679347	70.308210	101
El Médano 048	118	1	H5	1	19.5		5.20		24.679608	70.307022	101
El Médano 049	138	2	H4	3	19.0		4.81	E049	24.680426	70.308195	101
El Médano 050	52	1	H5	4	20.0		4.57		24.680422	70.309421	101
El Médano 051	28.9	1	L6	2	25.9		4.80		24.654874	70.343793	101
El Médano 052	66.5	1	H5	2	17.5		5.10		24.690605	70.328011	101
El Médano 053	17.9	1	H4/5	2	18.8		5.14	E053	24.722913	70.338758	101
El Médano 054	46.5	2	H5	2	18.5		5.11	E054	24.719358	70.338356	101
El Médano 055	34.3	1	H6	2	19.8		5.18		24.666243	70.313798	101
El Médano 057	10.8	1	H6	4	19.7		4.60		24.738258	70.363998	101
El Médano 058	11.8	1	H6	2	19.2		4.96	E001			101
El Médano 059	27	1	H4	3	16.9		4.74	E010	24.653190	70.342801	101
El Médano 060	29	2	H3	2	17.3	5.10	4.86	E060	24.691481	70.329590	101
El Médano 061	57	1	H5	2	18.2		5.23	E054	24.691327	70.330276	101
El Médano 062	22	2	L6	4	24.7		4.12		24.672236	70.311691	101
El Médano 063	23	4	H4	2	18.4		4.83	E063	24.679012	70.306675	101
El Médano 064	22	1	H4	4	18.2		4.61	E064	24.679188	70.309225	101
El Médano 065	11.5	1	H5	2	19.6		4.97	E045	24.720242	70.338401	101
El Médano 066	15.8	1	H5	2	18.3		4.92	E066	24.725644	70.331656	101
El Médano 067	20.4	1	L6	3	24.3		4.03	E067	24.669171	70.321398	101
El Médano 068	125	13	H4	2	17.4		5.24	E004	24.665531	70.321398	101
El Médano 069	65	1	H6	2	18.5		5.01		24.686401	70.329045	101
El Médano 070	50.5	3	L6	3	25.8		4.57		24.673641	70.307582	101

W = weathering grade (Wlotzka, 1993); magnetic susceptibility is given in log χ, with χ in 10-9 m3.kg-1. Possible pairing groups are indicated. PMD = percentage mean deviation (for type 3 only).

Appendix (A): Classification, physical properties and pairing of meteorites from the El Médano collection.

Official name	TKW (g)	Number of stones	Classification	W	Fa (%)	PMD Fa (%)	Magnetic susceptibility	Pairing group	Latitude S	Longitude W	Met Bull
El Médano 071	163	6	H5	2	18.0		5.19	E066	24.674285	70.309555	101
El Médano 072	19.9	1	H4	1	17.6		5.13		24.677365	70.309479	101
El Médano 073	67	1	LL6	3	28.8		3.92	E006	24.677298	70.309488	101
El Médano 074	42	1	H4	2	18.5		5.06	E074	24.677064	70.307748	101
El Médano 075	186	1	L4	3	24.7		4.55		24.721424	70.338867	101
El Médano 076	14.1	2	H5	2	18.6		5.25	E076	24.721814	70.338897	101
El Médano 077	72.0	1	L4	2	24.2		4.72		24.663659	70.321982	102
El Médano 078	1228	1	L6	3	24.4		4.47		24.678803	70.298130	101
El Médano 079	230	1	H5	2	18.5		5.13	E076	24.722526	70.338845	101
El Médano 080	24.5	1	L6	3	25.6		4.36		24.654248	70.343232	102
El Médano 081	13.4	1	H4	3	18.9		4.96		24.691336	70.329700	102
El Médano 082	22.5	1	H5	2	19.4		5.25		24.691237	70.330679	102
El Médano 083	12.6	1	H5	1	19.1		5.09	E083	24.672214	70.311600	102
El Médano 084	45	1	H5	2/3	19.1		4.93	E043	24.678312	70.309534	102
El Médano 085	12.9	1	H4	3	18.8		4.37		24.678679	70.308040	102
El Médano 086	1258	3	H4	1	18.4		5.12	E063	24.679059	70.306797	102
El Médano 087	13.9	1	H4	2	18.8		4.90	E049	24.679088	70.306989	102
El Médano 088	10.1	1	L6	3	24.9		4.37	E088	24.679474	70.308645	102
El Médano 089	296	2	L6	4	24.7		4.25		24.679495	70.309413	102
El Médano 090	18.8	1	L6	2	24.3		4.44		24.680333	70.308296	102
El Médano 091	17.8	1	H5	3	18.7		4.55	E091	24.721470	70.343662	102
El Médano 092	289	1	H6	3	18.3		4.84		24.719807	70.339052	102
El Médano 093	51.8	1	H4-6	2	19.9-19.8		4.95		24.722908	70.338655	102
El Médano 094	35.3	1	L6	1	24.5		4.74		24.723575	70.338759	102
El Médano 095	72	3	LL6	3	27.9		3.88		24.668380	70.320338	102
El Médano 096	11.1	1	acapulcoite		11.6		5.44		24.678756	70.297347	102
El Médano 097	229	1	L5-6	4-2	24.9		4.32		24.719460	70.338806	102
El Médano 098	135	2	L6	4	24.7		4.18		24.721395	70.338689	102
El Médano 099	10.5	1	H5	3	18.6		4.73	E099	24.721845	70.338742	102
El Médano 100	1.8		CM2	moderate	7.3	12.10	3.93		24.725488	70.340121	102

W = weathering grade (Wlotzka, 1993); magnetic susceptibility is given in log χ, with χ in 10-9 m3.kg-1. Possible pairing groups are indicated. PMD = percentage mean deviation (for type 3 only).

Appendix (A): Classification, physical properties and pairing of meteorites from the El Médano collection.

Official name	TKW (g)	Number of stones	Classification	W	Fa (%)	PMD Fa (%)	Magnetic susceptibility	Pairing group	Latitude S	Longitude W	Met Bull
El Médano 101	19.1	1	L6	3	24.5		4.64	E009	24.666423	70.320119	102
El Médano 102	65	1	H4/5	1	18.8		5.17	E053	24.668502	70.322432	102
El Médano 103	61	2	LL6	2	29.8		4.00	E103	24.663597	70.320779	102
El Médano 104	27	3	LL5	3	29.0		3.78		24.673343	70.310841	102
El Médano 105	16.7	1	H5/6	3	18.4		5.00	E105	24.673274	70.310716	102
El Médano 106	91	2	H5/6	2	18.9		4.98	E105	24.721842	70.339259	102
El Médano 107	10.3	1	H5/6	3	18.7		4.75		24.720276	70.338707	102
El Médano 108	15.5	1	H4	2	18.7		4.91	E063	24.665076	70.314196	102
El Médano 109	13.1	1	H3	2	17.2	5.7	5.02	E060	24.666783	70.313575	102
El Médano 110	28.8	1	LL6	4	32.0		3.41		24.659686	70.317043	102
El Médano 111	139	1	H5	4	18.8		4.39	E024	24.690661	70.327828	102
El Médano 112	23	1	H5	2	18.1		5.23		24.678904	70.307842	102
El Médano 113	37	1	L6	3	25.1		4.05		24.678902	70.307824	102
El Médano 114	24.4	1	H5	3	17.6		4.56		24.723351	70.340059	102
El Médano 115	84	1	H5	1	19.1		5.18		24.661445	70.325174	102
El Médano 116	46	2	H6	3	18.5		4.83	E038	24.677579	70.308935	102
El Médano 117	52	1	L6	3	25.6		4.68		24.675016	70.310204	102
El Médano 118	161	3	H5	3	18.4		4.99		24.723384	70.339234	102
El Médano 119	23.3	2	H5	2	18.3		5.09		24.719942	70.338682	102
El Médano 120	24.2	1	H5	2	19.5		4.94		24.719525	70.338754	102
El Médano 121	333	4	H5	3	18.2		5.09		24.723210	70.338991	102
El Médano 122	55	1	L5/6	3	25.7		4.29				102
El Médano 123	22.1	1	H5	1	19.5		5.21		24.663661	70.322933	102
El Médano 124	39	1	H5	1	18.2		5.23		24.657348	70.317527	102
El Médano 125	93	3	L6	3	23.7		4.49	E125	24.723383	70.338806	102
El Médano 126	584	1	H5	3	18.6		4.87	E099	24.726501	70.332939	102
El Médano 127	130	12	H5	1	18.3		5.20		24.675693	70.299647	102
El Médano 128	556	1	L6	2	24.8		4.55	E005	24.668901	70.321164	102
El Médano 129	27.8	1	L6	2	25.0		4.48	E005	24.663370	70.321451	102
El Médano 130	43.6	1	L6	3	24.5		4.21	E130	24.427460	70.299785	102

W = weathering grade (Wlotzka, 1993); magnetic susceptibility is given in log χ, with χ in 10-9 m3.kg-1. Possible pairing groups are indicated. PMD = percentage mean deviation (for type 3 only).

Appendix (A): Classification, physical properties and pairing of meteorites from the El Médano collection.

Official name	TKW (g)	Number of stones	Classification	W	Fa (%)	PMD Fa (%)	Magnetic susceptibility	Pairing group	Latitude S	Longitude W	Met Bull
El Médano 131	106	6	H4	3	19.1		4.86	E049	24.665471	70.321878	102
El Médano 132	670	5	H4	1	18.3		5.10		24.665551	70.322273	102
El Médano 133	397	4	LL6	1	29.8		4.00	E103	24.684355	70.329689	102
El Médano 134	20.5	1	H5	2	17.0		5.18		24.685247	70.329672	102
El Médano 135	71	1	L6	3	24.8		4.48	E088	24.684286	70.330379	102
El Médano 136	57	1	L5	3	24.3		4.28		24.685125	70.329914	102
El Médano 137	37	1	H5	2	18.0		5.05		24.673813	70.308351	102
El Médano 138	17.9	1	L6	3	24.8		4.20	E130	24.673976	70.310583	102
El Médano 139	11.3	1	H5	2	18.9		5.14				102
El Médano 140	11.5	1	H4/5	3	18.5		4.77		24.677588	70.310010	102
El Médano 141	752	4	L6	3	25.2		4.35	E044	24.679293	70.310065	102
El Médano 142	20.5	1	L6	3	24.8		4.54	E130	24.677601	70.308969	102
El Médano 143	59	2	H4	2	18.5		5.00	E074	24.677766	70.308377	102
El Médano 144	87	2	L4	2	24.9		4.70		24.677280	70.309652	102
El Médano 145	20.4	1	H5	2	18.0		5.01	E145	24.675890	70.310332	102
El Médano 146	10.9	1	H4	4	18.7		4.62	E064	24.675123	70.310110	102
El Médano 147	19.9	2	L6	3	26.0		4.50		24.723744	70.339536	102
El Médano 148	298	2	H5	2	18.5		4.95	E079	24.722895	70.339131	102
El Médano 149	99	1	H5	2	18.6		5.11	E079	24.722759	70.338855	102
El Médano 150	56	1	L6	3	23.4		4.60	E125	24.726663	70.332656	102
El Médano 151	12.6	3	H4	2	18.8		5.09	E043	24.675991	70.299321	102
El Médano 152	45	3	H4	1	18.7		5.23	E063	24.668485	70.313002	102
El Médano 158	38	1	H4	1	18.4		5.16	E063	24.678679	70.308040	102
El Médano 159	12.3	1	L6	3	24.4		4.32	E067	24.678880	70.309048	102
El Médano 160	88	1	H6	3	19.1		4.79		24.679418	70.309153	102
El Médano 161	91	1	H5	3	17.9		4.85	E145	24.718903	70.338931	102
El Médano 162	147	1	L4	1	23.4		4.89		24.427298	70.305827	102
El Médano 163	20.4	1	L6	3	24.3		4.04	E067	24.669171	70.321398	102
El Médano 164	282	13	H5	3	18.1		5.10	E054	24.719751	70.338660	102
El Médano 165	53	2	L6	3	25.1		4.50		24.720141	70.338625	102
El Médano 166	42	1	L5	2	24.3		4.79		24.723021	70.338890	102

W = weathering grade (Wlotzka, 1993); magnetic susceptibility is given in log χ, with χ in 10-9 m3.kg-1. Possible pairing groups are indicated. PMD = percentage mean deviation (for type 3 only).

Appendix (A): Classification, physical properties and pairing of meteorites from the El Médano collection.

Official name	TKW (g)	Number of stones	Classification	W	Fa (%)	PMD Fa (%)	Magnetic susceptibility	Pairing group	Latitude S	Longitude W	Met Bull
El Médano 167	163	3	H4	2	18.9		5.04	E063	24.664125	70.322416	102
El Médano 168	6.7	1	L6	3	25.0		4.6		24.725435	70.336680	102
El Médano 169	228	1	L6	3	23.6		4.33		24.719323	70.338304	102
El Médano 179	14.9	1	H3	3	17.6	2.5	4.61	E019	24.653337	70.342215	102
El Médano 180	166	1	H3-5	2	18.1/17.9	6.4/0.2	5.08		24.691692	70.328982	102
El Médano 181	33.5	2	L3	2	26.0	2.5	4.65		24.677766	70.308377	102
El Médano 182	89	3	H3	1	19.9	2.6	5.12		24.722964	70.338655	102
El Médano 183	6.9	1	H5	4	18.9		4.57	E091	24.721136	70.338777	102
El Médano 184	474	1	H5	1	19.0		5.29	E083	24.686297	70.309205	102
El Médano 185	172	14	H5	2	19.1		5.01		24.691273	70.327192	102
El Médano 186	219	3	H5	2	18.9		5.23	E045	24.678977	70.306612	102
El Médano 187	61	5	H5	3	18.4		4.83		24.678977	70.306612	102
El Médano 188	40	3	H6	4	18.5		4.51		24.723216	70.338813	102
El Médano 189	46	2	H6	2	18.1		5.18		24.723432	70.338793	102
El Médano 190	2220	10	H5	2	18.1		4.95	E145	24.722741	70.339039	102
El Médano 191	138	1	H5	2	17.9		5.05		24.719642	70.338566	102
El Médano 192	15.7	1	H5/6	3	18.7		4.99	E105	24.665178	70.318550	102
El Médano 195	25.2	1	H/L3	1	16.9	6	4.99		24.687015	70.327416	102
El Médano 196	18.8	1	LL3	2	18.6	10.7	4.03		24.678839	70.297479	102
El Médano 197	128	9	L6	3	24.9		4.40		24.672414	70.311699	102
El Médano 198	799	58	H5	2	20.1		5.06		24.672414	70.311699	102
El Médano 199	148	6	H6	1	18.9		5.19		24.719871	70.338693	102
El Médano 200	2.4		C3-ung	low	22.7	23.6	5.08				102
El Médano 202	5.5	1	L6	4	25.0		4.28		24.721442	70.343346	102
El Médano 203	2.3	1	LL6	3	31.2		3.84				102
El Médano 204	9.2	1	H5	2	18.0		5.22		24.665976	70.319825	102
El Médano 205	3.1	1	H5	3	18.6		5.06		24.658500	70.317433	102
El Médano 206	2.7	1	H6	3	19.6		4.88		24.664558	70.320423	102
El Médano 207	4.7	1	H5	3			4.80		24.665764	70.313683	102
El Médano 208	65	7	H6	3	19.2		4.85		24.719871	70.338693	102
El Médano 209	9.7	1	CO3						24.678829	70.310368	102
El Médano 210	2.7	1	H6	2	18.7		5.11		24.85	70.5333	

W = weathering grade (Wlotzka, 1993); magnetic susceptibility is given in log χ, with χ in 10-9 m3.kg-1. Possible pairing groups are indicated. PMD = percentage mean deviation (for type 3 only).

Appendix (B). Classification, physical properties and pairing of meteorites from the private collection.

Official name	TKW (g)	Number of stones	Classification	W	Fa (%)	PMD Fa (%)	Magnetic susceptibility	Met Bull
Catalina 002	61.1	1	LL3	4	18.0		3.60	101
Catalina 004	37.5	1	mesosiderite		35.7	1.4		101
Catalina 008	98	1	CO3	moderate	19.1	13.5	4.05	102
Catalina 009	5.2	1	CR2	moderate	1.3-31.8		4.86	102
Catalina 010	329	2	L5	2			4.59	102
Catalina 011	573	10	H5	2			5.10	102
Catalina 012	225	1	H6	2			4.75	102
Catalina 013	428	3	H4	1	18.0		5.13	102
Catalina 014	191	2	H4	1	19.3		5.19	102
Catalina 015	239	1	L5	1			4.90	102
Catalina 016	647	8	H4	2			5.20	102
Catalina 017	426	2	H5	1			5.23	102
Catalina 018	1018	1	L6	2			4.55	102
Catalina 019	3191	2	H4	2	18.4		5.10	102
Catalina 020	2084	38	L6	2			4.63	102
Catalina 021	320	11	H3	2	12.6	7.4	5.06	102
Catalina 022	77	5	L3	3	21.7	8.8	4.21	102
Catalina 023	53.5	2	H~6	2			5.03	102
Catalina 024	312	1	H4	1	18.2		5.39	102
Catalina 025	39	3	L~6	1			4.69	102
Catalina 026	845	5	H~5	1			5.22	102
Catalina 027	2408	7	L6	2	24.5		4.50	102
Catalina 028	4993	>100	H5	2	19.2		5.36	102
Catalina 029	169	5	H~5	2			4.75	102
Catalina 030	214	2	H~5	2			5.01	102
Catalina 031	1178	17	L~6	2			4.59	102
Catalina 032	1107	12	H4	2	19.4		5.08	102
Catalina 033	211	1	L~6	3			4.25	102
Catalina 034	20	3	LL5	4	26.8		4.05	102
Catalina 035	904	1	H~5	1			5.17	102

W = weathering grade (Wlotzka, 1993); magnetic susceptibility is given in log χ, with χ in 10-9 m3.kg-1. PMD = percentage mean deviation (for type 3 only).

Appendix (B): Classification, physical properties and pairing of meteorites from the private collection.

Official name	TKW (g)	Number of stones	Classification	W	Fa (%)	PMD Fa (%)	Magnetic susceptibility	Met Bull
Catalina 036	42	1	H~5	1			5.22	102
Catalina 038	332	6	H5	1			5.11	102
Catalina 039	135	4	H5/6	3			5.02	102
Catalina 040	73	1	H6	2			5.14	102
Catalina 041	27.1	2	H5	3			4.75	102
Catalina 042	291	1	H5	1			5.28	102
Catalina 043	252	1	H5	1			5.17	102
Catalina 044	300	1	H5	2			5.21	102
Catalina 045	29	6	LL5	3			4.09	102
Catalina 046	17.1	1	LL6	2			3.62	102
Catalina 047	237	23	H6	1			5.38	102
Catalina 048	97	4	LL5	2	26.3		4.05	102
Catalina 049	117	6	LL5	3			4.00	102
Catalina 050	23	2	LL5	3	29.9		3.99	102
Catalina 051	3470	1	H6	2			5.31	102
Catalina 052	295	10	L6	3	22.7		4.66	102
Catalina 053	692	1	H4	1	18.5		5.21	102
Catalina 054	1016	28	L6	1			4.68	102
Catalina 055	2405	2	H6	4			4.63	102
Catalina 056	65.4	1	LL6	4	30.0		3.20	102
Catalina 057	355	1	H6	2			5.28	102
Catalina 058	374	18	H6	1			5.20	102
Catalina 059	1906	31	H5	1			5.19	102
Catalina 060	30	2	H6	3	18.6		4.95	102
Catalina 061	364	2	LL6	3	29.8		3.53	102
Catalina 062	775	5	H5	1	18.5		5.11	102
Catalina 063	287	5	L6	4	24.5		4.22	102
Catalina 064	2730	>100	L6	4	24.2		4.35	102
Catalina 065	268	5	H4	3	18.8		4.85	102
Catalina 058	374	18	H6	1			5.20	102

W = weathering grade (Wlotzka, 1993); magnetic susceptibility is given in log χ, with χ in 10-9 m3.kg-1. PMD = percentage mean deviation (for type 3 only).

Appendix (B): Classification, physical properties and pairing of meteorites from the private collection.

Official name	TKW (g)	Number of stones	Classification	W	Fa (%)	PMD Fa (%)	Magnetic susceptibility	Met Bull
Catalina 059	1906	31	H5	1			5.19	102
Catalina 060	30	2	H6	3	18.6		4.95	102
Catalina 061	364	2	LL6	3	29.8		3.53	102
Catalina 062	775	5	H5	1	18.5		5.11	102
Catalina 063	287	5	L6	4	24.5		4.22	102
Catalina 064	2730	>100	L6	4	24.2		4.35	102
Catalina 065	268	5	H4	3	18.8		4.85	102
Catalina 066	5356	>100	L6	4	24.1		4.25	102
Catalina 067	20.5	2	H4	1	16.9		5.12	102
Catalina 068	314	3	H4	2	17.8		5.22	102
Catalina 069	436	>20	L4	1	22.4		4.79	102
Catalina 070	3	1	H6	1	19.2		5.00	102
Catalina 071	122	3	LL5	4			4.02	102
Catalina 072	>100	3794	L6	4	24.2		4.06	102
Catalina 073	178	>50	H4	2	17.2		4.78	102
Catalina 074	127	4	H5-6	1	17.1		5.10	102
Catalina 075	208	56	H5	2	19.0		5.02	102
Catalina 076	5349	35	L6	4			4.39	102
Catalina 077	1465	16	L5/6	3	24.6		4.60	102
Catalina 078	1458	2	L3	1	21.7	7	4.73	102
Colachi 001	81	1	LL6	2	31.3		3.65	102
El Médano 056	180	1	CK5		30.0	1.1	4.51	101
El Médano 153	6038	54	H3	2	16.6	4.6	4.99	102
El Médano 154	1047	1	L6	4	24.7		4.41	102
El Médano 155	517	1	H6	1			5.29	102
El Médano 156	161	1	L6 (elipse)	2	25.3		4.44	102
El Médano 157	620	1	H4	3	17.8		5.08	102
El Médano 170	3893	105	L4	2	23.3		4.80	102
El Médano 171	1821	1	H~5	1			5.15	102
El Médano 172	1097	1	H~5	2			5.20	102

W = weathering grade (Wlotzka, 1993); magnetic susceptibility is given in log χ, with χ in 10-9 m3.kg-1. PMD = percentage mean deviation(for type 3 only).

Appendix (B): Classification, physical properties and pairing of meteorites from the private collection.

Official name	TKW (g)	Number of stones	Classification	W	Fa (%)	PMD Fa (%)	Magnetic susceptibility	Met Bull
El Médano 173	448	1	L~6	2			4.61	102
El Médano 174	434	5	L~ 6	1			4.58	102
El Médano 175	147	1	L~ 6	2			4.38	102
El Médano 176	64	1	L6	2	24.5		4.64	102
El Médano 177	1198	1	H~5	1			5.10	102
El Médano 178	5758	166	H~5	2			5.25	102
El Médano 193	347	1	L6	3	24.3		4.42	102
El Médano 194	9521	3	H5	1			5.2	102
El Médano 201	3356	23	H5	2	18.5		4.98	102
Los Vientos 001	73	1	diogenite	minor				100
Los Vientos 002	30750	1	L6	1	23.2		4.86	100
Los Vientos 003	25450	3	H5	1	16.9		5.27	100
Los Vientos 004	29300	5	H5	1	16.4		5.30	100
Los Vientos 005	1431	38	H3	1	19.3	11.0	5.17	102
Los Vientos 006	230	1	H4	1			5.16	102
Los Vientos 007	701	12	H5/6	2	19.3		4.95	102
Los Vientos 008	1617	22	H5	1			5.26	102
Los Vientos 009	85	3	H5	1			5.21	102
Los Vientos 010	6800	6	H5	1			5.13	102
Los Vientos 011	300	1	L6	2			4.51	102
Los Vientos 012	5117	10	H5	1			5.30	102
Los Vientos 013	2016	1	H6	1			5.29	102
Los Vientos 014	565	2	L6 (elipse)	3			4.43	102
Los Vientos 015	772	13	H3	2	19.0	3.8	5.03	102
Los Vientos 016	1.9	1	LL3	3	13.8	8.7	4.13	102
Los Vientos 017	109	1	Ureilite	moderate	6.7-16.3		4.36	102
Los Vientos 018	308	16	L6	4	25.0		4.13	102
Los Vientos 019	263	2	H4	1	16.9		5.27	102
Los Vientos 020	8100	1	H4	2	17.6		5.20	102
Los Vientos 021	161	1	L~6	3			4.41	102

W = weathering grade (Wlotzka, 1993); magnetic susceptibility is given in log χ, with χ in 10-9 m3.kg-1. PMD = percentage mean deviation(for type 3 only).

Appendix (B): Classification, physical properties and pairing of meteorites from the private collection.

Official name	TKW (g)	Number of stones	Classification	W	Fa (%)	PMD Fa (%)	Magnetic susceptibility	Met Bull
Los Vientos 022	663	1	L~6	4	24.4		4.47	102
Los Vientos 023	7090	2	L6	2	25.2		4.71	102
Los Vientos 024	333	2	L~6	2			4.40	102
Los Vientos 025	506	3	L~6	2			4.42	102
Los Vientos 026	203	1	L~6	2			4.51	102
Los Vientos 027	131	1	L~6	3			4.46	102
Los Vientos 028	12110	1	H~5/6	2			5.18	102
Los Vientos 029	329	1	L6	2	24.3		4.41	102
Los Vientos 030	1489	3	H6	1			5.21	102
Los Vientos 031	81	9	L6	2			4.40	102
Los Vientos 032	29.4	1	H5	2			5.16	102
Los Vientos 033	457	>50	H6	4			4.77	102
Los Vientos 034	212	1	L6	3			4.42	102
Los Vientos 035	254	2	L6	3			4.38	102
Los Vientos 036	601	1	H5	2			5.18	102
Los Vientos 037	4789	1	H5	1			5.19	102
Los Vientos 038	566	1	L6	2			4.49	102
Los Vientos 039	180	2	L6	2	24.5		4.50	102
Los Vientos 040	1021	2	L6	2			4.53	102
Los Vientos 041	72	1	L6	2			4.54	102
Los Vientos 042	42	1	L6	4			4.33	102
Los Vientos 043	4.6	1	CR2	severe	0.4		4.76	102
Los Vientos 044	63	3	L6	2			4.52	102
Los Vientos 045	11900	2	H4	3	20.7		4.86	102
Los Vientos 046	5809	4	H5	2			5.10	102
Los Vientos 047	11074	684	L6	1			4.87	102
Los Vientos 048	115	7	H6	3			4.50	102
Los Vientos 049	2178	8	L6	3	24.4		4.51	102
Los Vientos 050	888	80	H4	4	16.6		4.96	102
Los Vientos 052	61.2	7	L3	1	22.1	3.6	4.64	102

W = weathering grade (Wlotzka, 1993); magnetic susceptibility is given in log χ, with χ in 10-9 m3.kg-1. PMD = percentage mean deviation(for type 3 only).

Appendix (B): Classification, physical properties and pairing of meteorites from the private collection.

Official name	TKW (g)	Number of stones	Classification	W	Fa (%)	PMD Fa (%)	Magnetic susceptibility	Met Bull
Los Vientos 053	968	1	H3	2	19.1	3	5.04	102
Mantos Blancos 002	6800	14	L6	3	24.0		4.38	102
Paposo 002	2407	1	L/LL4	1	26.5		4.37	100
Paposo 003	368	1	H6	2	18.8		5.44	101
Paposo 004	8250	1	L3.1	1	21.7	10.8	4.60	102
Paposo 005	1802	1	H5	2			5.07	102
Paposo 006	297	1	H3	1	15.7	4.4	5.03	102
Paposo 007	951	1	H3-5	2	14.4/18.3	7.0/0.2	5.12	102
Paposo 008	1035	1	H~5	1			5.26	102
Paposo 009	120	1	H~5	2			5.21	102
Paposo 010	1569	1	H~6	2			5.27	102
Paposo 011	418	7	L6	3			4.28	102
Paposo 012	670	1	H6	1	18.1		5.51	102
Paposo 013	1569	1	H6	2			5.27	102
Paposo 017	351.7	2	CR2	medium				103
San Juan 063	3384	19	H5	2			5.12	102
San Juan 064	656	40	L6	3			4.47	102
San Juan 065	459	14	H4	2	18.3		5.00	102
San Juan 066	441	11	L6	2	24.2		4.39	102
San Juan 067	450	20	H4	1	19.0		5.01	102
San Juan 068	2580	5	L6	3	24.5		4.49	102
San Juan 069	2787	45	H5	1			5.18	102

W = weathering grade (Wlotzka, 1993); magnetic susceptibility is given in log χ, with χ in 10-9 m3.kg-1. PMD = percentage mean deviation

Chapter 3: Chemistry

The following procedure is based on the work of several scientists over the last decades, for example (Vogt & Herpers 1988) and (Merchel & Herpers 1999). We adapted this procedure initially developed to extract any radionuclide of interest to those that can be measured at the French national Accelerator Mass Spectrometry (AMS) facility ASTER, i.e ^{10}Be, ^{26}Al, ^{36}Cl and ^{41}Ca.

The main purpose of this extraction procedure dedicated to target preparation for AMS measurements is to get rid of any interfering isobars. Table 4 lists the extracted elements and their isobars.

Table 4: Isobars of cosmogenic nuclides of interest.

Cosmogenic element	Isobars
^{10}Be	^{10}B
^{26}Al	^{26}Mg
^{36}Cl	^{36}S
^{41}Ca	^{41}K

To reduce the boron and magnesium isobars, the use of Teflon or polypropylene materials, instead of glass, was preferred.

3.1 Chemical extraction

The determination of concentrations using the AMS technique implies measuring elemental ratios that have to be fixed as soon as possible during the physico-chemical separation process to avoid any dependency on separation yields. To satisfy this requirement a significantly larger than natural amount of stable isotope (see §3.1.1 *Isotope carriers*) is added at the very beginning of the separation procedure.

Extracting Cl necessitates working in a chlorine-free room where no other chlorine compound can interfere with the Cl from the sample and from the carrier. Hence, we worked into two different rooms. The Cl-free room will be

called "Cl-laboratory", whereas the other room will be called "Be-laboratory" in the followings.

When it is indicated that a solution is to be centrifuged, unless specified, we centrifuge for 5 min at 3000rpm. Rinsing a precipitate is done by adding some solution (acid, base or mQ water), dispersing by stirring the precipitate and centrifuging again. Depending on its further use, the rinsing solution may be either discarded or kept.

Deionized water had a resistivity of 18.2 MΩ.

3.1.1 Isotope carriers

For Be, Al and Ca, we used as carriers ICP-MS standard solutions in HNO_3. For Cl, we used an in-house ^{35}Cl-enriched carrier with a $^{36}Cl/^{35}Cl$ ratio of $2.96.10^{-15} \pm 5.5.10^{-16}$ and a total Cl concentration of 6.92mg.g.

To the tube containing the sample we added

- 1-5mg Cl
- 1mg Al (Roth, 1000 mg/l ± 0.2% in HNO3 2%)
- 10-15mg Ca (Roth, 10 000 mg/l ± 0.2% in HNO3 2%)
- 1mg Be (Roth, 1000 mg/l ± 0.2% in HNO3 2% / HF 0.5%)

for iron meteorites or iron fraction.

and

- 1,5mg Cl
- 1mg Al
- 3-5mg Ca
- 0,3mg Be

for stony meteorites (weights are from (Merchel & Herpers 1999)).

Carrier solutions are weighed with a precision of 0.01mg.

3.1.2 Sample dissolution

To dissolve the sample, two methods related to the sample mineralogy are available: (1) if the sample is mainly silicates (chondrites, for example), a

mixture of concentrated HF (7ml) and concentrated HNO_3 (2ml) is used in Teflon digestion bombs for 1-2 days at 150°C; (2) if the sample is mainly Fe/Ni alloy, 10ml of 2N HNO3 are used in a centrifuge tube for 1-2 days.

We chose in this work to work exclusively with Fe/Ni alloys. For metal extraction procedure, see §3.1.16 *Iron fraction extraction*.

After dissolving for 1-2 days the samples in centrifuge tubes, they are centrifuged. The supernatant is poured into a new centrifuge tube. Solid residues are carefully rinsed, dried, and weighed as it is crucial to accurately and precisely know the amount of meteorite that was not dissolved.

3.1.3 First Chlorine precipitation

To precipitate AgCl, 1ml 10% $AgNO_3$ is added to the supernatant and the corresponding centrifuge tube settled over one night in the dark to avoid its exposure to light since silver chloride converts to Ag upon illumination. It is then centrifuged, and the supernatant that contains the other than Cl elements of interest (Be, Ca, Al) is poured into a new centrifuge tube that is sent to the Be-laboratory.

3.1.4 Removal of sulfur

Iron meteorites or iron fractions of meteorites contain sulfur. ^{36}S is an isobar of ^{36}Cl that must be removed before precipitating AgCl as an AMS target. To perform this purification, AgCl is dissolved by adding 2ml NH_3aq (25%) (AgCl is stable in acidic solution only), 1ml of milliQ water and 0.5ml of saturated $Ba(NO_3)_2$. The aim is to co-precipitate $BaSO_4$ with $BaCO_3$. The solution usually turns red at this point, most likely because of a minor co-precipitation of red iron hydroxide . The solution is stirred up and let stand overnight with the cap slightly open.

After having checked that the pH remained alkaline and thus prevented AgCl from precipitating, the tube is centrifuged to separate the $BaSO_4/BaCO_3$ precipitate. As some crystals of $BaSO_4/BaCO_3$ may stay in the solution, it is necessary to filter it, suing a PTFE syringe and a 0.45µm PTFE filter. $BaSO_4/BaCO_3$ precipitate is then rinsed (NH_3 + H_20), and the rinsing solution is filtered and kept.

3.1.5 Second precipitation of AgCl

1ml concentrated HNO_3 is added to the supernatant solution and the rinses resulting from the $BaSO_4/BaCO_3$ co-precipitation. That tube is then stirred and maintained one hour in the dark. The resulting AgCl precipitate is separated by centrifugation, the supernatant solution being discarded. To insure that the AgCl precipitate will not contain any remaining sulphur, it is rinsed once with 4ml of concentrated HNO_3, and twice with 5ml milliQ H_2O, the rinsing solutions being discarded. AgCl precipitate is then poured into a 1.5ml opaque micro-tube. The micro-tube is centrifuged and the supernatant carefully removed to eliminate any potentially polluting chemical elements and to speed up the drying step. Finally, the AgCl precipitate is dried a few hours at T=80°C and stored protected from light until sent to the accelerator for target preparation and AMS measurement.

All the previously described steps are performed in the Cl-laboratory.

3.1.6 Removal of silver

The supernatant solution obtained after the first AgCl precipitation that contains the other elements of interest is firstly ridded of the large amount of Ag^+ introduced to insure a quantitative precipitation of AgCl by adding 50 drops (circa 1.5ml) of 10.2N HCl. The solution usually turns yellow at this point while AgCl precipitates which again implies working protected from light. After centrifugation, the supernatant solution is transferred to a Teflon beaker, the precipitate carefully rinsed with again 50 drops of 10.2N HCl, centrifuged and the rinsing solution added to the previous supernatant solution. The resulting solution is heated to dryness at T=200°C on a clean hot plate*. To avoid any cross-contamination, using a lid and little Teflon "horseshoes" to lift the lid is necessary at this step. 150 drops (circa 4.5mL) of 7.1N HCl are then added in the beakers. All the residues of the heating should dissolve. The obtained solution is poured into a weighed centrifuge tube as well as the beaker rinsing solutions that result from 3 rinses with 1mL 7.1N HCl. Finally, weighing the centrifuge tube at the end of the described processes leads to the weight of the solution (see §3.6 *Result treatments*).

3.1.7 Aliquot for elementary concentrations

Knowing the elemental composition of the processed samples is essential to the processing of data obtained. To determine the elemental composition of the solutions, and therefore of the dissolved meteorites, a few percent aliquot (usually 300µl) is sampled from the solutions that were previously homogenized by stirring. The aliquot is poured into a weighed 1.5mL micro-tube, which is again weighed with the added aliquot (see §Result treatments) and sent for measurements (see §3.2 *ICP-MS (SARM)*).

3.1.8 Removal of iron

If the total iron amount in a solution exceeds 50mg, it has to be reduced before passing the solution through an ion exchange column. This is performed in a PTFE separating funnel extracting iron from 7.1N HCl solution by solvent extraction using 3 times 20ml of diisopropylether. The organic phase containing iron is discarded. The aqueous solution containing the elements of interest is evaporated to dryness at 150°C and the solid residue is dissolved in 1.5ml of 10.2N HCl.

3.1.9 Anion exchange column

An anion exchange column (height: 20cm; diameter: 1cm),with Teflon wool as a filter and DOWEX 1x8, 100-200 mesh as a resin is prepared.

The column is first cleaned using 30ml of milliQ water and conditioned using 20 ml of 10.2N HCl. The sample solution is added, followed by 0.5ml of 10.2N HCl corresponding to the beaker rinses. Be, Al, Ca and Ni are then eluted by 16ml of 10.2N HCl : all 18ml are collected in a centrifuge tube. If Mn carrier has been added, Mn can be collected with 100 ml of 7.1N HCl.

In order to be reusable, the Teflon beakers have to be rinsed with water, filled with diluted HCl and heated to 100°C for few hours to insure that any remaining elements have been eliminated.

3.1.10 Hydroxide precipitation

The eluate solution containing Be, Al, Ca and Ni evaporated down to 2-3ml in Teflon beakers is poured into a centrifuge tube as well as the Teflon beaker rinses that are 3 times 10-15 drops of 7.1N HCl. 30 drops of NH_{3aq} are then added to increase the pH at 8-9 which leads to the precipitation of

beryllium and aluminium hydroxides while calcium and nickel remain in solution. For Ni-rich meteorites, a blue hue due to Ni(II) hydroxide precipitate may thus appear. It disappears when adding a few more drops of NH_{3aq}. After centrifugation, the supernatant containing Ca + Ni is poured in a new tube and the hydroxide precipitate rinsed with 5ml of alkaline water (pH>7); the rinses being discarded.

3.1.11 Cation exchange column

The beryllium and aluminium hydroxides precipitate is dissolved overnight by 1ml of 1N HCl. A cation exchange step is applied to separate both elements. The same column type as for the anion exchange step (height: 20cm; diameter: 1cm) is filled with DOWEX 50x8, 100-200 mesh. It is first cleaned using 20ml milliQ water and conditioned using 20ml of 1N HCl. The sample solution is then added, followed by 0.5ml of 1N HCl corresponding to the beaker rinses. The first 40ml of 1N HCl added for this purpose as eluant are discarded since they elute boron, the main beryllium isobaric interference. Beryllium is finally eluted using 115ml of 1N HCl, and, thereafter, aluminium is eluted using 50ml of 4.5N HCl.

3.1.12 Aluminium and Beryllium target precipitation

Procedures to purify and precipitate Al and Be targets are identical. The solution is evaporated down to 2-3ml in Teflon beaker. A few drops of 7.1N HCl are added and the obtained solution is poured into a new centrifuge tube. To improve the recovery yield, the beaker is rinsed 3 times with a few drops of 7.1N HCl and the rinsing solutions are added to the centrifuge tube. Hydroxides are precipitated using NH_{3aq} added until reaching pH 8-9. After three washing cycles using alkaline water, the hydroxide precipitate is transferred into a quartz crucible. The precipitate is then evaporated to dryness at 150-200°C, heated for 15 minutes at 400°C on a hot plate. It is finally ignited at 900°C for 2h in a muffle furnace to obtain BeO or Al_2O_3. Since BeO is a carcinogenic compound, to wear an adapted mask is crucial.

3.1.13 Manganese precipitation

^{53}Mn is interesting because of its half-life of 3.74 10^6 Myrs, for CRE age and terrestrial ages. The procedure described below has not been realized in CEREGE, since we can not measure ^{53}Mn.

The 100ml obtained from the anion exchange column are evaporated to dryness in Teflon beaker. 5ml of milliQ water, 50 drops of concentrated HNO_3 and 0.5ml of H_20_2 are added, and the solution is heated to 150°C for 1h, lid closed. $KClO_3$ powder is added to oxidate Mn^{2+} to Mn^{4+}. We want to reduce the Cr isobar. The supernate is discarded. The Mn precipitate is dissolved again with 5ml of milliQ water, 50 drops of concentrated HNO_3 and 0.5ml of H_20_2, heated for 1h. After a last precipitation with $KClO_3$, the precipitate is carefully rinsed, then dried in a micro-tube at 80°C.

3.1.14 Nickel precipitation

^{59}Ni is produced by thermal neutrons reaction from ^{58}Ni. It is thus interesting to calculate pre-atmospheric sizes of meteoroid. The following procedure is exposed to the benefits of those who would specifically extract Ni for measurements (Chen *et al.* 2009).

The supernatant solution obtained from the precipitation of the Be and Al hydroxides and that contains Ca+Ni is centrifuged to get rid of any hydroxides that could remain on solution. 20-40 drops of an alcoholic solution of di-methyl-glyoxime that chelates Ni are added to the supernatant. A bright red precipitate ($Ni(dmgH)_2$ then forms. It is separated after a long lasting centrifugation from the supernatant that contains Ca. Ni precipitate can be dried at 110°C and ignited to nickel hydroxide at 600°C to prepare the AMS target.

3.1.15 Calcium target precipitation

To produce a Ca target free of Mg, oxalate has to be used to precipitate Ca as calcium oxalate and leave Mg in the solution. Every precipitation of Ca also allows getting rid of K, the main Ca isobaric interference.

The supernatant solution that contains Ca is heated at 125°C in a Teflon beaker covered with a Teflon lid. 60 drops of saturated oxalate $NH_{3aq}/(NH_4)_2C_2O_4$ (pH>7) are added and the Teflon beaker remains on the hot plate for at least 1h during which calcium oxalate (CaC_2O_4) precipitates. The content of the beaker is poured into a centrifuge tube for precipitate separation. After three washing cycles using hot water (rinsing solutions are discarded), the calcium oxalate precipitate is redissolved using 3ml of 22% HNO_3. 1ml of concentrated HF is then added to lead to an overnight CaF_2

precipitation. The obtained CaF_2 precipitate is carefully rinsed with water, transferred in a 1.5ml micro-tube and dried at 80°C for several hours.

3.1.16 Iron fraction extraction

The following procedure is adapted from Welten (1995).

The studied meteorite is roughly crushed in a metal grinder, then finely in an agate mortar. After each grinding step, the powder is placed within ethanol in an ultrasonic bath to remove attached silicates. The powdered sample is then subjected to magnetic separation in ethanol using a small handmagnet. The remaining magnetic powder is then dried, and grinded again. These steps are repeated 3 to 5 times.

Because magnetic particles gathered together, making it difficult to properly clean the powder of interest, the sample is demagnetized from time to time using a Molspin demagnetizer, a 30 mT alternative field being applied.

Following the grinding steps, the sample is placed within a 0.2N HCl solution for 30 minutes in an ultrasonic bath to dissolve troilite. Then, a diluted HF solution in a cold ultrasonic bath for 10 minutes is used to remove most of the remaining silicates. The resulting powder carefully rinsed with milliQ water is finally examined under a microscope and any remaining non-metallic minerals are handpicked and discarded.

Some authors disapprove the use of HCl before extracting the Cl. To check if the use of HCl has indeed an effect on the Cl isotopic ratios, we treated a piece of the iron meteorite Morasko 14 with HCl and then carefully rinsed it with milliQ water before the chemical extraction procedure. As shown in figure 4 the results for Morasko 14B are within uncertainties similar to those for Morasko 14A and Morasko 14C. Hence, we concluded that diluted HCl can be used for iron extraction.

3.1.17 Useful tips.

-When heating a solution, always clean the hot plate before and choose a PTFE hot plate. Hence, if a beaker is spilled by accident, you can recover most of the solution with a dropper.

- To prepare 10% $AgNO_3$, weight 3g of $AgNO_3$ powder in a vial and fill to 30g with milliQ water.

- To prepare saturated $Ba(NO_3)$, put milliQ water and a few drops of NH_3 in a vial, add $Ba(NO_3)_2$ until it is not dissolving anymore.

- To prepare alkaline water, add 3-4 drops of 25% NH_{3aq} to 0.5l of milliQ water. Check using a pH indicator that you have reach pH 8-9.

3.2 ICP-MS (SARM)

Considering the numerous production pathways involving multiple elemental targets, an accurate estimate of the production rates of interest (see §1.1.4) implies that the elemental concentrations of the studied samples have to be precisely determined. Aliquots of the studied samples were thus sent to the Service d'Analyse des Roches et des Minéraux (SARM) – CNRS – CRPG (Nançy, France) for such determinations.

Major element concentrations were measured using inductively coupled plasma optical emission spectrometry (Thermo Scientific ICP-OES Icap 6500), following the procedure described in (Carignan *et al.* 2001). Minor and trace element concentrations were measured using inductively coupled plasma mass spectrometry (ICP-MS).

Regarding iron meteorites or iron fractions, the main elements are of course Fe and Ni, Mg, and, when possible, S, Cr and P. Regarding stony meteorites or metal fractions from stony meteorites, Al, Ca, Mn, Si concentrations were also measured.

3.3 Sample pressing

The dried AgCl samples are compressed into a nickel sample holder and then stored for less than 12h in a 80°C oven, since AgCl is slightly hygroscopic. Nickel (grade: nickel 200) is preferred over others metals to reduce the ^{36}S contamination.

Because BeO, Al_2O_3 and CaF_2 are poor electrical and thermal conductors, they are mixed before being compressed into a copper sample holder with either, regarding BeO, niobium powder, or, regarding CaF_2 and Al_2O_3, Ag powder. The thus obtained Be, Al and Ca thermally and electrically conductive targets can be stored for long before being measured.

3.4 Chemistry blank

To quantify possible contamination resulting from the performed chemical procedures, a blank sample with initially no element of interest was processed following the same procedures as the samples. To reproduce as best as possible along the performed procedures the complexity of the chemical environments encountered, the iron meteorite Gibeon, whose cosmogenic nuclide concentrations have been reported as particularly low (Nishiizumi 1987), was chosen to process the chemical blank. After the previously described chemical processing, the cosmogenic nuclide concentrations measured in Gibeon are a least 2 orders of magnitude lower than in the majority of the studied samples.

For the few samples (4 ordinary chondrites and the iron meteorite Agoudal) in which low nuclide concentrations have been measured, a simple procedural blank has to be processed and measured (measurements under process).

3.5 Replica and validation of measurements

To test the reproducibility of the performed chemistry procedures, the same sample was duplicated not only within the same chemistry batch but also over different chemistry batches.

Morasko, an iron meteorite was duplicated within the same batch. Results for all measured cosmogenic nuclide concentrations are identical within uncertainties (see Fig. 4).

Cosmogenic nuclide concentrations in a shrapnel of Gebel Kamil, another iron meteorite, were measured every other batch. Results are identical within uncertainties. The Gebel Kamil duplicates also allow estimating the uncertainty associated to the chemical processing that may be applied to all other samples.

Some of my results may be compared with results from other laboratories. I chose the work of Ott *et al.* (2014) on Gebel Kamil iron meteorite. As shown on figure 4 , they are similar within uncertainties for ^{10}Be, ^{36}Cl and ^{41}Ca. Results for ^{26}Al are significantly different, though reproducible at CEREGE. This may be explained by a difference of sulphur and phosphorus content of the sample, and hence, a difference of ^{26}Al production rates.

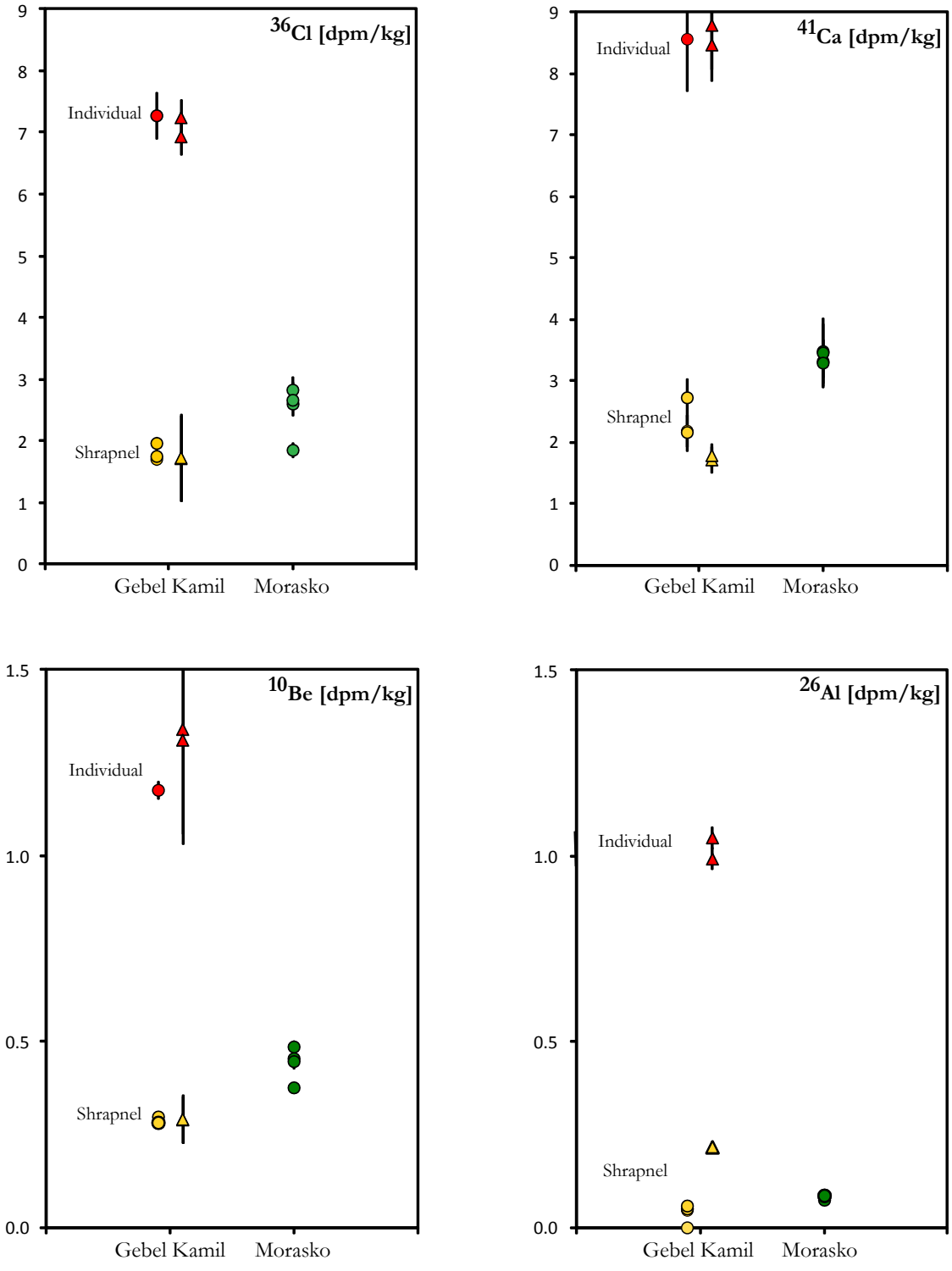

Figure 4: Cosmogenic radionuclides results for Gebel Kamil from our study (red and orange dots), from (Ott *et al.* 2014a) **(red and orange triangles) for Gebel Kamil individual (red) and Gebel Kamil schrapnels (orange). Results for Morasko from our study (green dots).**

3.6 Result treatments

3.6.1 Carrier weights

Carriers are carefully weighed with a precision of 0.01g to get $m_{carrier}$ in g. Knowing the carrier concentration $C_{carrier}$ in mg/g, the following equation gives the added mass of the stable element i $m_i^{carrier}$ in g

$$m_i^{carrier} = \frac{m_{carrier} \times C_{carrier}}{1000}$$

It is then possible to calculate the number of atoms $N_i^{carrier}$ with

$$N_i^{carrier} = \frac{\mathcal{N}_A \times m_i^{carrier}}{M_i}$$

where N_A is the Avogadro number in atoms and M_i the molar mass in g.mol^{-1}.

3.6.2 Elemental concentrations

SARM laboratory gives results in mg/L. To calculate the mass of a given element, the volume of the solution resulting from the dissolution of the meteorite sample has to be known. Before sampling the aliquot, the solution containing all elements but chlorine is weighed. The volumetric mass density of the solution has also to be known. Since an aliquot with a known-volume micropipette was taken and since it was weighed, the volumetric mass density is:

$$\rho = \frac{m_{aliquot}}{v_{aliquot}}$$

where $m_{aliquot}$ is in g and $v_{aliquot}$ in L.

The weight of a given element i is thus:

$$m_i\,[g] = C_i^{SARM} \times V_{solution}$$

where C_i^{SARM} is the SARM measured concentration in mg/L and $V_{solution}$ the volume of solution resulting of the dissolution of the sample.

Finally C_i the percentage of the element in wt% is:

$$C_i = \frac{m_i}{m_{sample}} \times 100$$

with m_{sample} the dissolved mass in g.

3.7 ASTER AMS measurements and activities calculations

The AMS national facility ASTER delivers results of radionuclide over stable nuclide ratio i^*/i, with an external uncertainty conservatively assumed to be 0.5% (Arnold *et al.* 2010). To calculate the radionuclide activity, the number of atoms of the radionuclide i N_i^* is first calculated as follows:

$$N_i^* = N_i^{carrier} \times \frac{i^*}{i}$$

N_i^* has then to be corrected for the chemistry blank. In our case, we substract the concentration measured in Gibeon (chemical blank, see above) corrected for the procedural blank concentration.

The activity in dpm/kg (disintegrations per minutes, per kilogram) is then given by:

$$A^i_{measured} = \frac{^{corrected}N_i^* \times ln2 \times 60}{365 \times 24 \times 3600 \times t_{1/2} \times m_{sample}}$$

where $t_{1/2}$ is the half-life of the radiogenic element i in years and m_{sample} in kg.

3.8 Uncertainties on cosmogenic activities

To estimate the uncertainty associated to cosmogenic nuclides activities, we follow the GUM method (Guide to the expression of Uncertainty in Measurement). GUM simplified method is:

- Identify the sources of uncertainties.
- Estimate the standard uncertainty associated with each source.
- Calculate the global uncertainty on the studied parameter, by using the propagation of errors.

First, the uncertainties associated to the sample chemical preparation have to be considered. They depend mainly on pipetting and weighing errors and are difficult to evaluate. As exposed in §3.5 *Replica and validation of measurements*, the

Gebel Kamil's schrapnel replicates have be considered to estimate **"chemistry procedure uncertainty".**

Then, there is an uncertainty associated to the AMS measurements ("**AMS measurement uncertainty**") depending on both the sample and the measured element.

3.8.1 Chemistry procedure uncertainties

As said earlier, we replicated the measurements of Gebel Kamil shrapnel to get an estimate of this uncertainty. The observed dispersion of the results is actually from a chemical procedure uncertainty in its strict meaning, and from the AMS measurement. Hence, if we consider the dispersion as only from the chemical procedure, we overestimate the uncertainty.

We calculate the relative uncertainty δA_{GK_shr} as follows:

$$\delta A_{GK\_shr} = \frac{\sigma_{GK\_shr}}{\sqrt{n}}$$

with σ_{GK_shr} the standard deviation for GK_shr measured activities and n the number of GK_shr replicas.

Since n is very low (n=3), δA_{GK_shr} is not a good approximation of the true standard deviation. Hence, we correct δA_{GK_shr} with t, the Student coefficient. t is tabulated: for n=3, and for a confidence interval of 68%, t=1,32.

The corrected value for δA_{GK_shr}, noted $\delta^* A_{GK\_shr}$ is:

$$\delta^* A_{GK\_shr} = 1.32 \times \frac{\sigma_{GK\_shr}}{\sqrt{3}}$$

Note that $\delta^* A_{GK\_shr}$ has to be estimated for each element.

Table 5 displays the absolute corrected chemistry procedure uncertainties for each radionuclide

Table 5: Corrected chemistry procedure uncertainties

Element	Uncertainty (%)
^{10}Be	1
^{26}Al	7
^{36}Cl	5
^{41}Ca	7

3.8.2 AMS and global uncertainties

Several uncertainties come from AMS measurement and have to be taken into account:

- the contribution of the chemistry blank,
- the uncertainty on the raw measurement,
- and an external error.

The uncertainty associated to the correction applied to take into account the contribution of the chemistry blank δA_{blank} is calculated as follows:

$$\left[A_{sample}\right]_{bk\ corr} = \left(A_{sample} \pm \delta A_{sample}\right) - \left(A_{bk} \pm \delta A_{bk}\right)$$

$$\left[\delta A_{sample}\right]_{bk\ corr} = \sqrt{\delta A_{sample}{}^2 + \delta A_{bk}{}^2}$$

the uncertainties associated to the raw measurements A_{sample} and A_{bk} resulting from the quadratic propagation

$$u = \sqrt[2]{\sum u_i^2}$$

of (1) the global uncertainty associated to the AMS measurement (δA_{sample}) which takes into account the number of events counted, the uncertainty associated to the mean of the standard ratio measured many times during a batch, the uncertainty associated to the theoretical standard ratio and the random error (minimized by increasing the number of observations), and of (2) the relative external error U_{ext} which is a multi-factor error including the stability of the measurement over time maximised at 0.5% for ^{10}Be. (Arnold *et al.* 2010). The external error might be the same for ^{26}Al and ^{41}Ca, and slightly higher for ^{36}Cl. This leads to:

$$\frac{\delta A_{sample}}{A_{sample}} = \sqrt{\left(\frac{\delta A_{sample}^{AMS}}{A_{sample}^{AMS}}\right)^2 + (U_{ext})^2}$$

and

$$\frac{\delta A_{blank}}{A_{blank}} = \sqrt{\left(\frac{\delta A_{blank}^{AMS}}{A_{blank}^{AMS}}\right)^2 + (U_{ext})^2}$$

Considering the chemistry procedure uncertainty $\frac{\delta^* A_{GK\_shr}}{A^{mean}_{GK\_shr}}$, the **total uncertainty** $\frac{\delta A^i_{sample}}{A^i_{sample}}$ associated to a cosmogenic nuclide i is:

$$\frac{\delta A^i_{sample}}{A^i_{sample}} = \sqrt{\left(\frac{\left[\delta A_{sample}\right]_{bk\ corr}}{\left[A_{sample}\right]_{bk\ corr}}\right)^2 + \left(\frac{\delta^* A_{GK\_shr}}{A^{mean}_{GK\_shr}}\right)^2}$$

3.9 Model calculations

As explained in §1.1.4, the cosmogenic nuclide production rates have to be modelled to allow modelling the activity of these nuclides in the meteorite at the time of the fall. We differentiate the models for iron meteorites and for chondrites.

3.9.1 Iron meteorites

Two models will be considered, though several others exist.

3.9.1.a Lavielle *et al.* (1999)

Lavielle and co-authors developed a semi-empirical model to calculate cosmic-ray exposure ages and terrestrial ages of iron meteorites having experienced a simple exposure history.

For exposure ages, Lavielle et al. favorized the $^{36}Ar/^{36}Cl$ relation, since $^{36}Ar/^{36}Cl$ is almost independent of shielding :

$$T_{CRE} = 511 \times \left(\frac{[^{36}Cl]}{[^{36}Ar]}\right)_0 \times \frac{[^{36}Ar]}{[^{36}Cl]}$$

with $[^{36}\mathrm{Cl}]_0$ and $[^{36}\mathrm{Ar}]_0$ the production rates (i.e. the activities for T_{terr} = 0 yr and T_{CRE} long enough to reach saturation state for radionuclides), and $[^{36}\mathrm{Ar}]$ and $[^{36}\mathrm{Cl}]$ the measured activities in dpm/kg.

They evaluated $\left(\frac{[^{36}\mathrm{Cl}]}{[^{36}\mathrm{Ar}]}\right)_0$ at 0.835±0.040, using cross sections measurement for Fe and Ni target elements.

Terrestrial ages equations are derived from (Nishiizumi *et al.* 1997) using the following equations:

$$\left[\frac{[^{36}Cl]}{[^{10}Be]}\right]_0 = 5.97 - 0.184[^{10}Be] - 0.024[^{10}Be]^2$$

with activities in dpm/kg

and:

$$T_{terr} = \frac{\ln\left(\frac{[^{36}Cl]}{[^{10}Be]}\right) - \ln\left(\frac{[^{36}Cl]}{[^{10}Be]}\right)_0}{\lambda_{10} - \lambda_{36}}$$

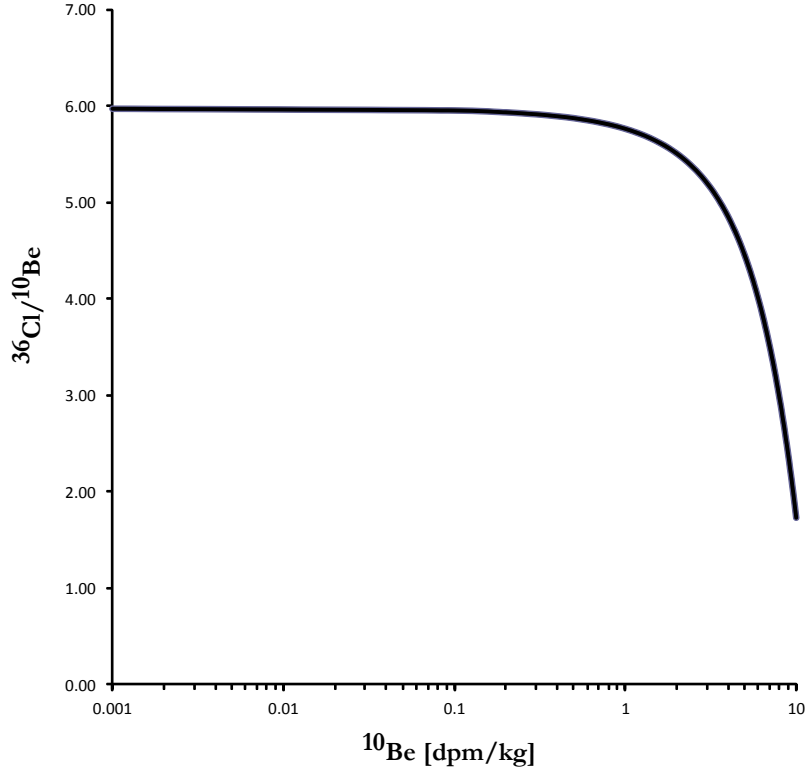

Figure 5: Best empirical fit line from Lavielle et al. (1999).

Figure 5 plots the semi-empirical results and the best-fit line for (Lavielle *et al.* 1999) model. If a sample's results intersect the line, its terrestrial age is equal to 0.

Lavielle et al. model is interesting for a quick overview of the data. For more precise results, taking into account the chemistry of the sample, the pre-atmospheric size and the shielding depth, or for calculations for non-iron meteorites, another model is needed.

3.9.1.b Ammon *et al.* (2009)

Ammon and co-authors designed a purely physical model for iron meteorites. It calculates the cross-sections for each target element (Fe, Ni, S, Si, Mg…), and depending on the bulk chemistry of the sample (see §3.2 *ICP-MS (SARM)*), models an activity for a specific radionuclide, for different pre-atmospheric radius (R) and shielding depth (S).

The production rate $P_i(R,d,M)$ for a cosmogenic nuclide i, with R the pre-atmospheric radius, S the shielding depth and M the solar modulation parameter is given by :

$$P_i(R,S,M) = \sum_{j=1}^{N} c_j \frac{\mathcal{N}_A}{A_j} \sum_{k=1}^{3} \int_0^{\infty} \sigma_{i,j,k}(E) \times J_k(E,R,S,M) dE$$

with

- N_A Avogadro's number,
- A_j the mass number of the target element,
- C_j the concentration of the target element i in g.g-1
- k an index for the reaction particle type
- $\sigma_{i,j,k}(E)$ the excitation function for the production of cosmogenic nuclide j from target element i
- J_k the differential flux density of k particles
- E the energy of the reacting particles.

The primary and secondary particles' spectra are calculated using Monte Carlo techniques.

Model calculations were compared for validation with measured results for both noble gases and radionuclides.

The uncertainties of the model calculations can be up to 20-40%, depending on the cosmogenic nuclide and on the target element, mainly because of the lack of experimental neutron cross sections.

Cross section calculations for sulphur (S) and phosphorus (P) are rather unreliable (Ammon *et al.* 2009, Leya & Masarik 2009) , and sulphur and phosphorus distributions are rather inhomogenous (Ammon *et al.* 2008). Hence, we did not consider, or with great cautiousness, the nuclides whose production significantly depends on the S and P target elements (^{26}Al, ^{10}Be and ^{21}Ne).

i Cosmic rays exposure age

For CRE ages, the most reliable ^{36}Cl/^{36}Ar dating system has been used. Most of the ^{36}Ar is produced from Fe and Ni via the radioactive progenitor ^{36}Cl, making the system almost independent for shielding.

Production rates for ^{36}Ar are calculated as follows:

$$[^{36}Ar]_0 = 2.296\times10^{-3}\times[^{36}Cl]_0$$

$[^{36}\mathrm{Cl}]_0$ being the activity (dpm/kg) corrected for terrestrial age, and depending on the pre-atmospheric radius.

CRE age is then calculated using

$$T_{CRE}[Ma] = \frac{^{36}Ar_{mes}}{2.296\times10^{-3}\times[^{36}Cl]_0}$$

with $^{36}\mathrm{Ar}_{\mathrm{mes}}$ the measured ^{36}Ar concentration in 10^{-8} cm^3 STP/g.

Other systems such as ^{26}Al-^{21}Ne, ^{10}Be-^{21}Ne or ^{38}Ar/^{10}Be-^{10}Be may also provide CRE ages. For reasons linked to the reliability of the production rate determination of ^{26}Al, ^{10}Be and ^{21}Ne exposed above, these cosmogenic nuclides were not used.

ii Terrestrial age

The ^{36}Cl-^{41}Ca system was chosen to provide terrestrial ages. The production rates of both elements are well constrained for iron meteorites, and the system enable calculation of ages up to 2 Myr, which is satisfactory for iron meteorites.

$$T_{terr} = \frac{\ln\left(\frac{[^{36}Cl]}{[^{41}Ca]}\right) - \ln\left(\frac{[^{36}Cl]}{[^{41}Ca]}\right)_0}{\lambda_{41} - \lambda_{36}}$$

with $\left(\frac{[^{36}Cl]}{[^{41}Ca]}\right)_0$ depending on the size of the meteorite and the shielding depth of the sample.

iii Radius and shielding depth

These parameters are determined by graphic interpolation with the model plots (Fig. 6) for single elements (corrected for terrestrial age if elements are radioactive), or for the system $^{4}He/^{38}Ar$ (Fig. 7) corrected for CRE age.

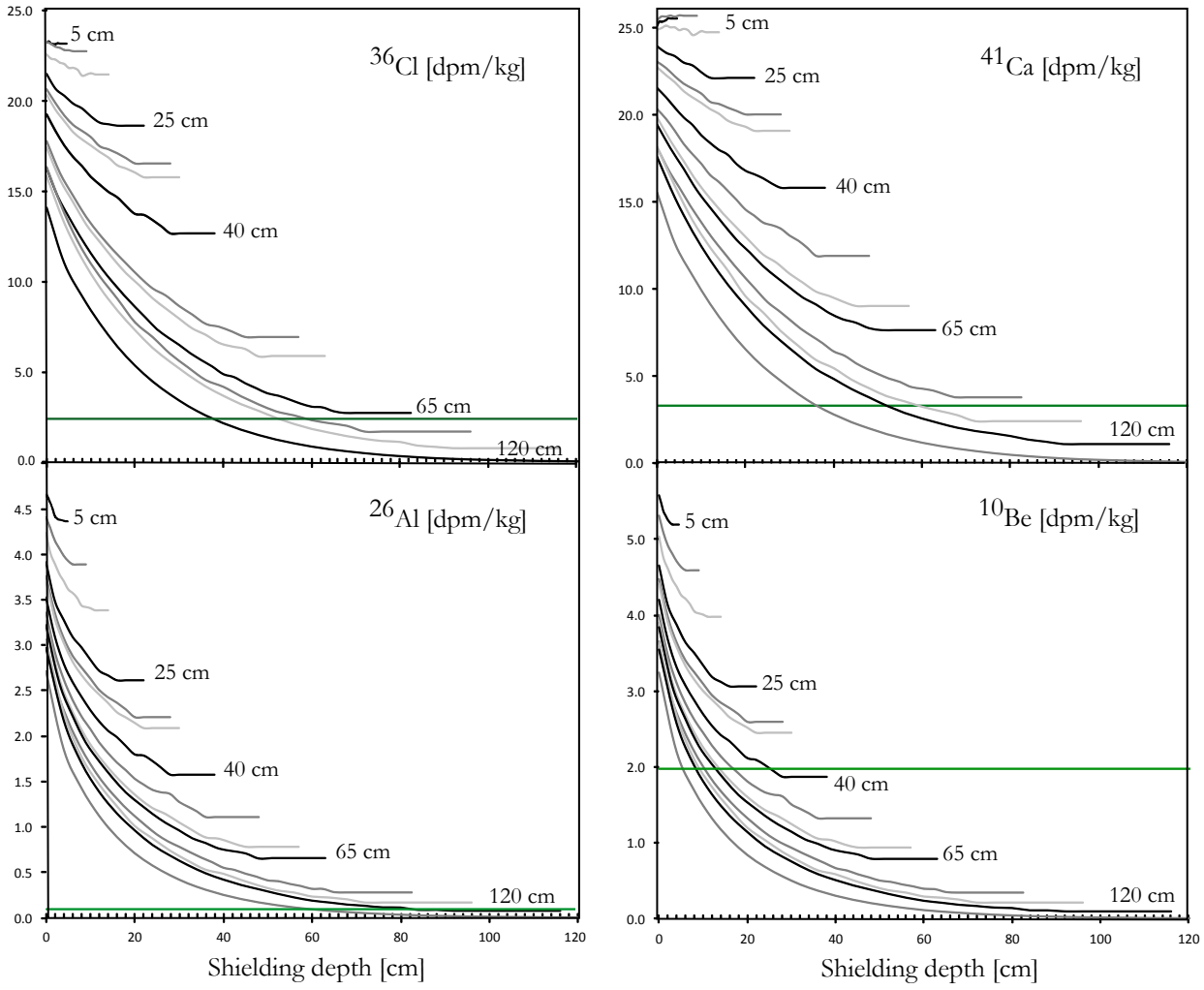

Figure 6: Cosmogenic nuclides production rates as a function of shielding depth and radius of the body. Green line show the measured nuclides for Morasko, non corrected for terrestrial age.

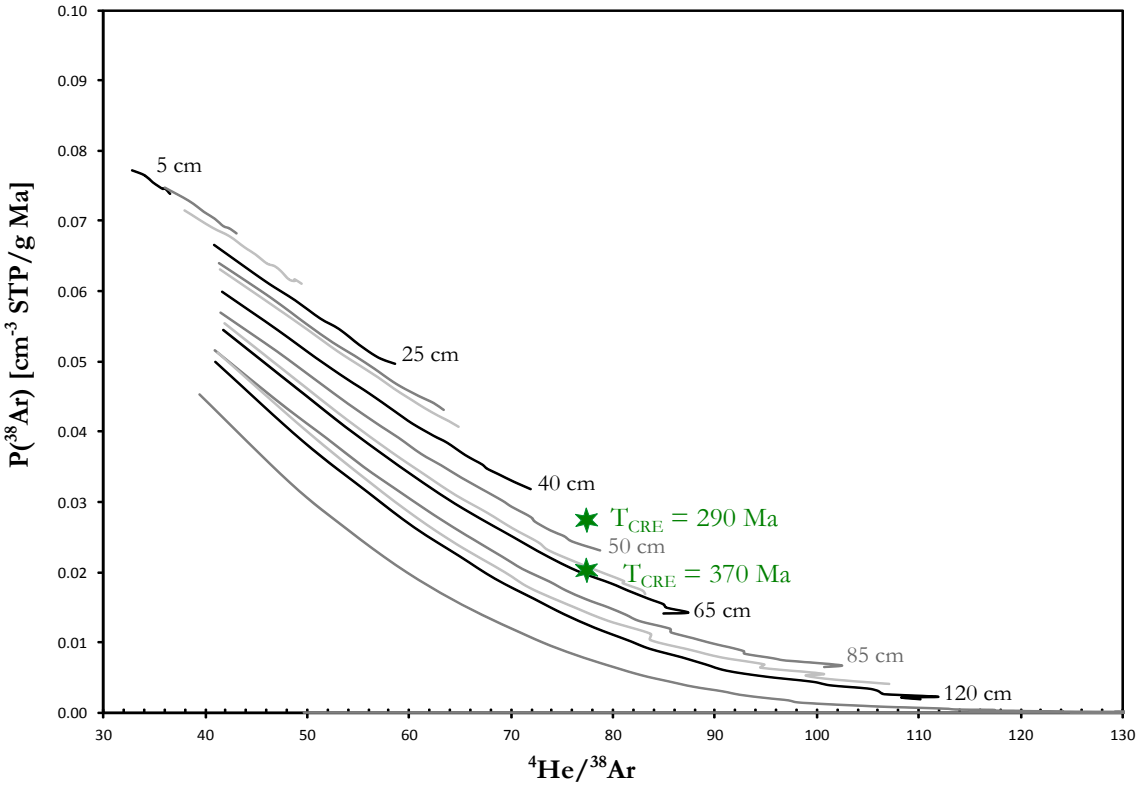

Figure 7: ^{38}Ar production rate as a function of ^{4}He/^{38}Ar ratios. Green stars show the results for Morasko iron meteorite, corrected for different CRE ages.

3.9.2 Chondrites and other stony meteorites (Leya & Masarik 2009).

Leya and Masarik developed a purely physical model for stony meteorites, based on the same equation as Ammon *et al.* (2009) described in § (Ammon *et al.* 2009). It calculates cosmogenic production rates for ordinary chondrites, and for carbonaceous chondrites. In the followings, only the ordinary chondrites results are used.

i CRE age

The reader will notice in §4 *Results* that cosmogenic gases were not measured for chondrites. It is indeed assumed that the chondrites spent enough time in space to reach saturation (10 times the half-life of a given radiogenic element), a hypothesis which is debatable but most likely reliable for short-lived radionuclides (^{36}Cl and ^{41}Ca). This corresponds to CRE ages older than 3 and 1 Myr, respectively. In some cases it has been shown that complex exposure

history (several episodes of fragmentation) may lead to errors on terrestrial ages and pre-atmospheric radius. Several cosmogenic nuclides are needed to determine complex exposure histories (Welten *et al.* 2008).

ii Terrestrial ages

The methods exposed here are for metal fraction of chondrites.

The $^{36}Cl/^{10}Be$-^{10}Be relation is slightly modified from (Lavielle *et al.* 1999).

$$\left[\frac{[^{36}Cl]}{[^{10}Be]}\right]_0 = 6.01 - 0.28[^{10}Be] - 0.009[^{10}Be]^2$$

and using again

$$T_{terr} = \frac{\ln\left(\frac{[^{36}Cl]}{[^{10}Be]}\right) - \ln\left(\frac{[^{36}Cl]}{[^{10}Be]}\right)_0}{\lambda_{10} - \lambda_{36}}$$

The $^{41}Ca/^{36}Cl$-^{36}Cl is the most reliable terrestrial age method for chondrites with ages between 40 kyr and 500 kyr. It is less dependent on CRE ages than the method exposed above.

The following relation, already used for iron meteorites, is used:

$$T_{terr} = \frac{\ln\left(\frac{[^{36}Cl]}{[^{41}Ca]}\right) - \ln\left(\frac{[^{36}Cl]}{[^{41}Ca]}\right)_0}{\lambda_{41} - \lambda_{36}}$$

$\left(\frac{[^{36}Cl]}{[^{41}Ca]}\right)_0$ is determined using the model for known radius and shielding depth.

For a rough first estimate, we can use the following empirical relation (Welten *et al.* 2006).

$$\left[\frac{[^{41}Ca]}{[^{36}Cl]}\right]_0 = 1.25 + 0.003[^{36}Cl] - 0.0006[^{36}Cl]^2$$

iii Radius and shielding depth

We graphically estimate R and S using radionuclides corrected for terrestrial ages.

3.10 Fixed point

After processing the sample, the data are listed in the DATA box and the parameters to be calculated listed in the UNKNOWNS box.

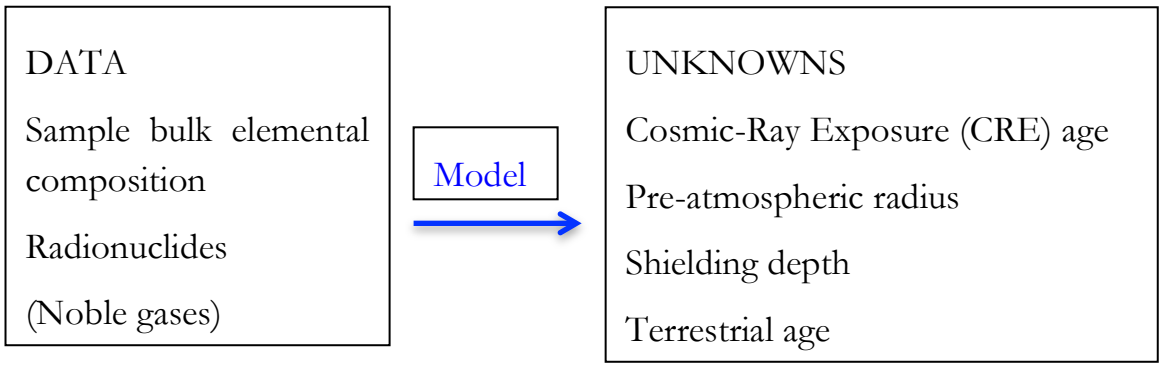

Since parameters are linked together, we try to find a set of values through a fixed-point method.

The equations derived from the first model (Lavielle *et al.* 1999) are used to obtain a first evaluation of the terrestrial and CRE ages (without considering R and S) and Ammon's or Leya's physical models are used to access to R and S. This leads to a first set of values for the Unknowns system.

This first set is then used to recalculate T_{terr}, T_{CRE}, R and S using exclusively Ammon's or Leya's physical models. A second set of values is thus obtained, which may or not be different from the first one.

These operations are iteratively repeated using dedicated software coded on Scilab (Appendix…) until there is no significant variation between two successive sets.

3.11 Uncertainties on model calculations

Formulas presented above link cosmogenic production rates from a model, and measured activities. We have explained how uncertainties on

measured activities are estimated. Uncertainties on cosmogenic nuclides production rates are of 10-15% (Ammon *et al.* 2009, Leya & Masarik 2009).

The uncertainty on a function $q = f(x_1, x_2, x_3,\ldots)$ linking several parameters is to be calculated using a propagation of uncertainties it gives a relative uncertainty by the following relation:

$$U_q = \sqrt[2]{\sum \left|\frac{\partial f}{\partial x_i}\right|^2 (U_{x_i})^2}$$

We apply this relation using the model uncertainties, and the uncertainties on cosmogenic nuclides activities (see §3.8 *Uncertainties on cosmogenic activities*) for uncertainties on CRE ages and terrestrial ages.

With the type of functions used to calculate terrestrial ages using two radionuclides 1 and 2 :

$$T_{terr} = \frac{\ln\left(\frac{[A_1]}{[A_2]}\right) - \ln\left(\frac{[A_1]}{[A_2]}\right)_0}{\lambda_2 - \lambda_1} = \frac{\ln(A_1) - ln(A_2) - ln(A_1)_0 + ln(A_2)_0}{\lambda_2 - \lambda_1}$$

the absolute uncertainty δT_{terr} is calculated with:

$$\delta T_{terr} = \sqrt{\left|\frac{1}{bA_1}\right|^2 \times {\delta A_1}^2 + \left|\frac{1}{bA_2}\right|^2 \times {\delta A_2}^2 + \left|\frac{1}{bA_{1_0}}\right|^2 \times {\delta A_{1_0}}^2 + \left|\frac{1}{bA_{2_0}}\right|^2 \times {\delta A_{2_0}}^2 + \left|\frac{c}{b}\right|^2 \times {\delta \lambda_2}^2 + \left|\frac{c}{b}\right|^2 \times {\delta \lambda_1}^2}$$

with $b = \lambda_2 - \lambda_1$ and $\mathrm{c} = \ln(A_1) - ln(A_2) - ln(A_1)_0 + ln(A_2)_0$.

With the type of function used to calculate CRE age, using two cosmogenic nuclides A_1 and A_2 :

$$T_{CRE}[Ma] = \frac{{}^{36}Ar_{mes}}{2.296\times10^{-3}\times[{}^{36}Cl]_0}$$

the absolute uncertainty δT_{CRE} is calculated with:

$$\delta T_{CRE} = a\sqrt{\left|\frac{1}{A_2}\right|^2 \delta A_1{}^2 + \left|\frac{A_1}{A_2^2}\right|^2 \delta A_2{}^2}$$

where $a = \frac{1}{2.296\times10^{-3}}$.

Since Ammon's and Leya's models consider discrete pre-atmospheric radius, we can't give an uncertainty on it. As for shielding depth, we can give a range of possible shielding depth, from different elements.

3.12 Conclusion

The chemical procedures implemented to extract cosmogenic radionuclides (^{10}Be, ^{26}Al, ^{36}Cl and ^{41}Ca) from meteorites for the measurements of their concentrations using the accelerator mass spectrometry technique have been exposed. The measurements performed on numerous replicates insure that reliable and reproducible data have been obtained using the established procedures.

We have gathered a large collection, statistically reliable enough to estimate a flux (chapter 2).

Using the chemistry protocol described in chapter 3 and the principles of dating exposed in chapter 1, we processed 24 ordinary chondrites from the ElM collection, and 12 iron meteorites from Europe, North Africa and Chile.

In the next chapter, the models and the relations used for calculating cosmic-ray exposure ages, terrestrial ages, pre-atmospheric radius and shielding depth are presented as well as the dedicated software developed to solve the system for these four linked parameters. It allows a quick and reliable determination of important information regarding the studied meteorites.

Chapter 4: Cosmogenic results and interpretation

4.1 Samples and results

4.1.1 Iron

4.1.1.a Choice of the samples

Twelve iron meteorites, listed in Table 6, were analysed.

As exposed in §Chemistry, Gebel Kamil, Gibeon and Morasko measurements were replicated, Gibeon being used as a chemistry blank.

Gebel Kamil (GK) is used to test the measurement reproducibility between both chemical batches and labs (Ott *et al.,* 2014). Note that GK_{ind} is a sample taken from the 83kg meteorite fragment, and that GK_{shr} are from the shrapnels. Two different fragments of Morasko, Morasko 13 and Morasko 14, were processed, Morasko 14A and Morasko 14C being replicates. Morasko 14B has been pre-treated with HCl to test the influence of metal extraction (see §Chemistry - Iron fraction extraction.). Two different fragments of Agoudal were processed as well.

Gibeon was chosen because of its low cosmogenic nuclides concentration.

Gebel Kamil (Egypt) was chosen as part of a collaboration with Luigi Folco, a scientist working on the Gebel Kamil crater, and because it has already been processed in another laboratory.

Saint-Aubin, La Caille and Mont-Dieu are iron meteorites fallen in France. They were chosen as part of a collaboration with the Muséum d'Histoire Naturelle de Paris.

Cerro del Inca, Guanaco and Dolores were found by different private hunters in Chile and studied to complete our Chilean collection. Cuenca del Tiburon is a small find (2.2kg) by a private hunter from near the Pampa de Mejillones DCA. It is in the process of declaration to the Meteorite Nomenclature Committee.

Morasko was chosen as part of collaboration with Pr. Andrzej Muszynski from Poland.

Agoudal was chosen as part of a collaboration with Pr. Hasnna Chennaoui and Maria Aboulahris from Morocco.

Tamentit (Algeria) is a large find (510 kg) from Sahara which is associated with the legend of an observed fall we want to reality check.

4.1.1.b Cosmogenic nuclides activities.

Table 6 shows the cosmogenic radionuclides activities for all iron meteorites. Activities and uncertainties are calculated following the method exposed in §ASTER AMS measurements.

In collaboration with Thomas Smith and Ingo Leya from the University of Bern, cosmogenic noble gases were measured on a selection of iron meteorites corresponding to the meteorites considered as the most relevant regarding our interests. Table 7 shows the noble gases results.

Table 6: Cosmogenic radionuclides activities of the iron meteorite samples (dpm/kg).

Sample name	^{36}Cl (dpm/kg)	^{41}Ca (dpm/kg)	^{10}Be (dpm/kg)	^{26}Al (dpm/kg)
GK_{ind}	7.28 ± 0.37	8.57 ± 0.86	1.175 ± 0.024	n.d.
$GK_{shr}A$	1.735 ± 0.043	2.72 ± 0.31	0.2978 ± 0.0098	0.0506 ± 0.0044
$GK_{shr}B$	1.94 ± 0.12	2.15 ± 0.29	0.2816 ± 0.0092	0.0561 ± 0.0055
$GK_{shr}C$	1.691 ± 0.096	2.17 ± 0.25	0.2801 ± 0.0092	0.0456 ± 0.0041
La Caille	4.65 ± 0.24	2.96 ± 0.31	0.903 ± 0.020	0.163 ± 0.012
Mont Dieu	9.03 ± 0.47	8.41 ± 0.78	1.687 ± 0.038	0.284 ± 0.022
St Aubin	3.65 ± 0.19	6.16 ± 0.83	1.075 ± 0.025	0.142 ± 0.019
Cerro del Inca	2.16 ± 0.11	0.129 ± 0.043	1.793 ± 0.036	0.204 ± 0.016
Guanaco	23.9 ± 1.2	23.8 ± 2.0	6.26 ± 0.11	0.985 ± 0.072
Cuenca del Tiburon	24.8 ± 1.3	26.6 ± 2.0	3.918 ± 0.077	n.d.
Dolores	n.d.	0.0029 ± 0.0038	1.335 ± 0.028	0.0994 ± 0.0083
Tamentit	14.86 ± 0.8	20.1 ± 1.8	4.065 ± 0.079	0.711 ± 0.054
Mo13	1.98 ± 0.11	3.31 ± 0.35	0.375 ± 0.012	0.0727 ± 0.0058
Mo14 A	2.54 ± 0.14	3.48 ± 0.44	0.452 ± 0.012	0.0849 ± 0.0069
Mo14 B	3.44 ± 0.21	3.45 ± 0.57	0.444 ± 0.017	0.0864 ± 0.0074
Mo14 C	3.27 ± 0.19	3.28 ± 0.38	0.484 ± 0.016	0.0851 ± 0.0065
Agoudal 1	0.607 ± 0.035	0.527 ± 0.074	0.119 ± 0.004	0.021 ± 0.002
Agoudal 2	0.0375 ± 0.0030	0.048 ± 0.019	0.0205 ± 0.0013	0.00088 ± 0.00076

Table 7: Noble gases results from selected iron meteorites [10^{-8} cm^3/g STP].							
Sample	^{3}He	^{4}He	^{20}Ne	^{21}Ne cosm.	^{22}Ne	^{36}Ar cosm.	^{38}Ar cosm.
Agoudal 1	8.38	44.88	0.119	0.100	0.100	0.36	0.57
Agoudal 2	5.19	26.26	0.194	0.187	0.189	0.58	0.93
La Caille	67.07	272.95	0.654	0.718	0.700	2.09	3.32
Saint-Aubin	146.41	602.61	1.388	1.527	1.550	4.95	7.85
Morasko 13	26.79	117.33	0.318	0.334	0.334	1.11	1.77
Morasko 14	28.76	127.21	0.266	0.278	0.280	0.89	1.41

4.1.1.c Calculations of CRE ages, terrestrial ages and physical parameters.

Table 8 shows the results of CRE ages, terrestrial ages, pre-atmospheric sizes and mass, shielding depth of the samples, and percentage of recovered mass with respect to the pre-atmospheric mass.

Table 8: CRE ages and terrestrial ages; pre-atmospheric radius and allowed range for shielding depth.						
Sample name	TCRE (Ma)	Tterr (ka)	Radius (m)	Shielding depth (cm)	Pre-atm. Mass (tons)	Mass recovered (%)
GK_{ind}	n.d.	20 ± 38	1	30-33	30	50
GK_{shr}	n.d.	20 ± 33	1	61-69	30	50
La Caille	135 ± 15	165 ± 33	0.65	38-43	9	12
Mont Dieu	n.d.	60 ± 37	0.5	21-29	4	3
St Aubin	520 ± 30	55 ± 41	0.85	37-46	20	2.5
Cerro del Inca	n.d.	690 ± 32	0.4	30-34	2	1.5
Guanaco	n.d.	27 ± 51	0.15	0-5	0.1	13
Cuenca del Tiburon	n.d.	5 ± 50	0.05	0-3	0.004	50
Dolores	n.d.	>1000	0.10	n.d.	0.03	13
Morasko	130 ± 15	25 ± 34	0.85	52-67	20	10
Tamentit	n.d.	9 ± 49	0.3	9-12	0.9	56
Agoudal	204 ± 90	105 ± 32	10	63-83	30 000	0.003

Data are interpreted in the forthcoming sections.

4.1.2 Chilean chondrites (Hutzler, 2014)

4.1.2.a Choice of the samples

To obtain an age spectrum representative of the collection, a random subsample of the collection should be taken.

In our case, we favoured the meteorites with a mass over 100g in order to be able to process enough material to finally obtain a clean and large enough metal fraction.

Table 9 lists the chosen samples with their petrographic types, weathering grade and total known weights. For more information, see Appendix in Chapter 2.

Note that CeC 006 and CeC 015 are possibly paired (see §2.2).

Table 9: Studied samples from the El Médano collection.

Official name	Petrographic type	Weath. grade	TKW (g)
CeC 006	L6	3	179
CeC 015	L6	3	115
CeC 020	H5	3	633
ElM 004	H4	1	151
ElM 017	L6	3	156
ElM 023	L6	3	115
ElM 025	H6	3	132
ElM 026	L6	3	154
ElM 037	L6	3	111
ElM 049	H4	3	138
ElM 075	L4	3	186
ElM 078	L6	3	1228
ElM 079	H5	2	230
ElM 086	H4	1	1258
ElM 089	L6	4	296
ElM 092	H6	3	289
ElM 097	L5-6	4	229
ElM 098	L6	4	135
ElM 111	H5	4	139
ElM 118	H5	3	161
ElM 126	H5	3	584
ElM 128	L6	2	556
ElM 135	L6	3	71
ElM 191	H5	2	138

4.1.2.b Radionuclides results

Table 10 shows the measured activities for the ordinary chondrites described above.

Table 10: Cosmogenic radionuclides activities of the chondrite samples (dpm/kg).

Sample name	^{36}Cl (dpm/kg)	^{41}Ca (dpm/kg)	^{10}Be (dpm/kg)	^{26}Al (dpm/kg)
CeC 006	0.0603 ± 0.0095	n.d.	0.713 ± 0.020	0.0226 ± 0.0034
CeC 015	6.89 ± 0.11	0.68 ± 0.15	6.47 ± 0.12	1.95 ± 0.15
CeC 020	1.608 ± 0.088	0.105 ± 0.033	0.993 ± 0.020	0.265 ± 0.020
ElM 004	10.03 ± 0.51	5.05 ± 0.41	4.619 ± 0.083	1.10 ± 0.08
ElM 017	11.99 ± 0.66	0.46 ± 0.17	24.75 ± 0.46	6.29 ± 0.48
ElM 023	15.49 ± 0.80	10.91 ± 0.91	6.15 ± 0.11	1.65 ± 0.12
ElM 025	2.37 ± 0.13	0.139 ± 0.047	5.65 ± 0.10	1.256 ± 0.093
ElM 026	11.40 ± 0.67	3.38 ± 0.38	4.976 ± 0.091	0.993 ± 0.074
ElM 037	16.01 ± 0.85	13.7 ± 1.1	5.0870 ± 0.0942	1.018 ± 0.078
ElM 049	0.286 ± 0.018	n.d.	1.539 ± 0.028	0.164 ± 0.013
ElM 075	0.980 ± 0.063	0.0185 ± 0.0092	2.385 ± 0.044	0.558 ± 0.042
ElM 078	13.08 ± 0.67	9.53 ± 0.79	5.250 ± 0.097	1.110 ± 0.083
ElM 079	6.96 ± 0.37	0.72 ± 0.15	5.49 ± 0.10	1.257 ± 0.097
ElM 086	8.30 ± 0.43	1.40 ± 0.16	5.290 ± 0.093	1.48 ± 0.11
ElM 089	4.28 ± 0.25	0.40 ± 0.13	6.32 ± 0.13	1.35 ± 0.10
ElM 092	2.29 ± 0.12	0.258 ± 0.048	1.877 ± 0.035	0.386 ± 0.030
ElM 097	0.756 ± 0.023	0.52 ± 0.16	3.859 ± 0.082	0.572 ± 0.045
ElM 098	2.01 ± 0.11	1.40 ± 0.16	0.588 ± 0.014	0.1110 ± 0.0089
ElM 111	0.711 ± 0.032	0.60 ± 0.27	9.60 ± 0.22	1.92 ± 0.15
ElM 118	7.941 ± 0.098	0.84 ± 0.18	5.168 ± 0.093	0.906 ± 0.068
ElM 126	5.099 ± 0.074	0.348 ± 0.081	7.00 ± 0.14	1.58 ± 0.12
ElM 128	16.99 ± 0.88	17.4 ± 1.4	6.34 ± 0.12	2.21 ± 0.17
ElM 135	1.001 ± 0.038	0.191 ± 0.071	3.568 ± 0.074	0.711 ± 0.054
ElM 191	1.88 ± 0.10	0.220 ± 0.058	3.042 ± 0.057	0.630 ± 0.048

4.1.2.c Terrestrial ages

Because the cosmogenic noble gases were not measured, CRE ages cannot be calculated. The models calculating cosmogenic production rates assume that the considered elements have reached saturation, i.e. have spent more than ten times their respective half-life in space. Is it reasonable to consider that the studied chondrites have spent enough time in space to saturate ^{36}Cl, ^{41}Ca, ^{26}Al and ^{10}Be?

The published CRE ages for stony meteorites range from 1 to 100 Ma (Schultz & Weber, 1996), with very few CRE ages lower than 5 Ma. Iron meteorites present longer CRE ages at roughly 600 Ma (McSween, 1999; Wieler & Graf, 2001).

We can therefore confidently assume that at least ^{36}Cl and ^{41}Ca were saturated. It is less certain for ^{26}Al and ^{10}Be which will thus have to be considered with care.

T_{terr} ^{36}Cl/^{10}Be and T_{terr} ^{36}Cl/^{41}Ca were calculated using the Leya model (2009) (see §3) using ^{10}Be and ^{36}Cl, and ^{10}Be and ^{41}Ca, respectively. T_{terr}^{36}Cl was calculated following Nishiizumi *et al.* (1989), using exclusively ^{36}Cl data with an average saturation activity of 22.8 ± 3.1 dpm/kg metal.

Table 11: Terrestrial ages of El Médano collection ordinary chondrites.

Official name	T_{terr} ^{36}Cl/^{10}Be (ka)	T_{terr} ^{36}Cl/^{41}Ca (ka)	T_{terr} ^{36}Cl (ka)	R (m)	Shielding depth (cm)
CeC 006	2345 ± 80	n.d.	2590 ± 100	n.d.	n.d.
CeC 015	709 ± 80	550 ± 33	520 ± 75	0.10	2-5
CeC 020	700 ± 80	670 ± 32	1150 ± 80	1.2	75-80
ElM 004	450 ± 80	200 ± 34	360 ± 80	0.65	46-50
ElM 017	1180 ±	770 ± 37	280 ± 80	0.10	2-5
ElM 023	250 ± 85	110 ± 38	170 ± 80	0.40	31-35
ElM 025	1300 ± 80	690 ± 33	980 ± 80	0.85	64-68
ElM 026	360 ± 80	300 ± 35	300 ± 80	0.20	0-5
ElM 037	360 ± 85	67 ± 40	150 ± 80	0.50	33-39
ElM 049	1890 ± 80	n.d.	1900 ± 80	n.d.	n.d.
ElM 075	1420 ± 80	950 ± 32	1370 ± 80	1.0	58-79
ElM 078	460 ± 80	110 ± 36	240 ± 80	0.65	28-32
ElM 079	665 ± 80	550 ± 33	515 ± 80	0.10	6-7.5
ElM 086	560 ± 80	430 ± 33	440 ± 80	0.20	1-6
ElM 089	1140 ± 80	580 ± 34	730 ± 80	0.65	30-34
ElM 092	930 ± 80	550 ± 32	1000 ± 80	1.2	60-75
ElM 097	1900 ± 80	140 ± 34	1500 ± 75	2.0	135-179
ElM 098	300 ± 80	150 ± 32	1000 ± 80	2.0	104-109
ElM 111	1950 ± 80	88 ± 12	1500 ± 80	3.0	138-145
ElM 118	570 ± 80	560 ± 33	460 ± 75	0.10	3-6
ElM 126	890 ± 80	650 ± 32	650 ± 75	0.20	0-5
ElM 128	410 ± 80	35 ± 42	130 ± 80	0.50	33-39
ElM 135	1590 ± 80	430 ± 33	1400 ± 75	2.0	100-106
ElM 191	1200 ± 80	540 ± 32	1100 ± 80	1.2	100-105

Note the CeC 006 and CeC 015 which were possibly paired, based on the criteria exposed in §2.2, have a significantly different terrestrial age which implies that the pairing is no longer possible.

4.2 Interpretation

4.2.1 Iron results

4.2.1.a Gebel Kamil (Egypt)

Gebel Kamil crater was identified in 2006 through a Google Earth survey (Folco *et al.,* 2011). Field trips revealed a well preserved 45m diameter wide crater and thousands of iron meteorite pieces (D'Orazio *et al.,* 2011). All specimens but one are shrapnels, i.e. fragments produced during the impact. The piece defined as the individual specimen weights 83kg, and shows well-developped regmaglypts.

Due to the freshness of the crater and the fact that prehistoric humans did not use the meteorite to shape tools, the impact is estimated to be <5000 ka.

The total recovered mass is around 1.7 tons which represents around 50% of the total mass still on the field. The pre-atmospheric radius of the impactor must have been of at least 0.45m to fit with a weight of 5 tons (Urbini *et al.,* 2012).

Gebel Kamil cosmogenic nuclides concentrations (both noble gases and radionuclides) have been measured by (Ott *et al.,* 2014). We measured only radionuclides in this work.

Combining ^{10}Be, ^{36}Cl and ^{41}Ca results for radius and shielding depth determination following the method exposed in §Chemistry lead to a pre-atmospheric radius between 65 and 120 cm, with a preferred value of 100 cm (corresponding to a pre-atmospheric mass of 30-40 tons). The individual and the shrapnels show significantly different shielding depths, with 30 to 35 cm depth for the individual, and 60-70 cm depth for the shrapnels. Terrestrial age of 20±30 ka is concordant with the young age inferred from the geomorphology of the crater.

Ott et al. (2014) propose a CRE age of approximately 366 ± 18 Ma. Considering geomorphological evidences, they however consider the meteorite terrestrial age to be short. The ^{36}Cl vs ^{41}Ca ratio for the individual (1.19

according to our measurements) compared to the expected saturation value of 1.34 complies with low terrestrial age. Shrapnels have an expected value of 1.57: only one of the shrapnel exhibit such a ratio ($GK_{shr}A$), whereas the others exhibit distinctly lower values of 1.10 and 1.28. It seems difficult to calculate the same terrestrial age for all samples without further investigation.

The presented pre-atmospheric radius and shielding depths agree with those from Ott et al. (2014). A radius of 1 m considering an iron meteorite impactor is enough to generate a crater of about 40 m in diameter.

4.2.1.b La Caille (France)

In 1828, two researchers, Thury and Brard, realized the metallic bench outside of the church in Caille (a village from the south of France) was indeed a large iron meteorite of 626 kg. It is said to have been found around 1650 a.d., and that it was an observed fall. It has been classified as an ungrouped octahedrite.

There is no available literature on La Caille cosmogenic nuclides concentrations.

According to our calculations, La Caille was 1.3m in diameter before entering the atmosphere and spent 135 ± 15 Ma in space, a low but not impossible CRE age. The deduced terrestrial age is 165 ± 30 ka. This age is surprisingly high for an iron meteorite from a non-arid area and implies that La Caille is not an observed fall.

Approximately 12% of the pre-atmospheric mass has been recovered. Considering the mass loss during the atmosphere entry and the mass loss due to terrestrial weathering, there may not be many more pieces of La Caille left on the ground.

4.2.1.c Mont Dieu (France)

Mont Dieu meteorite is a fine IIE octahedrite found in 1994 in the forest of Mont Dieu (France). Its total known weight is over 0.9 T.

Much work has been done on the mineralogy and the bulk and trace elements in Mont Dieu (Van den Borre *et al.* 2007, Van Roosbroek *et al.,* 2011). Van Roosbroek *et al.* (2012) considered Mont Dieu to result from the impact of a Fe-Ni impactor on an H-chondrite.

There is no available literature on Mont Dieu cosmogenic nuclides. We did not measure the cosmogenic noble gases concentrations because of a crystal of troilite in our prepared sample.

According to our calculations, Mont-Dieu was 1 m in diameter before entering the atmosphere and the studied sample led to a shielding depth of 20 to 30 cm. Roughly 3% of this pre-atmospheric mass has been recovered. Because of the location of find, the small pieces of Mont Dieu might have been totally weathered, and it is not certain that large pieces are still in the ground.

Terrestrial age of Mont-Dieu is 60 ± 35 ka, a relatively long residence time in a non-arid environment.

4.2.1.d Saint-Aubin (France)

Approximately 500 kg of a IIIAB iron meteorite have been found in 1968 by farmers in Saint-Aubin, France. Saint-Aubin presents large chromite crystals (Fehr & Carion, 2004). Noble gases ratios have been measured by Nishimura *et al.* (2008) in different phases (Fe-Ni metal and inclusions) of Saint-Aubin.

Pre-atmospheric size of Saint-Aubin was 1.7m in diameter, a result in agreement with the "very large meteoroid" announced by Nishimura and co-authors (2008).

Cosmogenic noble gases were measured on the bulk iron-nickel fraction without accessory minerals (chromite, troilite, schreibersite). Using the most reliable $^{36}Ar/^{36}Cl$ ratio, we calculate a CRE age of 520 ± 30 Ma, a rather normal age for an iron meteorite. Using ^{3}He, Nishimura et al. (2008) calculated a CRE age of 9-16 Ma. Our and Nishimura et al. (2008) results may differ by one order of magnitude. Whether this results from heterogeneities inside the meteoroid or from the measurements has still to be investigated.

Terrestrial age of Saint-Aubin is 55 ± 40 ka, compatible with a relatively recent fall.

4.2.1.e Agoudal (Morocco)

Several pieces of the IIAB of Agoudal iron meteorite have been recovered since 2011, for a total weight over one ton. Although none are validated, several hypotheses have been made concerning a potential related crater (Ibouh *et al.,*

2014, El Kerni *et al.,* 2014, Rochette *et al.,* 2014). Our study on Agoudal aims to provide new elements for this discussion.

Two different pieces of Agoudal were studied. One of these (Agoudal 2) exhibited cosmogenic nuclides concentrations, both radiogenic and noble gases, almost one order of magnitude lower than those of the other piece (Agoudal 1), which cannot be explained even considering a very large shielding depth. Lacking a proper explanation for these low concentrations, only the concentrations of the Agoudal 1 piece are taken into account.

Pre-atmospheric radius was calculated to be between 1.2 and 10 m. Even if Amon et al. (2009) model does not provide results for radius between 1.2 and 10 m, it is however most likely that Agoudal was several meters large before entering the atmosphere (between 55 and 30,000 tons).

The analysed piece was between 63 and 83 cm deep inside the meteoroid. Its CRE age is 204 ± 90 Ma, a standard value for iron meteorites. The terrestrial age of 105 ± 30 ka brings new insights into the discussion about the related crater.

4.2.1.f Tamentit (Algeria)

It was reported in 1865 that a mass of iron was lying in the Tamentit Oasis. The legend said that the fall has been observed around the 15th century and that the meteorite was then brought to Tamentit. It would then be the oldest recorded iron fall. In 1927, the large piece of around 510 kg was brought to the Muséum National d'Histoire Naturelle, in Paris. Tamentit has been classified as a IIIAB.

Tamentit was a small meteoroid of 60 cm in diameter. The analysed sample was close to the surface (9-12 cm shielding depth). Terrestrial age was calculated to be 9 ± 50 ka, consistent with the observed fall. We however recommend measuring ^{14}C to obtain a better constrained result.

4.2.1.g Morasko (Poland)

The first piece of Morasko iron meteorite has been found in 1914 near the town of Morasko, in Poland. Since, hundreds of pieces have been recovered for a total of more than 1 ton. So far the performed studies have concluded that they originate from the same iron meteorite. Eight circular ponds are noticeable in the strewnfield area. It is however still unclear if they are meteorite craters or

not, and if they are related to the Morasko iron meteorite. The "Morasko meteorite preserve" was created in 1976 to allow better preservation of the possible craters (Karwowski *et al.* 2011).

The biggest piece (261 kg) was found in 2012 by a joint expedition from Adam Mickiewicz University (Pr. A. Muszynski, A. Krzesinska), Aix-Marseille University (P. Rochette, A. Hutzler) and two private meteorite hunters. The meteorite was recovered 2.1m below the surface, allowing us to reasonably assume there are more large pieces still deep in the ground.

The Morako meteorite has been classified as a IAB-MG. It shows cm-large troilite and carbon inclusions, and inhomogenous cohenite.

Our work brings new insights into the study of the Morasko strewnfield and into the probability of finding more pieces that could be recovered.

Terrestrial age is estimated to be 25 ± 30 ka. If the ponds are craters associated with the Morasko meteorite, they should be less than 25 ka-old to have been emplaced after the last glaciation. Our results do not rule out such a possibility, but the associated uncertainties remain too large to allow definitive confirmation. This terrestrial age may however be better constrained by measuring cosmogenic nuclides concentrations, including in particular ^{14}C, in different pieces of the Morasko iron meteorite. The calculated Morasko meteorite CRE age is 130 ± 15 Ma. According to our calculation, the pre-atmospheric diameter was 1.7 m which leads to a pre-atmospheric mass of about 20 tons. About 10% of the pre-atmospheric mass has been recovered. Considering the mass loss during the atmosphere passage and the mass loss through terrestrial weathering, it is unsure if there are still large masses left in the ground.

4.2.1.h Cerro del Inca (Chile)

A single piece of iron meteorite of 20.6 kg was found in 1997 near a mine field in the Atacama Desert (Chile), east of Chug Chug DCA. It has been classified as a IIIF octahedrite. Cerro del Inca is part of the Chilean study we conducted in this work.

The pre-atmospheric radius was of 40 cm while the shielding depth was of 30-35 cm. The large terrestrial age of 690 ± 30 ka is not surprising for a Chilean meteorite, as exposed in the §Chondrites of this study.

4.2.1.i Dolores (Chile)

A 4.3 kg iron meteorite was found on a historical battlefield in 2001. Dolores was classified as a IIIAB meteorite. Dolores is an addition to the studied Chilean collection, though it is located far up north of our research fields.

Dolores shows extremely low cosmogenic nuclides concentrations with almost no more ^{41}Ca. It could correspond to a very old meteorite with a terrestrial age older than 1 Ma.

4.2.1.j Guanaco (Chile)

A 13.1 kg stone was found in 2000 near El Guanaco gold mine in Chile. Guanaco is located in the Catalina DCA. It has been classified as a IIG. It provides an additional terrestrial age to the studied Chilean collection.

The pre-atmospheric meteoroid radius was 15 cm. The Guanaco young terrestrial age of 27 ± 50 ka could be better constrained measuring it ^{14}C concentration (Schnitzer *et al.* 2012) although this technique is not yet well constrained for iron meteorites.

4.2.1.k Cuenca del Tiburon (Chile)

A small iron meteorite (2.2kg) was found near the Pampa de Mejillones DCA, in Chile by a private hunter, R. Martinez. It has not been classified or declared yet, Cuenca del Tiburon is a work name.

Cuenca del Tiburon was a small pre-atmospheric body being 10 cm in diameter, which implies that there was a maximum mass loss of 50% before discovery. The Cuenca del Tiburon calculated very low terrestrial age of 5 ± 50 ka could again be better constrained measuring its ^{14}C concentration.

4.2.2 Iron age spectra

In figure 8, we present the terrestrial age spectra for Chilean (data from MetBase and from this study) and non-chilean iron meteorites.

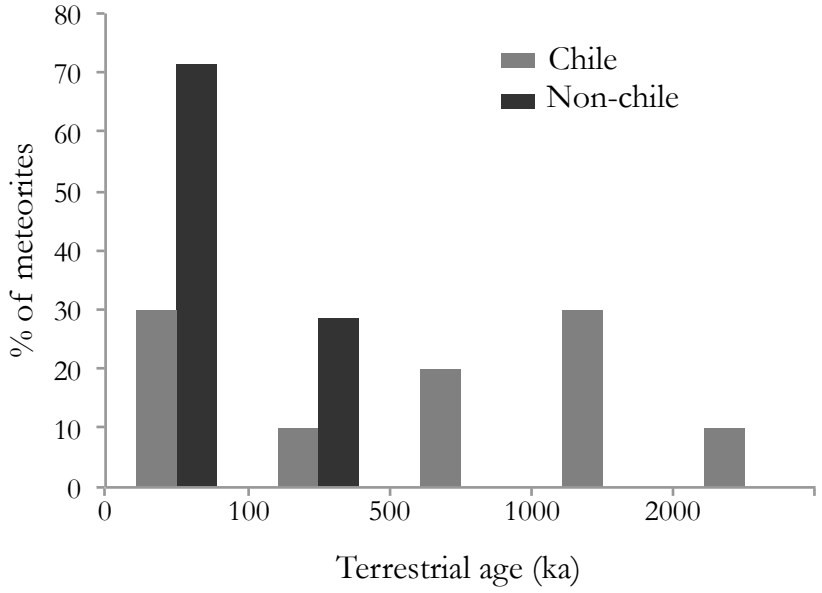

Figure 8: A histogram of terrestrial ages for 10 chilean iron meteorites (MetBase and this study) and 7 non-chilean iron meteorites (this study).

We distinctly notice that chilean iron meteorites tend to be older than non-chilean meteorites. This can be explained by the favorable conditions in Atacama desert (aridity and stability over 2 Ma), and also by the lack of pre-historic human occupation.

4.2.3 Chondrites

Twenty-five ordinary chondrites from the same Chilean collection have been dated with ^{14}C, in a collaboration with the University of Arizona (USA). Over 67% of the results were higher than 40 ka. This result confirms that cosmogenic isotopes with a longer half-life are better suited to work on this collection.

Terrestrial ages have been calculated with three different methods: T_{terr} $^{36}Cl/^{10}Be$, T_{terr} $^{36}Cl/^{41}Ca$ and T_{terr} ^{36}Cl (Leya & Masarik, 2009; Nishiizumi *et al.,* 1989).

Figure 9 presents the age spectra for the different methods.

As explained before, ^{10}Be is less reliable, because of the issue of the determination of sulfur and phosphorus concentrations in the sample. The ^{36}Cl method uses only one element, and hence does not get rid of the shielding effect. Hence, we consider the $^{41}Ca/^{36}Cl$ age spectrum to be the more reliable.

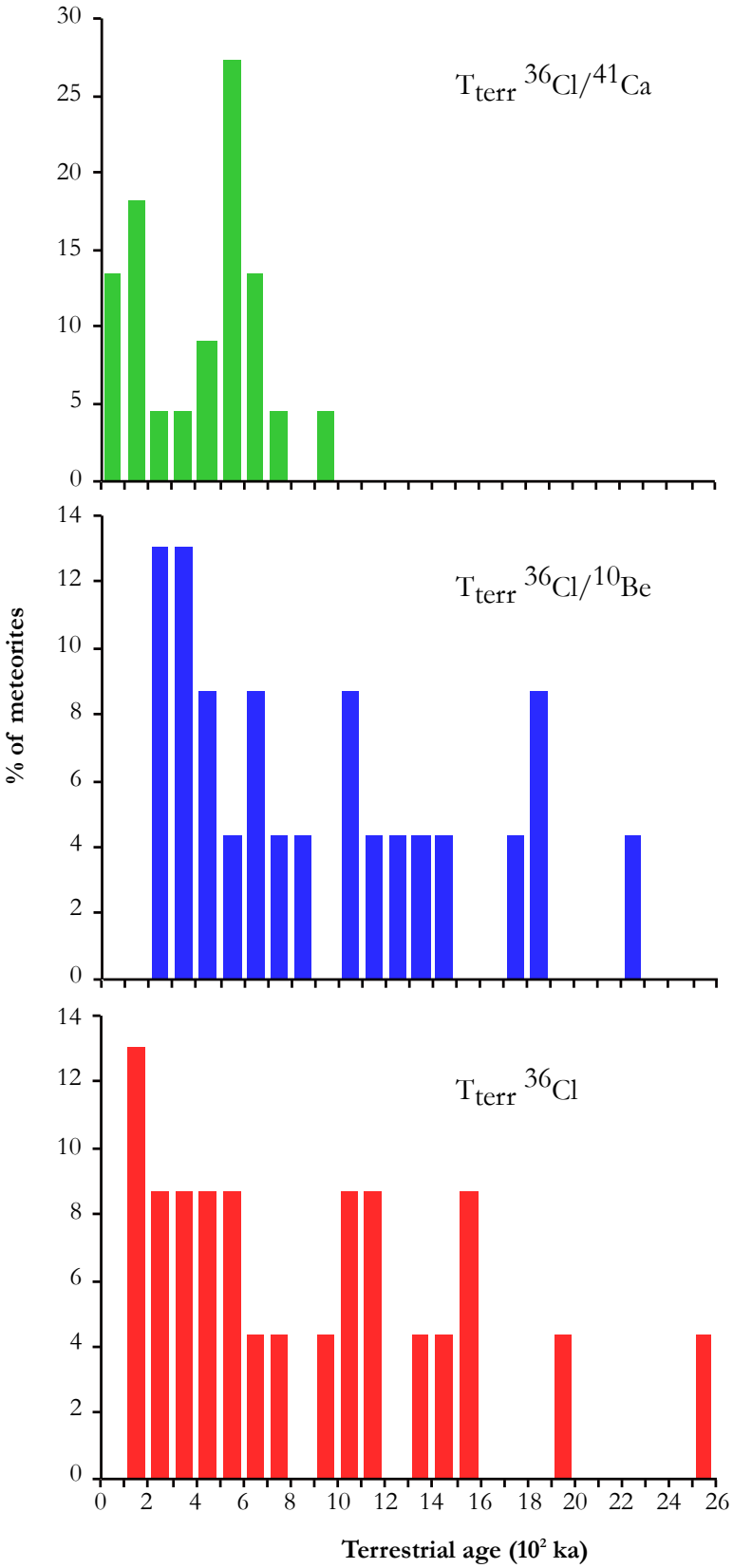

Figure 9: A histogram of terrestrial ages for the 25 studied ordinary chondrites from El Médano DCA for the three calculation methods.

The spectrum resulting from the ^{41}Ca method is flat up to 700 ka. We would have expected a spectrum decreasing with time, to account for the weathering and the disappearance of meteorites over time. One possible explanation for the lack of older meteorites is an insufficient sample size, another would be the presence of a wetter climate before 700ka.

The terrestrial ages of the El Médano DCA ordinary chondrites are distributed between 35 ka and 1 Ma ($^{41}Ca/^{36}Cl$ method) to over 2Ma ($^{10}Be/^{36}Cl$ and ^{36}Cl method). This distribution highlights much older terrestrial ages than for other hot desert collections, and similar to Antarctica age spectrum (fig. 10). According to these results, it is possible for a meteorite collection to be preserved for over 1 Ma in a hot desert environment, providing the environment is favorable enough (dry and stable enough).

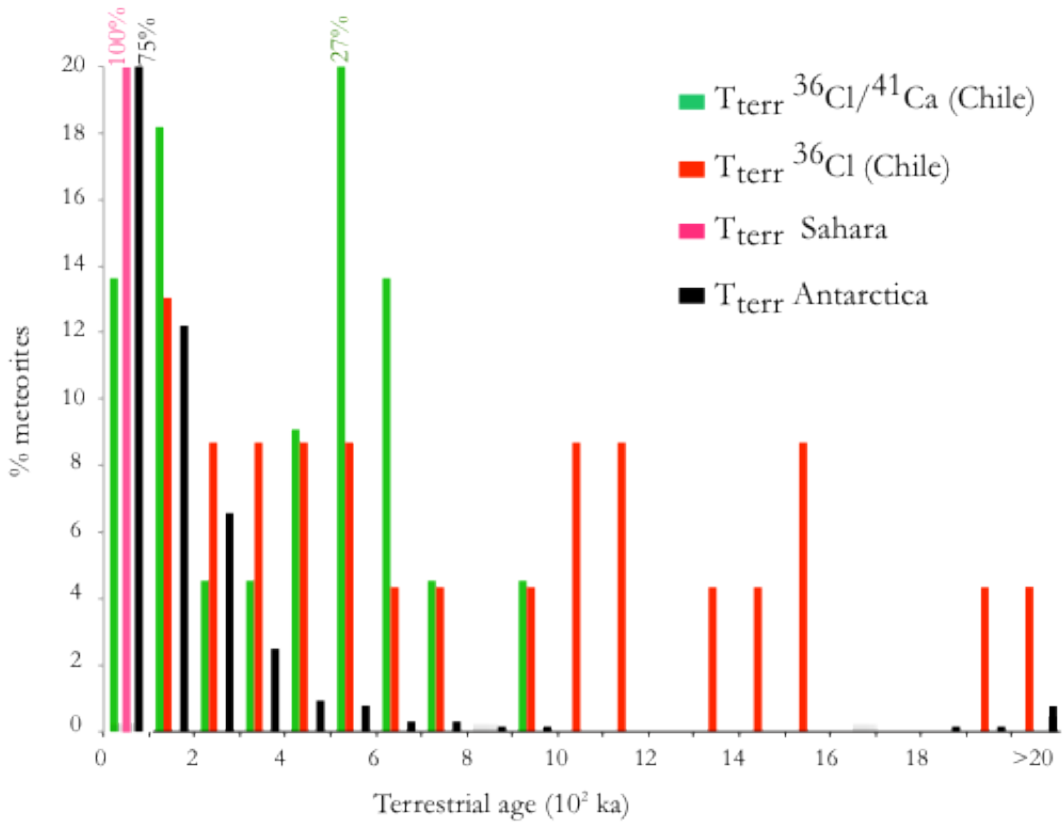

Figure 10: Histograms of terrestrial ages of ordinary chondrites for Chile (this study, green and red, 25 samples), Sahara (MetBase, pink, 112 samples) and Antarctica (MetBse, black, 639 samples).

It is also consistent with the §2.2 conclusions (Hutzler *et al.* n.d.) of an accumulation duration of about 1-2 Myr for meteorites in the El Médano DCA, in order to comply with the flux of 80 meteorites >10g/Ma/km^2 estimated in the literature (Halliday *et al.* 1989).

From §2.2, we calculated a concentration of meteorites of 168 met>10g/km^2 in El Médano DCA. The ^{41}Ca/^{36}Cl age spectrum shows a flat part until 700 ka, with 91% of the measured meteorites under this age. Hence, combining these two results, we obtain a flux of 218 met>10g/Ma/km^2 over the period 0-700 ka. It is by far higher than the flux estimated by Halliday (1989) (83 met>10g/Ma/km^2) and still higher than the flux estimated by Bland *et al.* (1996) (159 met>20g/Ma/km^2). If we try to evaluate the uncertainty associated with the flux result, we must take into account the uncertainties on measuring the searched areas, and the uncertainties linked to the bias calculations presented in §2.2. We can roughly estimate an uncertainty of 20%: it would make Bland's result and our result not so significantly different. Although the discrepancies may come from the fact that we did not evaluate the bias linked to the searched surface. Since the individual areas we searched in the El Médano DCA are small compared to typical strewn fields, we must correct the numbers of meteorites to take into account the effect described in Halliday *et al.* (1989). To use the example of Halliday et al. (1989), finding 10 different leaves in 1 m^2 in a forest does not mean you have 10 different trees in 1 m^2 This study is still under process, but it should reduce significantly the flux estimated here.

Conclusions and outlooks

My PhD aimed at developing chemical extraction procedures for radiogenic cosmogenic nuclides from extra-terrestrial matter. These methods are currently performed in few laboratories in the world but have never been introduced at CEREGE.

We chose two types of matrices to test the procedure: metal fraction of chondritic material and iron meteorites.

Extraction procedures were developed for ^{10}Be, ^{26}Al, ^{36}Cl and ^{41}Ca from extra-terrestrial matter. ^{59}Ni and ^{53}Mn extraction procedures were also tested but not routinely performed since the 6 MV (Megavolts) AMS national facility ASTER housed at CEREGE does not allow measuring these two nuclides. Chemical procedures were designed to obtain the purest sample as possible in term of the interfering isobars (^{10}B, ^{26}Mg, ^{36}S, ^{41}K). We used mostly ion-exchange resins and pH-controlled precipitations. The elements were then compressed into a nickel sample holder (AgCl) or into a copper sample holder with conductive powder (BeO with niobium powder ; CaF_2 and Al_2O_3 with silver powder), to be measured at the ASTER AMS national facility. The measurements have been demonstrated to be reproducible not only in the laboratory but also between different laboratories.

We chose 25 ordinary chondrites among 213 samples from a large Chilean collection (El Médano collection) that we collected, classified and analyzed. The collection was compared (in term of meteorite types, abundances, weathering…) with a Chilean collection recovered by private hunters. We also classified the 189 samples of this "private collection". We designed a mathematical model to help with the pairing of the meteorites of the El Médano's collection. Then a recovery density, before and after pairing, have been computed.

Quartz samples from the studied Chilean Dense Collection Areas were dated using ^{10}Be measurements. They led to exposure ages between 2 and 4 Ma. We dated (through collaboration with the University of Arizona, USA) 25 meteorites of the same collection using ^{14}C. 67% of the 25 samples led to ages older than 40 ka. It is thus consistent to use ^{36}Cl, ^{41}Ca and ^{10}Be to determine terrestrial ages instead of ^{14}C.

^{26}Al, ^{36}Cl, ^{41}Ca and ^{10}Be having been measured, we calculated terrestrial ages from the ^{36}Cl, ^{41}Ca and ^{10}Be data. We favored the results obtained

combining ^{36}Cl and ^{41}Ca, since cross sections are better constrained for these two nuclides contrary to ^{10}Be, and also because combining two nuclides helps getting rid of the shielding effect.

Using the number of falls per unit of surface (168 meteorites >10g/km^2 for the El Médano collection), and the terrestrial ages spectrum, we were able to calculate a flux of 218 meteorites >10g/km^2/Ma over a collection duration of about 700 ka. This flux is higher than any other flux from the literature: Halliday et al (1989) calculate 83 meteorites >10g/km^2/Ma for the current flux and Bland et al (1996) calculate a flux of 159 meteorites >20g/km^2/Ma over the last 50 ka, although if we consider a roughly estimated uncertainty of 20% on flux results, our estimate is similar to Bland et al. estimate.

These high fluxes could be explained by two hypotheses. First, we did not take into account the size of the discrete searched areas (a few thousands of m^2) compared to the typical size of a strewnfield, i.e. a few km^2. We are currently working on a way to quantify this bias that should significantly reduce the flux. Also, the flux we calculate in this study is in a longer timescale than the fluxes from the literature. The flux may have been higher in in the past, at a timescale of the order of 1 Ma.

Studied iron meteorites were seven large (>500kg TKW) iron meteorites from Europe and North Africa and four small (<20kg) Chilean meteorites. The terrestrial ages of the Chilean meteorites can be linked to the age spectrum of the El Médano collection. Large iron meteorites were studied for pre-atmospheric size, Cosmic Ray Exposure ages and terrestrial ages.

Stable nuclides (noble gases) were extracted from five out of the seven large iron meteorites, through collaboration with Thomas Smith and Ingo Leya from the University of Bern (Switzerland). These nuclides allowed us to determine the Cosmic Rays Exposure ages. The results were used to estimate if other pieces of some of the meteorites may still be found on and/or in the ground. They also provide new insights into the discussion about the link between the meteorites and nearby craters. As an example, terrestrial age of Agoudal (100 ka) is compatible with the estimated age of a large (a few hundreds of meters in diameter) crater detected nearby.

Based on our results, the Chilean collection appears to be the first one outside Antarctica that can probe the extra-terrestrial flux on the Ma timescale,

the other ones being restricted to the 10-100 ka timescale. It has the advantage over Antarctica to be less unaffected by secondary concentration processes on Earth, and thus can be used more readily to discuss the long term evolution of the flux of extra-terrestrial matter on Earth. Our first results point toward a possibly higher flux than the recent one, as well as a different composition of this flux (namely a different H/L ratio). Future investigations of the Chilean collection, as well as comparison with the Antarctic collection, may help to further evaluation the extra-terrestrial flux variability.

Concerning iron meteorites, we surmise that further systematic study of cosmonuclides in iron meteorites from various deserts will help understanding the long term history of these collection surfaces.

Conclusions et perspectives

Ma thèse avait pour but de développer des protocoles chimiques pour extraire des nucléides cosmogéniques radioactifs de la matière extra-terrestre. Ces méthodes sont réalisées actuellement dans quelques laboratoires, mais n'avaient jamais été introduites au CEREGE.

Nous avons choisi deux types de matrices pour tester les protocoles : la fraction métallique de chondrites ordinaires, et des météorites de fer.

Les protocoles ont été développés pour ^{10}Be, ^{26}Al, ^{36}Cl and ^{41}Ca. Les procédures d'extraction de ^{59}Ni et ^{53}Mn ont aussi été testées, mais n'ont pas été mises en place en routine, étant donné que le SMA de 6MV (Mégavolts) présent au CEREGE ne permet pas la mesure de ces deux éléments. Le protocole expérimental a été conçu afin d'obtenir les échantillons les plus purs en terme d'isobares (^{10}B, ^{26}Mg, ^{36}S, ^{41}K). Nous avons principalement utilisé des résines échangeuses d'ions et des précipitations à pH contrôlé. Les éléments extraits ont ensuite été compressés dans des cathodes en nickel (AgCl), ou dans des cathodes de cuivre avec une poudre conductrice de courant (BeO avec de la poudre de niobium ; CaF_2 et Al_2O_3 avec de la poudre d'argent), afin d'être mesurés par SMA sur l'instrument national ASTER. Les mesures sont reproductibles non seulement au laboratoire, mais aussi entre différents laboratoires.

Nous avons choisi 25 chondrites ordinaires parmi 213 échantillons d'une large collection chilienne (la collection El Médano), que nous avons collectée, classée et analysée. La collection a été comparée (en terme de types de météorites, de degré d'altération...) avec une autre collection chilienne collectée par des chasseurs privés. Nous avons développé un modèle mathématique pour faciliter l'appariement des météorites de la collection El Médano. Nous avons pu ainsi calculer une densité de récupération avant et après appariement.

Des galets de quartz des zones chiliennes étudiées ont été datés par la mesure de ^{10}Be. Nous avons trouvé des âges entre 2 et 4 Ma. Nous avons daté (dans le cadre d'une collaboration avec l'Université d'Arizona, aux Etats-Unis) 25 météorites de la même collection, en utilisant le ^{14}C. 67% de ces échantillons présentent un âge supérieur à 40 ka. Il est ainsi cohérent d'utiliser le ^{36}Cl, le ^{41}Ca et le ^{10}Be plutôt que le ^{14}C pour déterminer les âges terrestres.

Après avoir mesuré ^{26}Al, ^{36}Cl, ^{41}Ca et ^{10}Be, nous avons calculé les âges terrestres avec les données de ^{36}Cl, de ^{41}Ca et de ^{10}Be. Nous préférons les

résultats obtenus en combinant le ^{36}Cl et le ^{41}Ca, étant donné que les sections efficaces sont mieux définies pour ces deux éléments (au contraire de celles du ^{10}Be), et aussi car le fait de combiner deux éléments permet de diminuer l'effet de profondeur dans l'échantillon.

En utilisant le nombre de chutes par unité de surface (168 météorites >10g/km^2 pour la collection El Médano) et le spectre d'âges terrestres, nous avons pu calculer un flux 218 météorites >10g/km^2/Ma sur une période de 700 ka. Ce flux est plus important que les autres estimations disponibles dans la littérature : Halliday et al. (1989) calculent un flux actuel de 83 météorites >10g/km^2/Ma et Bland et al. (1996) présentent un flux de 159 météorites >20g/km^2/Ma sur les derniers 50 ka, bien que si on considère une estimation globale de 20% d'incertitude sur nos résultats, notre estimation est sensiblement identique à celle de Bland et al.

Ces flux importants peuvent être expliqués par deux hypothèses. Tout d'abord, nous n'avons pas pris en compte les différences de taille typique entre les zones de recherche (quelques centaines de m^2) et une ellipse de chute (quelques km^2). Nous travaillons actuellement sur un moyen de quantifier ce biais, ce qui devrait réduire le flux de façon significative. Deuxièmement, le flux que nous avons calculé est sur une période de temps beaucoup plus longue que les flux de la littérature. Le flux a pu être plus important dans le passé, sur une échelle de temps d'un million d'années.

Nous avons étudié sept grosses (>500kg TKW) météorites de fer et quatre petite (<20kg) météorites chiliennes. Les âges terrestres des météorites chiliennes peuvent être reliés au spectre d'âge de la collection El Médano. Les grosses météorites de fer ont été étudiées pour leur taille pré-atmosphérique, leur temps d'exposition dans l'espace, et leur âge terrestre.

Des isotopes stables (gaz rares) ont été extraits de cinq des sept grosses météorites de fer, via une collaboration avec Thomas Smith et Ingo Leya de l'Université de Bern (Suisse). Ces éléments nous ont permis de déterminer le temps d'exposition dans l'espace. Les résultats ont ensuite été utilisés pour déterminer si d'autres morceaux de certaines météorites pouvaient encore être découverts. Les résultats amènent aussi de nouveaux éléments dans la discussion à propos du lien entre certaines météorites et des cratères proches. À titre d'exemple, l'âge terrestre d'Agoudal (100ka) est compatible avec l'âge

estimé d'un large (quelques centaines de mètres de diamètre) cratère d'impact détecté à côté.

D'après nos résultats, la collection chilienne semble être la première (hors Antarctique) qui permette d'étudier le flux extra-terrestre sur une échelle de temps d'un Ma, les autres collections étant réduites à l'échelle 10-100 ka. La collection chilienne a l'avantage par rapport à l'Antarctique d'être non affectée par des processus de reconcentration, et peut ainsi être plus propice à l'étude de l'évolution sur le long terme du flux de matière extra-terrestre sur Terre. Nos premiers résultats concluent à un flux plus intense dans le passé, avec une composition potentiellement différente (un rapport H/L différent). Un travail plus poussé sur les collections chiliennes, ainsi qu'un comparaison avec les collections antarctiques pourrait aider à mieux contraindre la variabilité du flux extra-terrestre.

Nous pensons qu'une étude systématique poussée des isotopes cosmogéniques de météorites de fer de divers déserts pourrait aider à mieux comprendre l'histoire à long terme des surfaces de collecte.

REFERENCES

AMMON, K., MASARIK, J. & LEYA, I. 2008. Noble gases in Grant and Carbo and the influence of S- and P-rich mineral inclusions on the ^{41}K-^{40}K dating system. *Meteoritics & Planetary Science*, **43**, 685–699.

AMMON, K., MASARIK, J. & LEYA, I. 2009. New model calculations for the production rates of cosmogenic nuclides in iron meteorites. *Meteoritics & Planetary Science*, **44**, 485–503.

ARNOLD, M., MERCHEL, S., ET AL. 2010. The French accelerator mass spectrometry facility ASTER: Improved performance and developments. *Nuclear Instruments and Methods in Physics Research Section B: Beam Interactions with Materials and Atoms*, **268**, 1954–1959.

BENOIT, P.H. & SEARS, D.W.G. 1996. Rapid changes in the nature of the H chondrites falling to Earth. *Meteoritics & Planetary Science*, **31**, 81–86.

BENOIT, P.H., SEARS, H. & SEARS, D.W.G. 1993. The natural thermoluminescence of meteorites: 5. Ordinary chondrites at the Allan Hills Ice Fields. *Journal of Geophysical Research*, **98**, 1875.

BENOIT, P.H., SEARS, D.W.G., AKRIDGE, J.M.C., BLAND, P.A., BERRY, F.J. & PILLINGER, C. T. 2000. The non-trivial problem of meteorite pairing. *Meteoritics & Planetary Science*, **35**, 393–417.

BLAND, P.A., BERRY, F.J., SMITH, T.B., SKINNER, S.J. & PILLINGER, C.T. 1996. The flux of meteorites to the Earth and weathering in hot desert ordinary chondrite finds. *Geochimica et Cosmochimica Acta*, **60**, 2053–2059.

BLAND, P.A., BEVAN, A.W.R. & JULL, A.J.T. 2000. Ancient Meteorite Finds and the Earth's Surface Environment. *Quaternary Research*, **53**, 131–142.

BLAND, P.A., TOWNER, M.C., ET AL. 2014. Digital Expansion of the Desert Fireball Network. *In*: 77th Annual Meteoritical Society Meeting.

BROWN, E.T., EDMOND, J.M., RAISBECK, G.M., YIOU, F., KURZ, M.D. & BROOK, E.J. 1991. Examination of surface exposure ages of Antarctic moraines using in situ produced 10Be and 26Al. *Geochimica et Cosmochimica Acta*, **55**, 2269–2283.

BUNCH, T.E., WITTKE, J.H., IRVING, A.J. & KUEHNER, S.M. 2012. Estimation Of Petrologic Subtypes Of Unequilibrated Ordinary Chondrites From Systematics Of Chromium Distribution In Ferroan Olivine. *In*: *43rd Lunar and Planetary Science Conference.*

CARIGNAN, J., HILD, P., MEVELLE, G., MOREL, J. & YEGHICHEYAN, D. 2001. Routine Analyses of Trace Elements in Geological Samples using Flow Injection and Low Pressure On-Line Liquid Chromatography Coupled to ICP-MS: A Study of Geochemical Reference Materials BR, DR-N, UB-N, AN-G and GH. *Geostandards Newsletter*, **25**, 187–198.

CHEN, J.H., PAPANASTASSIOU, D.A. & WASSERBURG, G.J. 2009. A search for nickel isotopic anomalies in iron meteorites and chondrites. *Geochimica et Cosmochimica Acta*, **73**, 1461–1471.

CHMELEFF, J., VON BLANCKENBURG, F., KOSSERT, K. & JAKOB, D. 2010. Determination of the 10Be half-life by multicollector ICP-MS and liquid scintillation counting. *Nuclear Instruments and Methods in Physics Research Section B: Beam Interactions with Materials and Atoms*, **268**, 192–199.

CLARKE, J.D.A. 2006. Antiquity of aridity in the Chilean Atacama Desert. *Geomorphology*, **73**, 101–114.

D'ORAZIO, M., FOLCO, L., ZEOLI, A. & CORDIER, C. 2011. Gebel Kamil: The iron meteorite that formed the Kamil crater (Egypt): Gebel Kamil iron meteorite. *Meteoritics & Planetary Science*, **46**, 1179–1196.

DUNAI, T.J. 2010. *Cosmogenic Nuclides Principles, Concepts and Applications in the Earth Surface Sciences*. Cambridge; New York, Cambridge University Press.

DUNAI, T.J., GONZÁLEZ LÓPEZ, G.A. & JUEZ-LARRÉ, J. 2005. Oligocene–Miocene age of aridity in the Atacama Desert revealed by exposure dating of erosion-sensitive landforms. *Geology*, **33**, 321.

EL KERNI, H., CHENNAOUI AOUDJEHANE, H., ET AL. 2014. Agoudal (High Atlas Mountains): Confirmation and First Studies of a Remnant of a Post Mid-Jurassic Impact Structure in Morocco. *In*: 77th Annual Meteoritical Society Meeting.

EUGSTER, O., HERZOG, G.F., MARTI, K. & CAFFEE, M.W. 2006. Irradiation Records, Cosmic-Ray Exposure Ages, and Transfer Times of Meteorites. *In*: Lauretta, D. S. & McSween, H. Y. (eds) *Meteorites and the Early Solar System II*. Tucson : Houston, University of Arizona Press ; In collaboration with Lunar and Planetary Institute, The University of Arizona space science series, 829–851.

FEHR, K.T. & CARION, A. 2004. Unusual large chromite crystals in the Saint Aubin iron meteorite. *Meteoritics & Planetary Science*, **39**, A139–A141.

FOLCO, L., DI MARTINO, M., ET AL. 2011. Kamil Crater (Egypt): Ground truth for small-scale meteorite impacts on Earth. *Geology*, **39**, 179–182.

FRIES, M., MATSON, R., SCHAEFER, J., FRIES, J., HANKEY, M. & ANDERSON, L. 2014. Worldwide Weather Radar Imagery may allow Substantial Increase in Meteorite Fall Recovery. *In*: 77th Annual Meteoritical Society Meeting.

GATTACCECA, J., EISENLOHR, P. & ROCHETTE, P. 2004. Calibration of *in situ* magnetic susceptibility measurements. *Geophysical Journal International*, **158**, 42–49.

GATTACCECA, J., VALENZUELA, M., ET AL. 2011. The densest meteorite collection area in hot deserts: The San Juan meteorite field (Atacama Desert, Chile): San Juan meteorite dense collection area (Atacama, Chile). *Meteoritics & Planetary Science*, **46**, 1276–1287.

GOLDSMITH, Y., STEIN, M. & ENZEL, Y. 2014. From dust to varnish: Geochemical constraints on rock varnish formation in the Negev Desert, Israel. *Geochimica et Cosmochimica Acta*, **126**, 97–111.

GROSSMAN, J.N. & BREARLEY, A.J. 2005. The onset of metamorphism in ordinary and carbonaceous chondrites. *Meteoritics & Planetary Science*, **40**, 87–122.

HALLIDAY, I. 1964. The Variation in the Frequency of Meteorite Impact with Geographic Latitude. *Meteoritics*, **2**, 271–278.

HALLIDAY, I., BLACKWELL, A.T. & GRIFFIN, A.A. 1989. The flux of meteorites on the Earth's surface. *Meteoritics*, **24**, 173–178.

HALLIDAY, I., BLACKWELL, A.T. & GRIFFIN, A.A. 1991. The frequency of meteorite falls: Comments on two conflicting solutions to the problem. *Meteoritics*, **26**, 243–249.

HARVEY, R.P. & CASSIDY, W.A. 1989. A statistical comparison of Antarctic finds and modern falls: Mass frequency distributions and relative abundance by type. *Meteoritics*, **24**, 9–14.

HEZEL, D.C., SCHLÜTER, J., KALLWEIT, H., JULL, A.J.T., AL FAKEER, O.Y., AL SHAMSI, M. & STREKOPYTOV, S. 2011. Meteorites from the United Arab Emirates: Description, weathering, and terrestrial ages: Meteorites from the United Arab Emirates. *Meteoritics & Planetary Science*, **46**, 327–336.

HUSS, G.R. 1990. Meteorite infall as a function of mass: Implications for the accumulation of meteorites on Antarctic ice. *Meteoritics*, **25**, 41–56.

HUTZLER, A., GATTACCECA, J., ET AL. n.d. Description of a very dense meteorite collection area in western Atacama: insight into the long-term composition of the meteorite flux to Earth using a new pairing method.

IBOUH, H., MICHARD, A., CHARRIÈRE, A., BENKADDOUR, A. & RHOUJJATI, A. 2014. Tectonic–karstic origin of the alleged 'impact crater' of Lake Isli (Imilchil district, High Atlas, Morocco). *Comptes Rendus Geoscience*.

JULL, A.J.T. 2006. Terrestrial Ages of Meteorites. *In*: Lauretta, D. S. & McSween, H. Y. (eds) *Meteorites and the Early Solar System II*. Tucson : Houston, University of Arizona Press ; In collaboration with Lunar and Planetary Institute, The University of Arizona space science series, 889–905.

KARWOWSKI, L., PILSKI, A.S., MUSZYNSKI, A., ARNOLD, S., NOTKIN, G. & GURDZIEL, A. 2011. New Finds in the Morasko Meteorite Preserve, Poland. *Meteorites*, **1**, 21–28.

KORSCHINEK, G., BERGMAIER, A., ET AL. 2010. A new value for the half-life of 10Be by Heavy-Ion Elastic Recoil Detection and liquid scintillation counting. *Nuclear Instruments and Methods in Physics Research Section B: Beam Interactions with Materials and Atoms*, **268**, 187–191.

KUTSCHERA, W., AHMAD, I. & PAUL, M. 1992. Half-Life Determination of 41Ca and Some Other Radioisotopes. *Radiocarbon*, **34**, 436–446.

LAVIELLE, B., MARTI, K., JEANNOT, J.-P., NISHIIZUMI, K. & CAFFEE, M. 1999. The 36Cl–36 Ar–40K- 41 K records and cosmic ray production rates in iron meteorites. *Earth and planetary science letters*, **170**, 93–104.

LEYA, I. & MASARIK, J. 2009. Cosmogenic nuclides in stony meteorites revisited. *Meteoritics & Planetary Science*, **44**, 1061–1086.

MASON, B. 1966. The enstatite chondrites. *Geochimica et Cosmochimica Acta*, **30**, 23–39.

MCSWEEN, H.Y. 1999. *Meteorites and Their Parent Planets.*, 2nd ed. Cambridge ; New York, Cambridge University Press.

MERCHEL, S. & HERPERS, U. 1999. An update on radiochemical separation techniques for the determination of long-lived radionuclides via accelerator mass spectrometry. *Radiochimica Acta*, **84**, 215–219.

MERCHEL, S., ARNOLD, M., ET AL. 2008. Towards more precise 10Be and 36Cl data from measurements at the 10−14 level: Influence of sample preparation. *Nuclear Instruments and Methods in Physics Research Section B: Beam Interactions with Materials and Atoms*, **266**, 4921–4926.

MUÑOZ, C., GUERRA, N., MARTÍNEZ-FRÍAS, J., LUNAR, R. & CERDA, J. 2007. The Atacama Desert: A preferential arid region for the recovery of meteorites—Find location features and strewnfield distribution patterns. *Journal of Arid Environments*, **71**, 188–200.

NISHIIZUMI, K. 1987. 53Mn, 26Al, 10Be and 36Cl in meteorites: Data compilation. *International Journal of Radiation Applications and Instrumentation. Part D. Nuclear Tracks and Radiation Measurements*, **13**, 209–273.

NISHIIZUMI, K. 2004. Preparation of 26Al AMS standards. *Nuclear Instruments and Methods in Physics Research Section B: Beam Interactions with Materials and Atoms*, **223-224**, 388–392.

NISHIIZUMI, K., ELMORE, D. & KUBIK, P.W. 1989. Update on terrestrial ages of Antarctic meteorites. *Earth and Planetary Science Letters*, **93**, 299–313.

NISHIIZUMI, K., CAFFEE, M.W., JEANNOT, J.-P., LAVIELLE, B. & HONDA, M. 1997. A systematic study of the cosmic-ray-exposure hitory of iron meteorites : Beryllium10-Chlorine36/Beryllium10 terrestrial ages. *In*: *Meteoritics & Planetary Science*. A100.

NISHIIZUMI, K., IMAMURA, M., CAFFEE, M.W., SOUTHON, J.R., FINKEL, R.C. & MCANINCH, J. 2007. Absolute calibration of 10Be AMS standards. *Nuclear Instruments and Methods in Physics Research Section B: Beam Interactions with Materials and Atoms*, **258**, 403–413.

NISHIMURA, C., MATSUDA, J. & KURAT, G. 2008. Noble gas content and isotope abundances in phases of the Saint-Aubin (UNGR) iron meteorite. *Meteoritics & Planetary Science*, **43**, 1333–1350.

OBERST, J., MOLAU, S., ET AL. 1998. The 'European Fireball Network': Current status and future prospects. *Meteoritics & Planetary Science*, **33**, 49–56.

OTT, U., MERCHEL, S., ET AL. 2014a. Cosmic ray exposure and pre-atmospheric size of the Gebel Kamil iron meteorite. *Meteoritics & Planetary Science*, **49**, 1365–1374.

OTT, U., MERCHEL, S., ET AL. 2014b. Cosmic ray exposure and pre-atmospheric size of the Gebel Kamil iron meteorite. *Meteoritics & Planetary Science*, **49**, 1365–1374.

PRETTYMAN, T.H., HENDRICKS, J.S. & REEDY, R.C. 2014. Effects of Metoroid Shape on Cosmogenic Nuclide Production. *In*: 77th Annual Meteoritical Society Meeting. 325.

PRIOR, G.T. 1920. The Classification of Meteorites 1. *Mineralogical Magazine*, **19**, 51–63.

ROCHETTE, P., SAGNOTTI, L., ET AL. 2003. Magnetic classification of stony meteorites: 1. Ordinary chondrites. *Meteoritics & Planetary Science*, **38**, 251–268.

ROCHETTE, P., GATTACCECA, J., ET AL. 2008. Magnetic classification of stony meteorites: 2. Non-ordinary chondrites. *Meteoritics & Planetary Science*, **43**, 959–980.

ROCHETTE, P., GATTACCECA, J., ET AL. 2009. Magnetic classification of stony meteorites: 3. Achondrites. *Meteoritics & Planetary Science*, **44**, 405–427.

ROCHETTE, P., CHENNAOUI AOUDJEHANE, H., EL KERNI, H., QUESNEL, Y., UEHARA, M., ABOULAHRIS, M. & HUTZLER, A. 2014. Reconciling Impact Evidence and Meteorite Strewnfield in Agoudal (Morocco): Field, Geomorphology and Geophysical Evidences. *In*: 77th Annual Meteoritical Society Meeting.

RUBIN, A.E., SCOTT, E.R.D. & KEIL, K. 1997. Shock metamorphism of enstatite chondrites. *Geochimica et Cosmochimica Acta*, **61**, 847–858.

RUSSELL, S.S., ZOLENSKY, M., ET AL. 2005. The Meteoritical Bulletin, No. 89, 2005 September. *Meteoritics & Planetary Science*, **40**, A201–A263.

RUZICKA, A., GROSSMAN, J.N. & GARVIE, L. 2014. The Meteoritical Bulletin, No. 100, 2014 June. *Meteoritics & Planetary Science*, **49**, E1–E101.

SCHLÜTER, J., SCHULTZ, L., THIEDIG, F., AL-MAHDI, B.O. & AGHREB, A.E.A. 2002. The Dar al Gani meteorite field (Libyan Sahara): Geological setting, pairing of meteorites, and recovery density. *Meteoritics & Planetary Science*, **37**, 1079–1093.

SCHMITZ, B., TASSINARI, M. & PEUCKER-EHRENBRINK, B. 2001. A rain of ordinary chondritic meteorites in the early Ordovician. *Earth and Planetary Science Letters*, **194**, 1–15.

SCHNITZER, C.J., JULL, A.J.T., BIDDULPH, D., ZAHN, D., CHENG, L., BURR, G.S. & MCHARGUE, L. 2012. New studies of 14C and 10Be in iron meteorites. *In*: 75th Annual Meteoritical Society Meeting.

SCHULTZ, L. & WEBER, H.W. 1996. Noble gases and H chondrite meteoroid streams: No confirmation. *Journal of Geophysical Research*, **101**, 21177.

SCOTT, E.R.D., KEIL, K. & STOEFFLER, D. 1992. Shock metamorphism of Carbonaceous Chondrites. *In*: Lunar and Planetary Science Conference. 1207.

STÖFFLER, D., KEIL, K. & EDWARD R.D, S. 1991. Shock metamorphism of ordinary chondrites. *Geochimica et Cosmochimica Acta*, **55**, 3845–3867.

STONE, J.O. 2000. Air pressure and cosmogenic isotope production. *Journal of Geophysical Research*, **105**, 23753.

URBINI, S., NICOLOSI, I., ET AL. 2012. Geological and geophysical investigation of Kamil crater, Egypt: Kamil crater, Egypt. *Meteoritics & Planetary Science*, **47**, 1842–1868.

VAN DEN BORRE, N., GOETHALS, H., HERTOGEN, J. & CLAEYS, P. 2007. Mont Dieu Iron Meteorite: Petrography and Geochemistry. *In*: 70th Annual Meteoritical Society Meeting.

VAN ROOSBROEK, N., GODERIS, S., DEBAILLE, V., HUBLET, G. & CLAEYS, P. 2011. Mont Dieu a IIE Non-Magmatic Iron Meteorite with Chondrules. *In*: 74th Annual Meteoritical Society Meeting.

VAN ROOSBROEK, N., GODERIS, S., DEBAILLE, V., VALLEY, J.W. & CLAEYS, P. 2012. Formation of the Mont Dieu IIe Non Magmatic Iron Meteorite, and Origin of its Silicate Inclusions. *In*: 43rd Lunar and Planetary Science Conference.

VAN SCHMUS, W.R. & WOOD, J.A. 1967. A chemical-petrologic classification for the chondritic meteorites. *Geochimica et Cosmochimica Acta*, **31**, 747–765.

VOGT, S. & HERPERS, U. 1988. Radiochemical separation techniques for the determination of long-lived radionuclides in meteorites by means of accelerator-mass-spectrometry. *Fresenius Zeitschrift für Analytische Chemie*, **331**, 186–188.

WEISBERG, M.K., MCCOY, T.J. & KROT, A.N. 2006. Systematics and Evaluation of Meteorite Classification. *In*: Lauretta, D. S. & McSween, H. Y. (eds) *Meteorites and the Early Solar System II*. Tucson : Houston, University of Arizona Press ; In collaboration with Lunar and Planetary Institute, The University of Arizona space science series, 19–52.

WELTEN, K.C. 1995. *Exposure Histories and Terrestrial Ages of Antarctic Meteorites*. University of Utrecht.

WELTEN, K.C., NISHIIZUMI, K., ET AL. 2006. Terrestrial ages, pairing, and concentration mechanism of Antarctic chondrites from Frontier Mountain, Northern Victoria Land. *Meteoritics & Planetary Science*, **41**, 1081–1094.

WELTEN, K.C., NISHIIZUMI, K., ET AL. 2008. The complex exposure histories of the Pitts and Horse Creek iron meteorites: Implications for meteorite delivery models. *Meteoritics & Planetary Science*, **43**, 1321–1332.

WIELER, R. & GRAF, T. 2001. Cosmic Ray Exposure History of Meteorites. *In*: Peucker-Ehrenbrink, B. & Schmitz, B. (eds) *Accretion of Extraterrestrial Matter Throughout Earth's History*. Boston, MA, Springer US, 221–240.

WLOTZKA, F. 1993. A Weathering Scale for the Ordinary Chondrites. *In*: *Meteoritics & Planetary Science*. 460–460.

ZOLENSKY, M.E., WELLS, G.L. & RENDELL, H.M. 1990. The accumulation rate of meteorite falls at the earth's surface - The view from Roosevelt County, New Mexico. *Meteoritics*, **25**, 11–17.

ZOLENSKY, M.E., BLAND, P.A., BROWN, P. & HALLIDAY, I. 2006. Flux of Extraterrestrial Materials. *In*: *Meteorites and the Early Solar System II*. The University of Arizona space science series, 869–888.

APPENDIX

APPENDIX A : Kohout et al. (2014)

The Meteoritical Society

Meteoritics & Planetary Science 1–14 (2014)
doi: 10.1111/maps.12325

Density, porosity, mineralogy, and internal structure of cosmic dust and alteration of its properties during high-velocity atmospheric entry

T. KOHOUT[1,2*], A. KALLONEN[1], J.-P. SUURONEN[1], P. ROCHETTE[3], A. HUTZLER[3], J. GATTACCECA[3,4], D. D. BADJUKOV[5], R. SKÁLA[2], V. BÖHMOVÁ[2], and J. ČUDA[6]

[1]Department of Physics, University of Helsinki, Helsinki 00014, Finland
[2]Institute of Geology, Academy of Sciences of the Czech Republic, Prague CZ-16502, Czech Republic
[3]Aix-Marseille Université/CNRS, CEREGE UM34, Aix-en-Provence 13545, France
[4]Department of Earth, Atmospheric, and Planetary Sciences, Massachusetts Institute of Technology, 77 Massachusetts Avenue, Cambridge, Massachusetts 02139, USA
[5]V. I. Vernadsky Institute of Geochemistry and Analytical Chemistry RAS, Moscow 119991, Russia
[6]Regional Centre of Advanced Technologies and Materials, Departments of Physical Chemistry and Experimental Physics, Palacky University Olomouc, Olomouc 78371, Czech Republic
[*]Corresponding author. E-mail: tomas.kohout@helsinki.fi

(Received 12 December 2013; revision accepted 06 May 2014)

Abstract–X-ray microtomography (XMT), X-ray diffraction (XRD), and magnetic hysteresis measurements were used to determine micrometeorite internal structure, mineralogy, crystallography, and physical properties at μm resolution. The study samples include unmelted, partially melted (scoriaceous), and completely melted (cosmic spherules) micrometeorites. This variety not only allows comparison of the mineralogy and porosity of these three micrometeorite types but also reveals changes in meteoroid properties during atmospheric entry at various velocities. At low entry velocities, meteoroids do not melt and their physical properties do not change. The porosity of unmelted micrometeorites varies considerably (0–12%) with one friable example having porosity around 50%. At higher velocities, the range of meteoroid porosity narrows, but average porosity increases (to 16–27%) due to volatile evaporation and partial melting (scoriaceous phase). Metal distribution seems to be mostly unaffected at this stage. At even higher entry velocities, complete melting follows the scoriaceous phase. Complete melting is accompanied by metal oxidation and redistribution, loss of porosity (1 ± 1%), and narrowing of the bulk (3.2 ± 0.5 g cm^{-3}) and grain (3.3 ± 0.5 g cm^{-3}) density range. Melted cosmic spherules with a barred olivine structure show an oriented crystallographic structure, whereas other subtypes do not.

INTRODUCTION

Cosmic dust recovered on Earth in the form of interplanetary dust particles (IDPs) and micrometeorites is, together with larger meteorites, a valuable source of primitive extraterrestrial material. The cosmic dust input to Earth is in the 5–300 t/d range, depending on the method of observation (Plane 2012). Micrometeorites and IDPs represent material released from asteroids and comets (e.g., Nesvorny et al. 2006; Nesvorný et al. 2010) into interplanetary space, material which carries important information about the composition and structure of asteroid surfaces and cometary dust. Thus, knowledge of the physical properties of cosmic dust is essential in interpreting the surface material and physical properties of asteroids and comets, as well as in modeling the atmospheric entry of cosmic dust (meteor phenomena).

The physical properties of larger, centimeter- to decimeter-sized extraterrestrial samples, meteorites, have undergone extensive study. Consolmagno et al. (2008) reviewed their bulk and grain density and porosity measured mostly using gas pycnometry and the Archimedean glass bead method.

Smaller, millimeter- to micrometer-sized interplanetary dust particles and micrometeorites have received much less study. Traditional measurement methods used on meteorites cannot be applied to these particles due to their small size. For this reason, little is known about the physical properties of cosmic dust.

Early research deduced the particle size and density of interplanetary dust from the morphology of micrometeorite impact craters on lunar rocks (e.g., Brownlee et al. 1976; Nagel et al. 1976). Either scanning electron microscopy (SEM) or synchrotron x-ray fluorescence (SXRF) later served to determine density and porosity of recovered IDPs and micrometeorites. Shape and volume were deduced from 2-D or stereo images, and mass was usually deduced from observed mineral grain sizes and their known mineralogical density or from SXRF data. Based on these methods, the average bulk density of cosmic dust is typically around 2 g cm^{-3} with most values between 0.6 and 5.5 g cm^{-3}. Flynn and Sutton (1991) reported a bimodal distribution (averaging 1–2 and 2.7 g cm^{-3}) for interplanetary dust. However, Love et al. (1994) reported a unimodal distribution averaging around 2 g cm^{-3}. Some dust particles have been found to have bulk densities as low as 0.3 and as high as 6.2 g cm^{-3}. While the mid-upper range of these values is similar to the bulk densities of meteorites, values below 1 g cm^{-3} are significantly lower, indicating porosities exceeding 50%. Published porosity values of IDPs show similarly wide variation. While Corrigan et al. (1997) reported porosity values between 0 and 10% (similar to that of larger chondritic meteorites), Rietmeijer and Nuth (2000) report densities as low as 0.1 g cm^{-3} for a few dust particles with porosities of up to 90%.

Recently, new methods such as X-ray microtomography (XMT, also known in the literature as μ-CT) have been employed (Okazawa et al. 2002; Tsuchiyama et al. 2004; Taylor et al. 2011). XMT scans provide fully 3-D volumetric X-ray attenuation maps of both the exterior and interior of the sample, providing a significant improvement over 2-D SEM imaging. However, XMT resolution with the majority of X-ray tube sources is limited to approximately 1 μm depending on the imaging geometry, the size of the source, and the resolution of the detector.

In this study, we present the physical properties, internal structure, and mineralogy derived from XMT scans and X-ray diffraction (XRD) measurements of 32 micrometeorites of various melted, partially melted and unmelted types. By comparing their properties, we evaluate changes in the physical properties of micrometeoroids as a function of their atmospheric velocity.

STUDY MATERIAL

Micrometeorites can be recovered from specific areas where they are concentrated or where they accumulate. Favorable concentration areas include sediments formed by melting ice caps (e.g., Maurette et al. 1987) or moraine sediments (e.g., Harvey and Maurette 1991). Areas of favorable accumulation include stable surfaces in desert settings, whether in Antarctica (Rochette et al. 2008) or in hot deserts (Gattacceca et al. 2011). In this study, we report measurements of the physical properties of cosmic dust in the form of 32 micrometeorites collected from the northern ice cap of the Novaya Zemlya archipelago in Russia (Badjukov and Raitala 2003; Badjukov et al. 2010) and from soils collected in the central depression of the Atacama desert (Gattacceca et al. 2011). Based on the classification by Genge et al. (2008), the collection includes various types of micrometeorites ranging from melted (glassy, porphyritic olivine, and barred olivine S-type [silicate] cosmic spherules) to partly melted (scoriaceous) to well-preserved unmelted ones (mostly fine grained).

INSTRUMENTS AND METHODS

XMT Measurements

The XMT scans were collected at the Department of Physics, University of Helsinki with custom-built Nanotom 180 NF tomography equipment (Phoenix|x-ray Systems and Services, part of GE Measurement Systems and Solutions, Germany, Fig. 1). Its high-voltage (20–180 kV) nanofocus X-ray tube and variable imaging geometry enable the XMT equipment to scan objects with a diameter from 10 cm to 50 μm, and with a submicron voxel size (the edge length of one cubic volume element) for objects smaller than 2 mm. All micrometeorites from the Atacama collection and micrometeorites 1–6 from the Novaya Zemlya collection were placed in conical plastic tubes, which were closed at one end, and secured with cotton. The plastic tubes were then glued to a sample holder and placed on a rotating stage. For the smaller micrometeorites (11–19 from the Novaya Zemlya collection), the plastic tube was omitted, and the micrometeorites were glued directly onto a carbon fiber sample holder with acetone-soluble glue. We measured one micrometeorite at a time and moved the rotation stage as close to the X-ray source as possible to maximize the magnification. The acquisition parameters varied slightly due to differences in measurement geometry resulting from small variations in the micrometeorite mounting. The X-ray tube acceleration voltage was 80 kV, and the tube

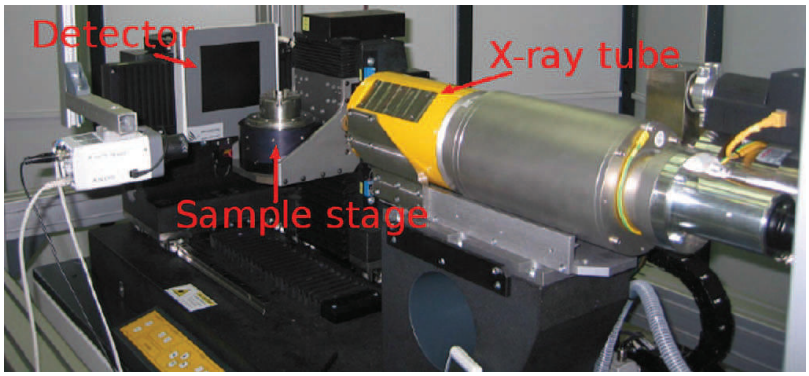

Fig. 1. The X-ray microtomography setup.

current was 180 μA. The micrometeorites were imaged over a full 360° circle with an angular step between 0.5° and 0.225° (corresponding to 720–1440 projection images). Each projection image was composed of an average of 8–16 transmission images, and exposure times for each transmission image varied between 500 and 2000 ms. The voxel sizes of the tomograms ranged from 0.63 to 0.25 μm, depending on the size of the micrometeorite. The resulting realistic resolution after 3D reconstruction is approximately 1 μm.

The methodology for processing XMT data is complex. Sixteen-bit integer (grayscale) volumes were reconstructed from the projection images with the datos|x software (Phoenix|x-ray) and digitally filtered to remove noise. On most samples, 3D median smoothing with a 3 × 3 × 3 or 5 × 5 × 5 voxel kernel was used. Gaussian smoothing with a 5 × 5 × 5 voxel kernel was used in the case of some cosmic spherules with initially good contrast and very low porosity (micrometeorites nos. 9.1 through 10.3). More sophisticated edge-preserving methods (5 × 5 × 5 voxel kernel bilateral or anisotropic diffusion filtering) were applied in the case of two unmelted micrometeorites (nos. 15 and 19) with noisier data and results were compared with the median smoothed data. It was found that the choice of filter did not significantly affect the results. The grain volume of the micrometeorites was calculated based on a manually selected gray value threshold, which separated dark (low gray value) areas representing empty space (both inside and outside the sample) from bright (high gray value) areas representing the solid micrometeorite material. One micrometeorite (no. 13) was found to contain large areas of intermediate gray value, interpreted as a partial volume effect due to pores that are smaller than the resolution of the scan. The grain volume included only a fraction of this semiporous phase, with the proportionality constant computed linearly from the respective gray values of the three phases (bulk, semi-porous, and pore space). We used two methods to calculate bulk volume. The first method incorporated a morphological closing followed by a hole-filling algorithm, which filled all pores not connected to the exterior.

The second method incorporated a convex hull algorithm. This convex hull method is suitable only for quasi-spherical objects (melted cosmic spherules or highly porous unmelted micrometeorites, such as micrometeorite 19), as it fills concave surface features and thus provides an upper limit for the bulk volume. Avizo Fire 7.0.1 software (Visualization Sciences Group) was used to compute the segmentation, morphological operations, and volume. The pore volume was then determined as the difference between the bulk and grain volumes. Our XMT scans have 10-fold higher resolution than scans in previous XMT studies of micrometeorites, such as Taylor et al. (2011), and are comparable to synchrotron source-based observations by Okazawa et al. (2002) and Tsuchiyama et al. (2004, 2011).

The mass of the larger micrometeorites (cosmic spherules) was measured using Sartorius M2P microbalance at 1 μg accuracy and precision. Subsequently, bulk and grain densities were calculated from the bulk and grain volumes and mass.

XRD Measurements

After XMT scanning, selected larger micrometeorites were investigated with XRD measurements, utilizing a second X-ray tube (IμS, Incoatec, Germany) and an area detector (Pilatus 1M, Dectris, Switzerland) incorporated into the XMT scanner. A detailed description of the combined XMT/XRD system is given in Suuronen et al. (2014). In brief,

the XRD measurements were performed using an approximately 200 × 200 μm^2 beam of molybdenum K_α-radiation (λ = 0.709 Å) and an area detector in perpendicular transmission geometry. Based on the XMT reconstruction, the beam was aimed at a specified subvolume of the micrometeorite (in most cases, the center of the micrometeorite) using the sample manipulator stage of the XMT scanner. The recorded scattering patterns were analyzed for mineralogical composition and degree of crystallite orientation in the micrometeorites with Matlab software, using the 111-diffraction peak from a silicon standard to determine the sample-to-detector distance. To sample a greater portion of the reciprocal space in the well-ordered micrometeorites, a second diffraction pattern was measured at a 90° angle to the first one.

Electron Microscopy

To verify the compositional results derived from XMT scans, three micrometeorites were analyzed using a TESCAN VEGA 3XM scanning electron microscope (SEM) with a Bruker QUANTAX200 energy dispersive X-ray spectrometer (EDS) and CAMECA SX-100 electron probe microanalyzer (microprobe) at the Institute of Geology, Academy of Sciences of the Czech Republic.

Magnetic Properties Measurements

Hysteresis properties were measured using a Princeton Measurements Model 3900 vibrating sample magnetometer (VSM) at the Department of Physics, University of Helsinki for the Novaya Zemlya, and at CEREGE, Aix-Marseille University for the Atacama collection. Hysteresis loops were measured up to ±1.2 T (±1 T for the Atacama collection) field. Correction for the paramagnetic component was subsequently applied. Magnetite content was calculated from the ratio of the saturation magnetization of the micrometeorite to the saturation magnetization of the magnetite (approximately 50 $Am^2\ kg^{-1}$).

RESULTS

Micrometeorite Texture and Structure

XMT revealed various textures and structures of the micrometeorites studied. Melted cosmic spherules in our collection include barred and cryptocrystalline olivine or glassy subtypes (Fig. 2). Three micrometeorites (nos. 9.3, 9.10, 10.4) contained coarse-grained inclusions most likely of relict material, and one micrometeorite (no. 4) contained a large metal inclusion. One cosmic spherule with a barred structure (no. 2) was polished and analyzed with SEM-EDS. Submicron magnetite grains within the olivine lamellae were identified (Fig. 3). The size of these magnetite grains is roughly equivalent to the XMT resolution, so they show only a grainy texture in the XMT images. Weathering of the spherules due to long-term exposure on the Earth's surface, as evidenced by a selective dissolution of lamellae at the surface of the spherules (nos. 2, 5, 10.5, and 10.9) or by a rim of different density and the textured material of some of the Atacama spherules (nos. 10.3, 10.11, 10.12, 10.13, and 10.14), does not seem pervasive.

Partly melted scoriaceous micrometeorites nos. 11, 14, and 16 (Fig. 4) show a relatively homogeneous silicate matrix with spherical vesicles of various sizes. Vesicles of submicron size (below the XMT resolution) are likely to exist within the micrometeorites, so the total porosity of the micrometeorites may be even higher. Micrometeorite no. 16 contains a bright metallic phase. A polished section of this micrometeorite was prepared and observed with a microprobe (Fig. 5). The matrix consisted of enstatite and low-Ca pyroxene, and the metallic phase was identified as FeNi metal (5–10 wt% Ni). The composition of this micrometeorite is similar to that of ordinary chondrites.

In addition to rounded vesicles, micrometeorite 14 contains linear cracks and thus seems to be not only scoriaceous, but also mechanically fractured. The micrometeorite also has an apparent magnetite rim (Fig. 4).

Unmelted micrometeorites nos. 12, 13, 15, 18, and 19 (Fig. 4) show various textures and structures from compact (with metal-rich inclusions observed in micrometeorite no. 12) to highly porous and fragmented (micrometeorite no. 19). A polished section of micrometeorite 12 was analyzed using a microprobe (Fig. 6) and hydrated silicates were found to be the main micrometeorite constituents. The bright phase in the BSE (backscattered electrons) images was identified as iron oxides. Sulfur was detected in the center of some bright phase grains, which points to their likely origin as oxidation products of troilite. In some unmelted micrometeorites, we observed a magnetite rim.

Mineralogy and Crystallography

A combination of the XRD and the magnetic hysteresis measurements permits the determination of the dominant mineralogical phases. From the XRD patterns (examples shown in Fig. 7), olivine was found to be the major constituent of all the cosmic spherules. One scoriaceous and one unmelted micrometeorite that we measured also contained olivine. The olivine

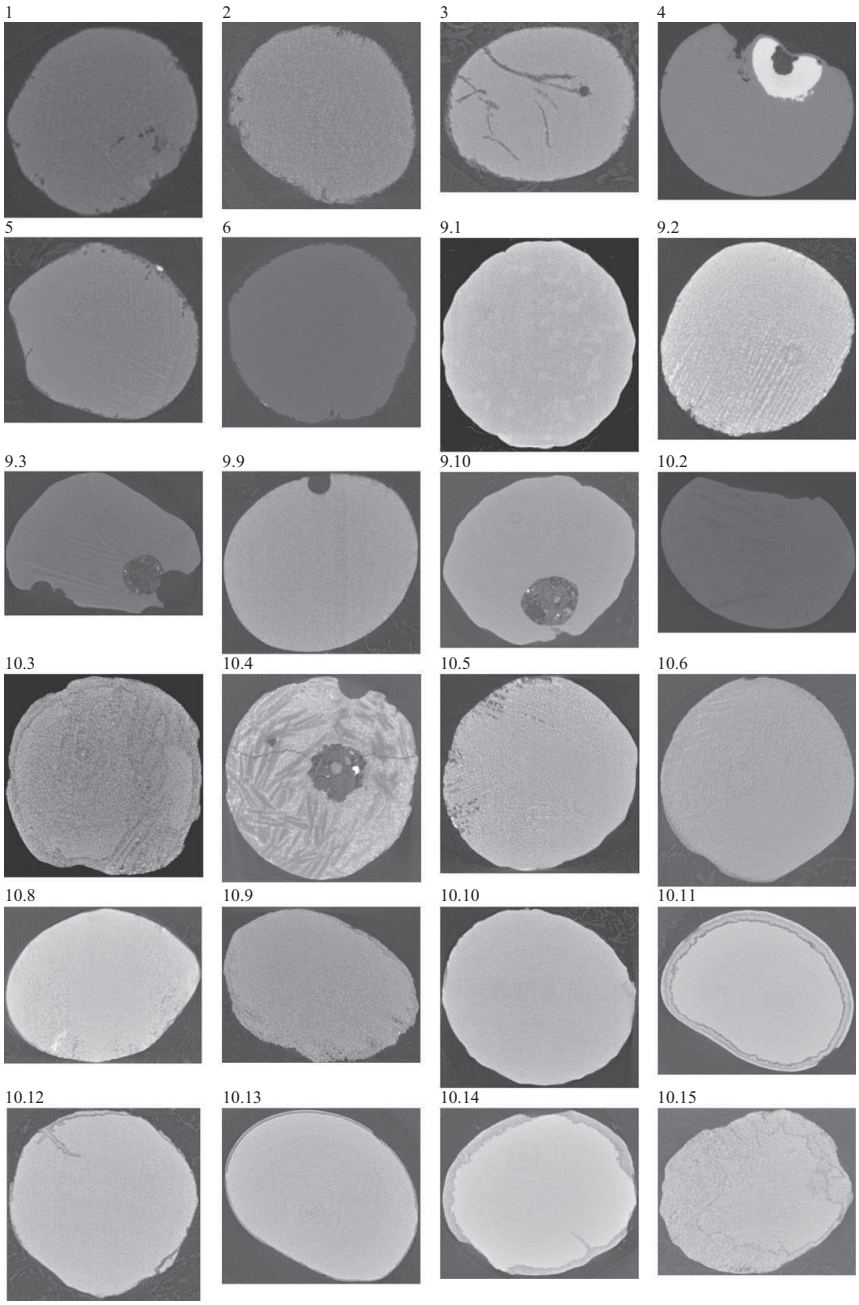

Fig. 2. Tomography sections of entirely melted micrometeorites (cosmic spherules). The weathering effects can be seen on some micrometeorites (partial dissolution extending from the surface on spherules nos. 2, 5, 10.5, and 10.9; weathering rim on spherules no. 10.3, 10.11, 10.12, 10.13, and 10.14). Micrometeorite size and origin are indicated in Table 1. Spherules nos. 9.3, 9.10, and 10.4 contain an inclusion—probably composed of pristine material.

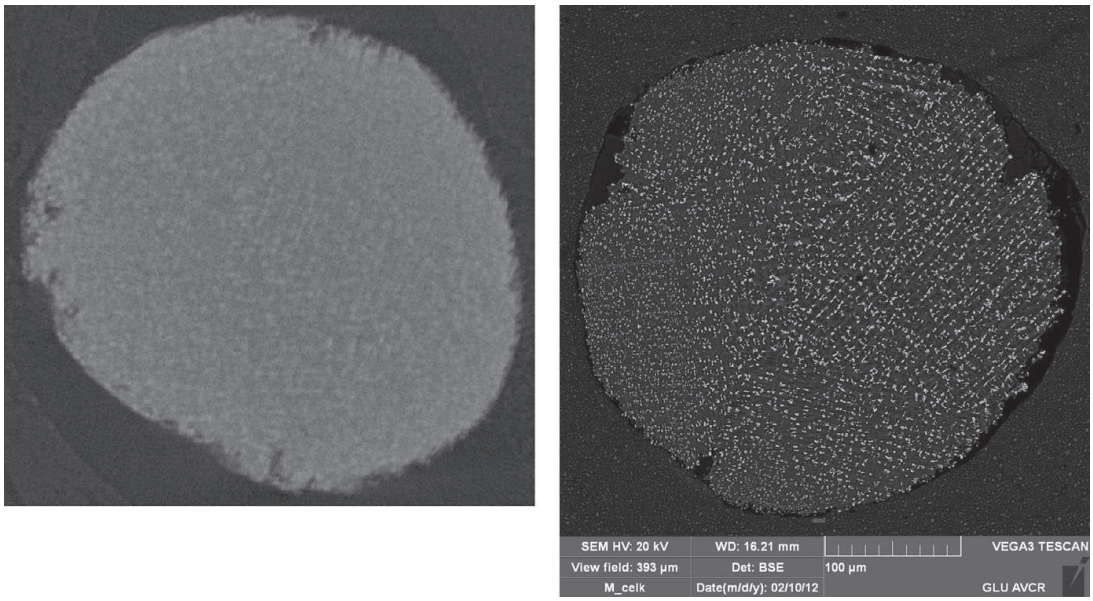

Fig. 3. Comparison of the cosmic spherule no. 2 tomography section (left) with electron microscope (backscattered electrons) image (right) of sample 2 (sections are not of the same orientation). The barred olivine structure with submicron magnetite grains can be observed.

compositions varied widely from Mg to Fe rich (Tables 1 and 2).

In some cosmic spherules, we observed a weak pattern of magnetite. Because we measured the XRD data in only one or two orientations, not all minor phases are necessarily detected in the XRD pattern. This is especially true for the micrometeorites with a high degree of crystallite orientation. As noted in the previous section, SEM-EDS analysis confirmed the presence of magnetite in one cosmic spherule. The measured saturation magnetization values support the presence of a ferromagnetic phase in most of the cosmic spherules, even in those in which the XRD showed no such phases (Tables 1 and 2).

One drawback of our XRD setup is its limited detection capability resulting from the measurement geometry. However, this measurement approach enables us to determine the level of preferred crystallographic orientation or randomization. An XRD pattern composed of localized point reflections is typical for a micrometeorite with a preferred orientation of its crystallographic structure. Micrometeorites with some variation in the crystalline orientation show short arcs in the XRD pattern, whereas an XRD pattern dominated by circles (resembling a powder diffraction pattern) is typical of polycrystalline micrometeorites with randomized crystallographic orientations. We observed all three types of the XRD patterns noted above (Fig. 8). In general, melted cosmic spherules with barred olivine structure show mostly preferred crystallographic orientations, whereas glassy cosmic spherules are mostly disoriented (Table 1). One partly melted scoriaceous micrometeorite showed a randomized pattern, and the one unmelted micrometeorite showed an oriented pattern (Table 2).

With cosmic spherules nos. 9.3 and 9.10, it was possible to aim X-ray beam on the inclusions within the spherule and compare the resulting XRD patterns and plots with those omitting the inclusion (Fig. 7). Figure 9 demonstrates the measurement geometry for spherule no. 9.3. This spherule shows an overall partly oriented pattern and spherule no. 9.10 shows an overall disoriented pattern. In both cases, additional weak point-like reflections (oriented pattern) related to presence of the inclusion are visible and additional peaks are observed in the identical regions of the XRD plots. It is impossible to identify corresponding mineral due to a low intensity of the inclusion signal.

Physical Properties

The physical properties of the micrometeorites are summarized in Tables 1 and 2 together with error estimates based on repeated measurements of selected

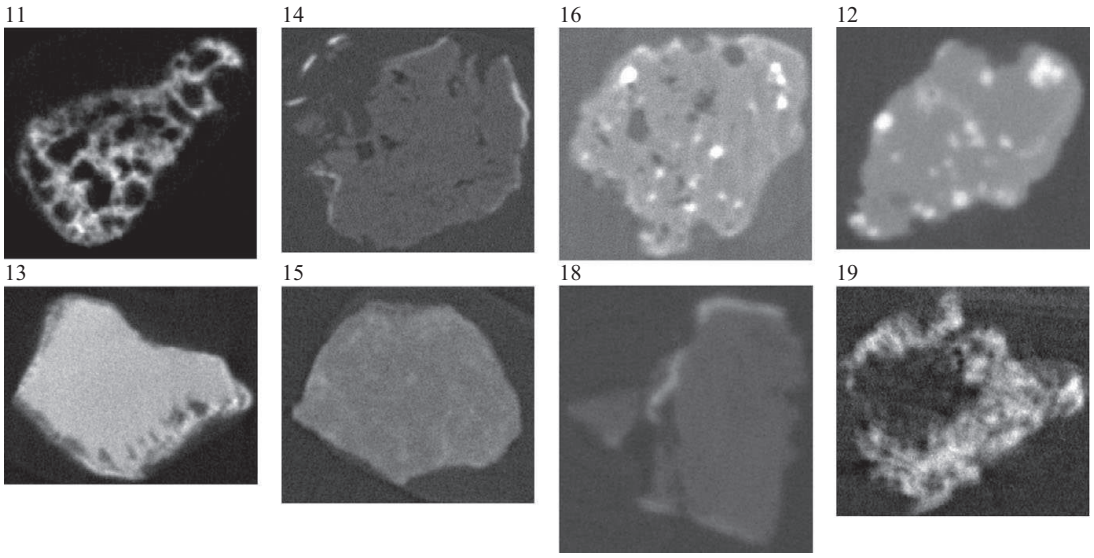

Fig. 4. Tomography sections of the partially melted (scoriaceous) micrometeorites nos. 11, 14, and 16 and unmelted micrometeorites nos. 12, 13, 15, 18, and 19. Micrometeorite size and origin are indicated in Table 2.

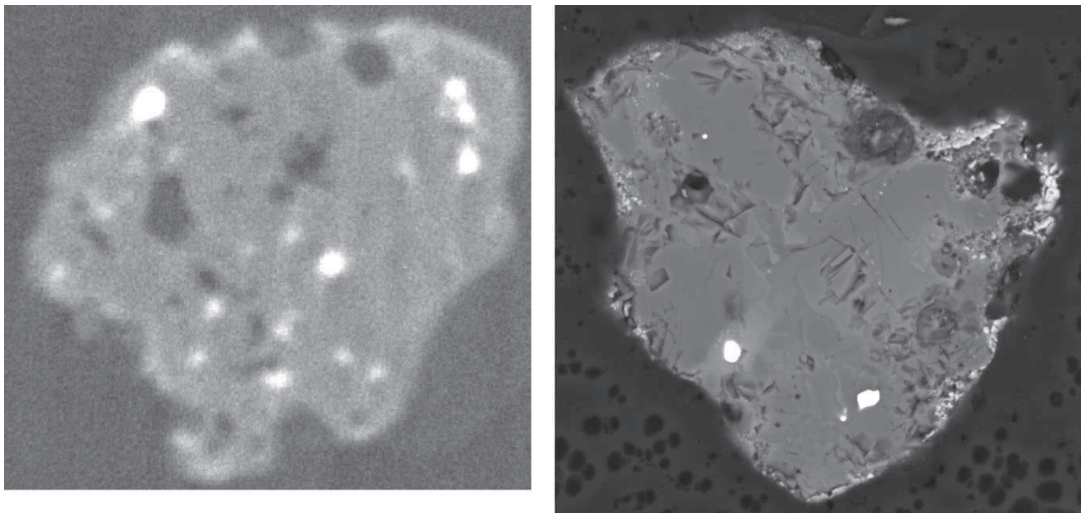

Fig. 5. Comparison of the micrometeorite no. 16 tomography section (left) with electron microscope (backscattered electrons) image (right, sections are not of the same orientation). The matrix is composed of enstatite and low-Ca pyroxene, while the bright fraction is FeNi metal. The magnetite rim surrounding the sample perimeter can be also seen.

micrometeorites. The physical properties of the cosmic spherules of melted silicate (S) type are quite uniform and reveal no apparent trends with subtypes (barred, cryptocrystalline olivine, or glassy) apart from the single porphyritic spherule (10.4) showing slightly higher porosity and grain density. The measured porosities were found to be low ($1 \pm 1\%$), and the bulk and grain densities were relatively uniform (3.2 ± 0.5 and 3.3 ± 0.5 g cm^{-3}, respectively) Only one spherule (no. 4) was found to be significantly denser (bulk and grain density 5.6 and 5.7 g cm^{-3}, respectively) due to the presence of a large metallic inclusion.

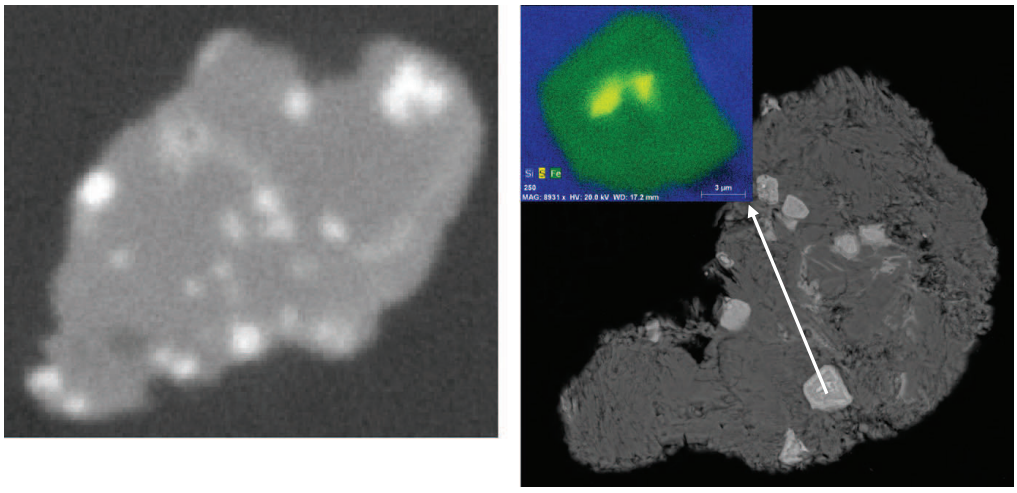

Fig. 6. Comparison of the micrometeorite no. 12 tomography section (left) with electron microscope (backscattered electrons) image (right, sections are not of the same orientation). The matrix is composed of hydrated silicates, while the bright fraction is iron oxides. Inset: In some of the oxide grains, sulfur can be found in their center (Fe: green, S: yellow, Si: blue).

With the partially melted, scoriaceous, and unmelted micrometeorites, it was only possible to determine the porosity. We could not determine density due to the small particle size. Scoriaceous micrometeorites have higher porosities, ranging from 16% up to 27% (Table 2). Pristine unmelted micrometeorites show wider variation in their porosity than do the previous two classes. The fine-grained unmelted micrometeorites typically have porosities in the range of 0–12% (Table 2). One highly porous fragmental micrometeorite (no. 19) has a porosity exceeding 50% (Fig. 10). This value represents the highest porosity in our data set.

In Table 2, a bulk and grain density estimate is given to one scoriaceous (no. 11) and one unmelted (no. 13) micrometeorite. The grain density is in this case inferred from observed mineralogy (4.0 g cm^{-3} for intermediate olivine and 3.5 g cm^{-3} for magnesium-rich olivine) and bulk density is subsequently calculated from grain density and observed porosity.

A complete set of all XMT and XRD figures and videos is available in Supporting Information section of the online version of the paper.

DISCUSSION

The physical properties of micrometeorites fall within the range of previously published values (Flynn and Sutton 1991 [unmelted IDPs], Love et al. 1994 [unmelted IDPs], Corrigan et al. 1997 [unmelted IDPs], Okazawa et al. 2002 [scoriaceous and unmelted micrometeorites], Tsuchiyama et al. 2004 [scoriaceous and unmelted micrometeorites], Taylor et al. 2011 [all micrometeorite types], Tsuchiyama et al. 2011 [Itokawa regolith particles]). Our micrometeorite set contains examples of melted, partially melted, and unmelted cosmic dust particles and the observed trends in porosity (low porosity of melted micrometeorites, high porosity of scoriaceous micrometeorites, and high porosity variations among unmelted ones) are consistent with these studies. In this work, we measured all micrometeorites with the same instrumentation and methodology, thereby enabling direct comparison of various types.

Comparing the physical properties, especially the porosity, of cosmic spherules (melted micrometeorites) with those of partially melted or unmelted meteorites enables us to evaluate changes in meteoroid properties as a function of the atmospheric entry velocity and angle (Fig. 11). Unmelted micrometeorites represent nearly pristine cosmic dust which entered the atmosphere slowly, typically between 11.2 and 15 km s^{-1} and at a rather shallow entry angle (Love and Brownlee 1991). Thermal changes, if any, are limited to the presence of the magnetite rim at the perimeter of some micrometeorites (Fig. 4). Such a magnetite rim is analogous to the fusion crusts covering a pristine meteorite interior of larger meteorites. The physical properties of these micrometeorites remain nearly unchanged and are representative of the cosmic dust in Earth's vicinity. These micrometeorites seem to be rather heterogeneous with a widely variable porosity (0–12%). This is within

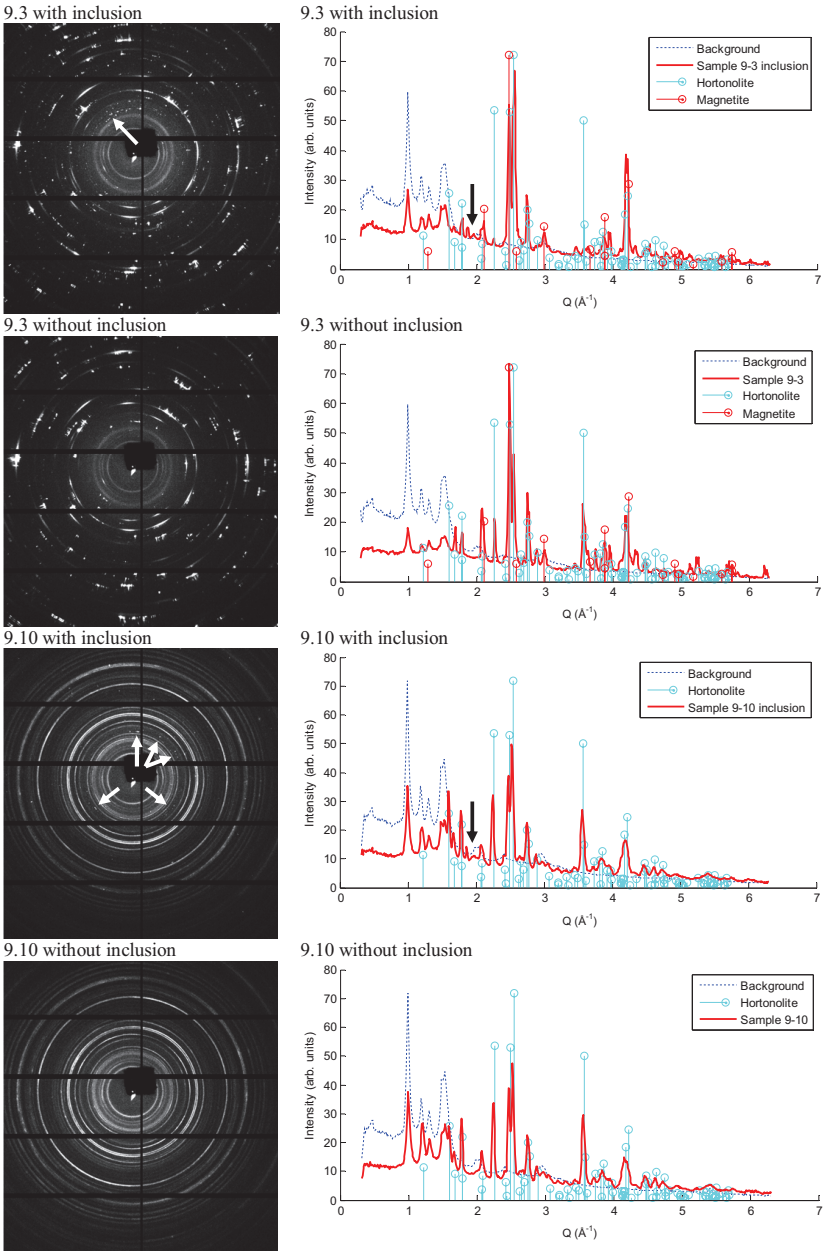

Fig. 7. Comparison of the cosmic spherules nos. 9.3 and 9.10 X-ray diffraction patterns and plots focused on the inclusion (left) with the ones offset from it (right). Additional point-like reflections originating from the inclusion are marked with arrows.

Table 1. List of cosmic spherules with their physical properties, mineralogy, and tentative classification. Approximate size is a rough approximation of the mean diameter. Mass is given with 1 μg accuracy and bulk volume is given up to two significant digits.

Micrometeorite number	Type	Origin	Approximate size (μm)	Mass (μg)	V_B (10^6 μm^3)	ρ_B (g cm^{-3})	ρ_G (g cm^{-3})	p (%)	Mineralogy major	Mineralogy minor	M_s (Am^2 kg^{-1})	Mt (wt%)	Structure
1	S-BO	NZ	320	53	16	3.5	3.6	1	Ol (Mg)	Mt			O
2	S-BO	NZ	390	86	24	3.6	3.7	2	—	—	9.0	18	—
3	S-BO	NZ	170	93	28	3.4	3.4	1	—	—	8.2	16	—
4	S-PO	NZ	190	181	32	5.6	5.7	0	—	—	22.7	45	—
5	S-G	NZ	330	61	19	3.3	3.4	3	—	—	5.1	10	—
6	S-G	NZ	450	125	38	3.3	3.4	1	—	—	5.6	11	—
9.1	S-PO	AT	630	326	110	3.0	3.0	0	Ol (int.)	n.d.	4.0	8	RO
9.2	S-BO	AT	530	235	73	3.2	3.2	1	Ol (Mg)	Mt	8.1	16	O
9.3	S-BO, rel	AT	850	489	170	2.9	2.9	1	Ol (int.)	Mt	5.0	10	PO
9.9	S-BO	AT	550	254	81	3.1	3.1	0	Ol (Mg)	Mt	5.8	12	O
9.10	S-G, rel	AT	590	258	87	3.0	3.0	1	Ol (int.)	n.d.	2.0	4	RO
10.2	S-BO	AT	610	254	83	3.0	3.0	0	Ol (int.)	n.d.	2.8	6	O
10.3	S-BO	AT	670	353	120	3.1	3.1	0	Ol (Fe)	Mt	8.3	17	O
10.4	S-PO, rel	AT	720	501	166	3.0	3.2	5	Ol (int.)	Mt	4.8	10	O
10.5	S-BO	AT	670	398	124	3.2	3.2	1	Ol (int.)	Mt	8.4	17	O
10.6	S-BO	AT	710	310	102	3.0	3.0	0	Ol (int.)	Mt	9.6	19	O
10.8	S-BO	AT	630	265	80	3.3	3.3	0	Ol (Fe)	Mt	15.8	32	O
10.9	S-BO	AT	680	338	110	3.1	3.1	0	Ol (int.)	Mt	10.1	20	O
10.10	S-G	AT	550	247	82	3.0	3.0	0	Ol (int.)	Mt	3.7	7	RO
10.11	S-G	AT	670	292	102	2.9	2.9	0	Ol (int.)	Mt	7.4	15	RO
10.12	S-G	AT	600	300	97	3.1	3.1	1	Ol (int.)	Mt	5.0	10	RO
10.13	S-G	AT	700	405	135	3.0	3.0	1	Ol (int.)	Mt	2.0	4	RO
10.14	S-G	AT	630	266	91	2.9	2.9	0	Ol (int.)	Mt	5.1	10	PO
10.15	S-BO	AT	600	236	81	2.9	2.9	0	Ol (int.)	Mt	11.0	22	O
Error				±1	±1	±0.1	±0.1	±3			±0.1	±1	

CS = cosmic spherule, BO = barred olivine, G = glass, PO = porphyritic olivine, rel = containing relict grain(s), NZ = Novaya Zemlya, AT = Atacama, V_B = bulk volume, ρ_B = bulk density, ρ_G = grain density, p = porosity, Ol (Fe) = iron-rich olivine, Ol (Mg) = magnesium-rich olivine, Ol (int.) = intermediate olivine, Mt = magnetite, O = preferred orientation of the crystallographic structure, PO = partly oriented crystallographic structure, RO = randomized crystallographic structure, n.d. = not determined.

Table 2. List of partially melted and unmelted micrometeorites with their physical properties, mineralogy, and tentative classification. Approximate size is a rough approximation of the mean diameter. Bulk volume is given up to two significant digits.

Micrometeorite number	Type	Origin	Approximate size (μm)	Mass (μg)	V_B (10^6 μm^3)	ρ_B (g cm^{-3})	ρ_G (g cm^{-3})	p (%)	Mineralogy major	Mineralogy minor	Structure
11	PM-Sc	NZ	230	—	1.6	3.0	4.0	25	Ol (int.)	n.d.	RO
14	PM-Sc	NZ	160	—	1.3	—	—	27	—	—	—
16	PM-Sc	NZ	170	—	1.4	—	—	16	—	—	—
12	UM-Fg	NZ	210	—	2.8	—	—	0	—	—	—
13	UM-Fg	NZ	230	—	1.0	3.1	3.5	12	Ol (Mg)	Mt	O
15	UM-Fg	NZ	170	—	—	—	—	0	—	—	—
18	UM-Fg	NZ	120	—	0.55	—	—	9	—	—	—
19	UM-P	NZ	150	—	1.2	—	—	51	—	—	—
Error					±0.2	±0.3	±0.3	±5			

PM = partially melted, UM = unmelted, Sc = scoriaceous, Fg = fine grained, P = porous, NZ = Novaya Zemlya, V_B = bulk volume, ρ_B = bulk density, ρ_G = grain density, p = porosity, Ol (Mg) = magnesium-rich olivine, Ol (int.) = intermediate olivine, Mt = magnetite, O = preferred orientation of the crystallographic structure, RO = randomized crystallographic structure, n.d. = not detected.

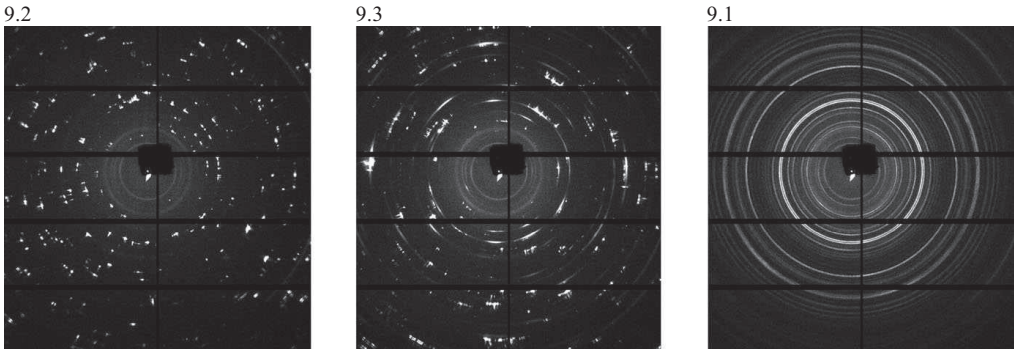

Fig. 8. Examples of X-ray diffraction patterns of cosmic spherules with preferred orientation of the crystallographic structure (no. 9.2), partly oriented crystallographic structure (no. 9.3), and randomized crystallographic orientations (no. 9.1).

range of various chondritic meteorites (Consolmagno et al. 2008) and thus may resemble meteorite fine-grained matrix. The highly porous micrometeorite (no. 19) with porosity around 50% represents a class of its own and its appearance resembles dust aggregate particles similar to those experimentally prepared by Wurm and Blum (1998). Unfortunately, we were not able to determine its mineralogy due to its small size.

Partially melted, scoriaceous micrometeorites represent dust particles that enter the atmosphere at slightly higher velocities, typically in the range of 12–20 km s^{-1} and at steeper entry angles (Love and Brownlee 1991). Whereas fragmental micrometeorites such as no. 19 would likely disintegrate completely during entry under such conditions, more compact micrometeorites survive the greater heating and stress. The heat generated during meteoroid deceleration partially melts and evaporates volatiles, resulting in the growth of large vesicles within the silicate matrix. However, the extent of melting is insufficient to cause homogenization of the meteoroid, oxidation of metal (FeNi metal is preserved in the micrometeorite no. 16, Fig. 5), or to change its shape from irregular to quasi-spherical, but partial melting does result in higher micrometeorite porosity (25–30%).

In contrast, cosmic spherules (melted micrometeorites) represent dust particles entering the atmosphere at high velocities, typically over 15 km s^{-1} and at steeper angles (Love and Brownlee 1991). Heating during atmospheric entry completely melts the meteoroid, causes loss of up to half of its initial mass, and changes its shape to a droplet-like quasi-sphere (Love and Brownlee 1991). Meteoroid homogenization and metal oxidation into magnetite lower and narrow the range of the bulk (3.2 ± 0.5 g cm^{-3}) and grain (3.3 ± 0.5 g cm^{-3}) densities and reduce the porosity. Thus, density and porosity values are lower compared with chondritic meteorites (Consolmagno et al. 2008)

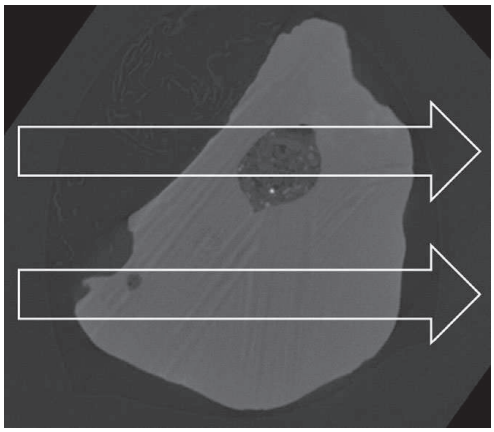

Fig. 9. The measurement geometry of the cosmic spherule no. 9.3 with X-ray paths aimed at and omitting the inclusion.

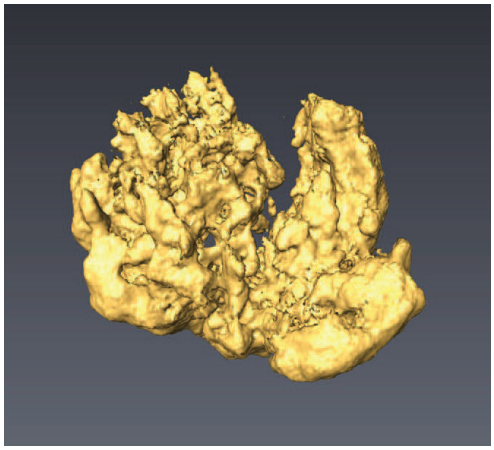

Fig. 10. Surface rendering of the fragmental unmelted micrometeorite no. 19.

or chondritic (LL) Itokawa regolith particles (Tsuchiyama et al. 2011). The compact nature of the cosmic spherules resembles chondrules (being melt product, however, in different red-ox conditions) rather than chondritic matrix. The spherule no. 4 has higher densities (bulk and grain density 5.6 and 5.7 g cm^{-3}, respectively) similar to stony-iron meteorites (Consolmagno et al. 2008) due to presence of a large metallic inclusion.

We must therefore bear in mind that the melted cosmic spherules could originally have been more porous, larger, and of a wider density range (as unmelted cosmic dust particles are). Upon atmospheric entry, their porosity most likely increases initially, when partial melting occurs (scoriaceous phase), and is subsequently lost as the micrometeorites reach an entirely melted stage and solidify into spherules. Based on modeling by Love and Brownlee (1991), this transformation lasts only for the first few seconds.

Our micrometeorite density and porosity values also reveal similarities to those of shower and sporadic meteoroids derived from camera observations. Babadzhanov and Kokhirova (2009) report grain densities ranging from 2.2 to 3.4 g cm^{-3} and porosities ranging from 0 to 83% for shower meteoroids. Borovička et al. (2010) report porosities in similar range. Babadzhanov (2001) and Bellot Rubio et al. (2002) report lower bulk density values of 0.4–2.9 and 0.45–1.9 g cm^{-3}, respectively, requiring most likely significant porosity. Our values also most closely resemble the bulk density and porosity values of group I (3.7 g cm^{-3}, approximately 0%) and group II (2.07 g cm^{-3}, approximately 50%) meteoroids described in Ceplecha et al. (1993) and ReVelle (2001). Through comparison of these values with our results, we conclude that these meteors in their luminous phase represent either scoriaceous phase (meteors with densities below 3 g cm^{-3}, and significant porosity, e.g., group II) or the terminal molten phase (meteors with densities over 3.7 g cm^{-3} and absent porosity, e.g., group I). This comparison is valid for meteoroids of similar size to the studied micrometeorites.

CONCLUSIONS

The described XMT, XRD, and magnetic hysteresis methodology enables imaging of the internal structure of micrometeorites, as well as determination of the mineralogy, crystallography, and physical properties at approximately μm resolution. Our study sample set consists of unmelted, partially (scoriaceous) melted, and completely melted (cosmic spherules) micrometeorites, which allows comparison of the mineralogy and porosity of these three types of micrometeorites, as well as revealing changes in meteoroid properties during atmospheric entry at various velocities. At low velocities, the meteoroid does not melt, and its physical properties do not change significantly. At higher velocities, meteoroid porosity increases due to the evaporation of volatiles and partial melting (scoriaceous phase). Metal distribution seems largely unaffected at this stage. At even higher velocities, complete melting follows the scoriaceous phase, accompanied by metal oxidation and redistribution, loss of porosity, and narrowing of the

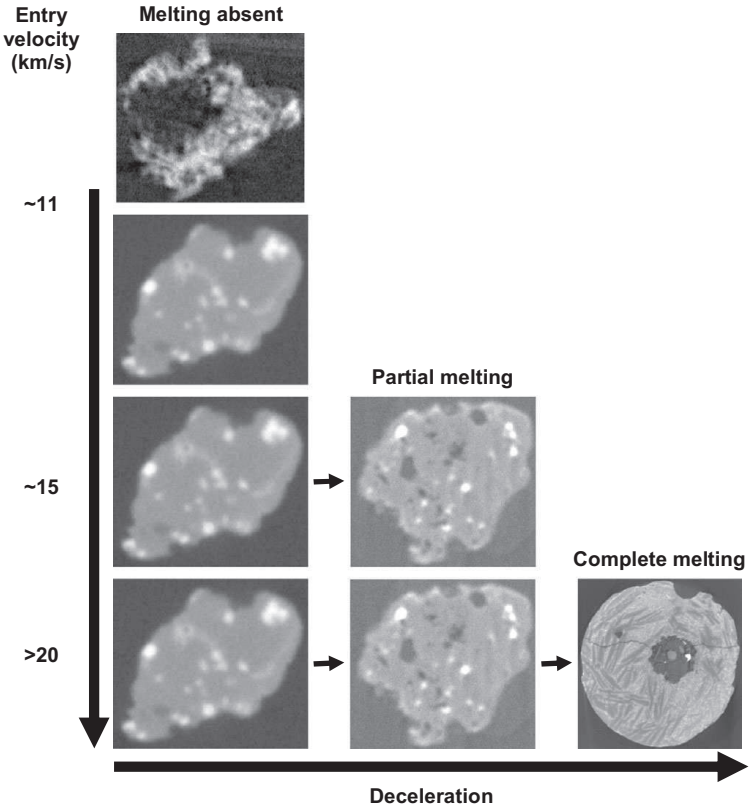

Fig. 11. Evolution of meteoroid physical properties as a function of its entry velocity.

density range. Melted cosmic spherules with a barred olivine structure show a preferred orientation in their crystallographic structure, whereas glassy cosmic spherules are mostly disoriented. Inclusions present in some cosmic spherules show an oriented crystallographic structure. The porosity behavior (initial increase followed by total loss during high velocity entry) is an especially important fact for consideration in modeling meteor phenomena.

Acknowledgments—We would like to thank to the reviewers Daniel Britt and Joe Friedrich for constructive comments on the manuscript and to associate editor Mike Zolensky for editorial handling. This work is supported by Academy of Finland project No. 257487 and Ministry of Education, Youth and Sports of the Czech Republic grant No. LH12079. We are also thankful for support from the Operational Program Research and Development for Innovations–European Regional Development Fund (CZ.1.05/2.1.00/03.0058) and Operational Program Education for Competitiveness–European Social Fund (CZ.1.07/2.3.00/20.0017, CZ.1.07/2.3.00/20.0170, CZ.1.07/2.3.00/20.0155, and CZ.1.07/2.3.00/20.0056) of the Ministry of Education, Youth and Sports of the Czech Republic.

Editorial Handling—Dr. Michael Zolensky

REFERENCES

Babadzhanov P. B. 2001. Fragmentation and densities of meteoroids. *Astronomy & Astrophysics* 384:317–321. doi:10.1051/0004-6361:20020010.

Babadzhanov P. B. and Kokhirova G. I. 2009. Densities and porosities of meteoroids. *Astronomy & Astrophysics* 495:353–358. doi:10.1051/0004-6361:200810460.

Badjukov D. D. and Raitala J. 2003. Micrometeorites from the northern ice cap of the Novaya Zemlya archipelago,

Russia: The first occurrence. *Meteoritics & Planetary Science* 38:329–340.
Badjukov D. D., Brandstätter F., Raitala J., and Kurat G. 2010. Basaltic micrometeorites from the Novaya Zemlya glacier. *Meteoritics & Planetary Science* 45:1502–1512. doi:10.1111/j.1945-5100.2010.01125.x.
Bellot Rubio L. R., Martínez González M. J., Ruiz Herrera L., Licandro J., Martínez-Delgado D., Rodríguez-Gil P., and Serra-Ricart M. L. 2002. Modeling the photometric and dynamical behavior of Super-Schmidt meteors in the Earth's atmosphere. *Astronomy & Astrophysics* 389:680.
Borovička J., Koten P., Spurný P., Čapek D., Shrbený L., and Štork R. 2010. Material properties of transition objects 3200 Phaethon and 2003 EH_1. *Icy Bodies of the Solar System, Proceedings of the International Astronomical Union, IAU Symposium* 263(5):218–222. doi:10.1017/S174392131000178X.
Brownlee D. E., Hörz F., Tomandl D. A., and Hodge P. W. 1976. Physical properties of interplanetary grains. In *The study of Comets, part 2*, edited by Donn B., Mumma M., Jackson W., A'Hearn M., and Harrington R. Washington, D.C.: NASA Goddard Space Flight Center. pp. 962–982.
Ceplecha Z., Spurný P., Borovička J., and Keclikova J. 1993. Atmospheric fragmentation of meteoroids. *Astronomy & Astrophysics* 279:615.
Consolmagno G., Britt D., and Macke R. 2008. The significance of meteorite density and porosity. *Chemie der Erde* 68:1–29. doi:10.1016/j.chemer.2008.01.003.
Corrigan C. M., Zolensky M. E., Dahl J., Long M., Weir J., Sapp C., and Burkett P. J. 1997. The porosity and permeability of chondritic meteorites and interplanetary dust particles. *Meteoritics & Planetary Science* 32:509–515.
Flynn G. J. and Sutton S. R. 1991. Cosmic dust particle densities—Evidence for two populations of stony micrometeorites. Proceedings, 21st Lunar and Planetary Science Conference. pp. 541–547.
Gattacceca J., Valenzuela M., Uehara M., Jull T., Giscard M., Rochette P., Braucher R., Suavet C., Gounelle M., Morata D., Munayco P., Bourot-Denise M., Demory F., and Bourlès D. 2011. The densest meteorite collection area in hot deserts: The San Juan meteorite field (Atacama Desert, Chile). *Meteoritics & Planetary Sciences* 46:1276–1287.
Genge M. J., Engrand C., Gounelle M., and Taylor S. 2008. The classification of micrometeorites. *Meteoritics & Planetary Science* 43:497–515.
Harvey R. P., and Maurette M. 1991. The origin and significance of cosmic dust from the Walcott Neve, Antarctica. Proceedings, 21th Lunar and Planetary Science Conference. pp. 569–578.
Love S. G. and Brownlee D. E. 1991. Heating and thermal transformation of micrometeoroids entering the earth's atmosphere. *Icarus* 89:26–43.
Love S. G., Joswiak D. J., and Brownlee D. E. 1994. Densities of stratospheric micrometeorites. *Icarus* 111:227–236.
Maurette M., Jehanno C., Robin E., and Hammer C. 1987. Characteristics and mass distribution of extraterrestrial dust from the Greenland ice cap. *Nature* 328:699–702.
Nagel K., Neukum G., Fechtig H., and Gentner W. 1976. Density and composition of interplanetary dust particles. *Earth and Planetary Science Letters* 30:234–240.
Nesvorný D., Vokrouhlický D., Bottke W. F., and Sykes M. 2006. Physical properties of asteroid dust bands and their sources. *Icarus* 181:107–144.
Nesvorný D., Jenniskens P., Levison H. F., Bottke W. F., Vokrouhlický D., and Gounelle M. 2010. Cometary origin of the zodiacal cloud and carbonaceous micrometeorites. Implications for hot debris disks. *The Astrophysical Journal* 713:816–836. doi:10.1088/0004-637X/713/2/816.
Okazawa T., Tsuchiyama A., Yano H., Noguchi T., Osawa T., Nakano T., and Uesugi K. 2002. Measurement of densities of Antarctic micrometeorites using X-ray microtomography. *Antarctic Meteorites* XXVII: 137–139.
Plane J. M. C. 2012. Cosmic dust in the earth's atmosphere. *Chemical Society Reviews* 41:6507–6518. doi:10.1039/c2cs35132c.
ReVelle D. O. 2001. Bolide dynamics and luminosity modeling: Comparisons between uniform bulk density and porous meteoroid models. In *Proceedings of the Meteoroids 2001 Conference*, edited by Warmbein B. ESA-SP 495, Kiruna, Sweden, 513–517.
Rietmeijer F. J. M. and Nuth J. A. 2000. Collected extraterrestrial materials: Constraints on meteor and fireball compositions. *Earth, Moon and Planets* 82–83: 325–350.
Rochette P., Folco L., Suavet C., van Ginneken M., Gattacceca J., Perchiazzi N., Braucher R., and Harvey R. P. 2008. Micrometeorites from the transantarctic mountains. *Proceedings of the National Academy of Sciences* 105:18206–18211. doi:10.1073/pnas.0806049105.
Suuronen J.-P., Kallonen A., Hänninen V., Blomberg M., Hämäläinen K., and Serimaa R. 2014. Bench-top x-ray microtomography complemented with spatially localized x-ray scattering experiments. *Journal of Applied Crystallography* 47:471–475. doi:10.1107/S1600576713031105.
Taylor S., Jones K. W., Herzog G. F., and Hornig C. E. 2011. Tomography: A window on the role of sulfur in the structure of micrometeorites. *Meteoritics & Planetary Science* 46:1498–1509.
Tsuchiyama A., Okazawa T., Noguchi T., Yano H., Osawa T., Nakamura T., Nakamura K., Nakano T., Uesugi K., and Yasuda H. 2004. Density and porosity measurement of Antarctic micrometeorites using microtomography. *Meteoritics & Planetary Science* 39:A107.
Tsuchiyama A., Uesugi M., Matsushima T., Michikami T., Kadono T., Nakamura T., Uesugi K., Nakano T., Sandford S. A., Noguchi R., Matsumoto T., Matsuno J., Nagano T., Imai Y., Takeuchi A., Suzuk Y., Ogami T., Katagiri J., Ebihara M., Ireland T. R., Kitajima F., Nagao K., Naraoka H., Noguchi T., Okazaki R., Yurimoto H., Zolensky M. E., Mukai T., Abe M., Yada T., Fujimura A., Yoshikawa M., and Kawaguchi J. 2011. Three-Dimensional Structure of Hayabusa Samples: Origin and Evolution of Itokawa Regolith. *Science* 26:1125–1128. doi:10.1126/science.1207807
Wurm G. and Blum J. 1998. Experiments on preplanetary dust aggregation. *Icarus* 132:125–136. doi:10.1006/icar.1998.5891.

SUPPORTING INFORMATION

Additional supporting information may be found in the online version of this article:

Appendix S1: A complete set of all XMT and XRD figures and videos.

APPENDIX B: Pairing meteorites (Matlab).

Fonction de pairing

```
% Ce programme calcule des facteurs d'appariement pour des météorites, à partir de la donnée
% de certains paramètres (position, type pétro, etc.) pour ces météorites.

% - Ne pas oublier d'importer MatrixData, matrice de données, avec les paramètres en colonnes et
% les météorites en lignes. Les trois premières colonnes doivent être dévolues  à la latitude, la
% longitude et l'altitude.
% - Ne pas oublier de vérifier que pour chaque paramètre, une fonction de calcul a été définie
% (sinon, par défaut, la fonction est constante égale à 1).

s=size(MatrixData)
nl=s(1)
nc=s(2)

Seuil = 0.85

% Seuil est la valeur au-dessus de laquelle un facteur final d'appariement est considéré
% suffisant pour que les météorites soient appariables.

PoidsParametres = input(['Veuillez indiquer les poids des paramètres par un vecteur de taille '
num2str(nc) ' : '], 's')

% Le vecteur PoidsParametres attribue un poids à chaque type de données, poids qui sera utilisé
% dans le calcul de la moyenne géométrique des facteurs partiels. Le même poids doit être
% attribué aux trois premières colonnes, qui correspondent à la distance entre les météorites.
% Si le poids est de 0, la donnée ne sera pas considérée.

PoidsParametres = str2num(PoidsParametres)

mat=zeros(nl,nl)
mat2=zeros(nl,nl)

% Ces matrices accueilleront les résultats de l'algorithme.

for i = 1:nl
   for k = 1:nc
      if MatrixData(i,k) == 9999
            IsDataAvailable(i,k) = 0;
      else
         IsDataAvailable(i,k) = 1;
      end
   end
end
```

```
% Toute donnée non disponible pour une météorite doit être signalée dans MatrixData par la
% valeur 9999. Cette valeur est détectée, et reportée par un 0 dans IsDataAvailable (les données
% disponibles étant indiquées par des 1), qui est une matrice de la même taille que Matrixdata.

if PoidsParametres(1) > 0
   for i = 1:nl
      for j = 1:nl
         par(i,j,3) = DistanceVersFacteur(CoordonneesVersDistance(MatrixData(i,1),
MatrixData(j,1), MatrixData(i,2), MatrixData(j,2), MatrixData(i,3), MatrixData(j,3)));
      end
   end
else
   par(:,:,3) = ones (nl,nl)
end

% Si la distance n'a pas reçu de poids nul, on applique les fonctions CoordonneesVersDistance
% puis DistanceVersFacteur aux coordonnées de chaque paire de météorites. Les résultats, des
% facteurs partiels d'appariement, sont stockés dans le tableau par(.,.,3). Sinon, on y stocke des
% 1.

for k=4:nc

% Tous les autres paramètres se traitent de la même manière. C'est l'objet de cette boucle.

   if PoidsParametres(k) > 0
      for i=1:nl
         for j=1:nl

% On traite, pour chaque paramètre à poids positif, tous les couples de météorites possibles.

            BoolCalc = IsDataAvailable(i,k)*IsDataAvailable(j,k);
            if BoolCalc == 1

% Pour chaque couple, on vérifie que la donnée est disponible pour les deux grâce à
% IsDataAvailable,ce que transcrit le booléen BoolCalc.

            par(i,j,k) = (ParametresVersFacteurs (MatrixData(i,k), MatrixData(j,k),
k))^(PoidsParametres(k));
            else
            par(i,j,k) = 1;

% SI les données sont disponibles , on utilise la fonction ParametresVersFacteurs pour
% obtenir un facteur partiel brut, que l'on élève à une puissance correspondant à son poids.
% Sinon, on prend un facteur égal à 1.

            end
         end
      end
   else
   par(:,:,k)= ones(nl,nl);
   end
```

```
 par
 end

% Si le poids est nul, on prend directement la valeur 1 pour s'épargner des calculs. A ce stade, on
% a calculé pour chaque couple et chaque donnée un facteur.

for i=1:nl
   for j=1:nl
      for k=3:nc-1
         par(i,j,k+1)=par(i,j,k)*par(i,j,k+1);

% Pour chaque couple, on multiplie entre eux tous les facteurs partiels, stockés en par( ., ., nc)

      end
      ComputedData = IsDataAvailable(i,:).*IsDataAvailable(j,:).*PoidsParametres;
      NbComputedData = sum(ComputedData) - (2* PoidsParametres(1));
      mat(i,j)=par(i,j,nc)^(1/NbComputedData);
   end
end

% On calcule ensuite pour chaque couple le nombre n(i,j) de données (pondérées) utilisées pour
% le calcul, en prenant en compte les données éventuellement indisponibles. On prend alors la
% racine n-ème du facteur calculé. On obtient ainsi la moyenne géométrique pondérée des
% facteurs partiels.

for i = 1:nl
   for j = 1:nl
      if mat(i,j) > (Seuil)
      mat2(i,j) = 1;
      end
   end
end

% La matrice mat contenant les résultats calculés précédemment, on remplit ensuite la matrice
% mat2 en regardant pour chaque couple si le facteur calculé est au-dessus du seuil.

mat
mat2

% On renvoie ensuite les résultats.

fid=fopen('Resultats.txt','w');
for i = 1:nl
   for j = 1:nl
   fprintf(fid,'%d\t' , mat(i,j));
   end
   fprintf(fid,'\n');
end
fclose(fid);

% Cette partie du code sert à transcrire la matrice mat des facteurs finaux dans un fichier texte
```

```
% appelé Resultats, qui doit être dans le dossier où se trouvent les codes.

fid=fopen('Resultats2.txt','w');
for i = 1:nl
   for j = 1:nl
   fprintf(fid,'%d\t' , mat2(i,j));
   end
   fprintf(fid,'\n');
end
fclose(fid);
% Cette partie du code sert à transcrire la matrice mat2 des pairings possibles  dans un fichier
% texte appelé Resultats2, qui doit être dans le dossier où se trouvent les codes.
```

Coordonnees vers distance

```
function [z ] = CoordonneesVersDistance( lat_1, lat_2, long_1, long_2, alt_1, alt_2 )

% Cette fonction calcule la distance entre deux points à partir de leurs latitudes, longitudes et
% altitudes.
% Les latitudes et longitudes doivent être fournies en degrés décimaux  et non en degrés puis
% minutes, secondes, etc. Les altitudes sont données en kilomètres.

a_angle = abs(lat_1 - lat_2);
b_angle = abs(long_1 - long_2);
 a_angle = (a_angle*2*pi)/360;
b_angle = (b_angle*2*pi)/360;
a = a_angle*alt_1;
b = b_angle*cos(lat_1)*alt_1;
c = abs(alt_1 - alt_2);
z = sqrt(a^2 + b^2 + c^2);

end

% On commence par déterminer les écarts de latitudes et longitudes, puis on les convertit en
% radians,
% On calcule les longueurs d'arc correspondant à ces écarts d'angles en multipliant par les bons
% rayons (i.e. l'altitude pour la latitude, et le rayon du parallèle défini par la latitude pour la
% longitude), et enfin on calcule la différence d'altitudes. Le théorème de Pythagore conclut.
% Le résultat est donné en kilomètres
```

Distance vers facteur

```
function [ p ] = DistanceVersFacteur( d )

if d < 0.01
   p = 1;
elseif d < 10
   p = 0.85;
elseif d < 20
   p = 0.83;
elseif d < 30
```

```
    p = 0.8;
elseif d < 40
    p = 0.75;
elseif d < 50
    p = 0.3;
else
    p = 0;
end

end

% La fonction DistanceVersFacteur ne rentre pas dans le cadre de la fonction précédente car elle
% ne reçoit pas une valeur pour chaque météorite, mais une unique valeur pour le couple. Cette
% fonction est par défaut une fonction par paliers.
```

Parametres vers facteurs

```
function [output ] = ParametresVersFacteurs( x_i, x_j, k)

if k == 1
    output = FonctionCalcul1( x_i, x_j);
elseif k == 2
    output = FonctionCalcul1( x_i, x_j);
elseif k == 3
    output = FonctionCalcul1( x_i, x_j);
elseif k == 4
    output = FonctionCalcul2( x_i, x_j);
elseif k == 5
    output = FonctionCalcul2( x_i, x_j);
elseif k == 6
    output = FonctionCalcul3( x_i, x_j);
elseif k == 7
    output = FonctionCalcul2( x_i, x_j);
elseif k == 8
    output = FonctionCalcul3( x_i, x_j);
else
    output = 1;
end

% Cette fonction prend en entrées les valeurs d'un type de données pour deux météorites, et le
% numéro de ce type de données. Il applique aux valeurs la fonction de calcul appropriée.
% C'est ici qu'on choisit quelle fonction de calcul on applique à quel type de données.
```

Fonction de calcul

```
function [z ] = FonctionCalcul1 ( x_i, x_j )

sigma = 1;
z = exp((-(abs(x_i - x_j))^2)/(2*sigma^2))   ;

end
```

```
% Un exemple de fonction de calcul. Ici, on a choisi de prendre une gaussienne en la différence
% entre les deux données. L'écart-type sigma est par défaut réglé à 1, et doit être ajusté pour
% que la fonction de calcul donne un facteur correspondant à la réalité expérimentale.
```

APPENDIX C: Calculations of CRE ages, terrestrial age and pre-atmospheric size (Scilab).

Here are presented the different scripts we used.
Script has to be put in different files :
-file dessin.sce
-file mindistance.sce
-file rayoncourbes.sce
-file chondrites.sce
-file iron.sce
-file iron_no_gaz.sce

Chondrites.sce is used for radiongenic nuclides on chondrites.
Iron.sce and **iron_no_gaz.sce** are used for iron meteorites, depending whether noble gaz are available or not.

Dessin.sce, **mindistance.sce** and **rayoncourbes.sce** are used with all three files above.

File “dessin.sce”

Fonction « dessin “

```
// La fonction 'dessin' prend en entrée un tableau de type Amon, une concentration et un
// shielding
// Elle ne renvoie rien.
// Elle trace dans la fenêtre graphique courante l'ensemble des courbes représentant la
// concentration en fonction du shielding, l'horizontale y=C, et est centrée sur le point
// d'intersection de l'horizontale et de la courbe correspondant au R choisi

function dessin(tableauAmon,C,S)
  decoupage = couper(tableauAmon);
  n = size(decoupage,2);
  decoupage = [decoupage,size(tableauAmon,1)+1];

  for i=1:n
    mini = decoupage(i);
    maxi = decoupage(i+1)-1;
    abscisse = tableauAmon(mini:maxi,2);
    ordonnee = tableauAmon(mini:maxi,4);
    plot2d(abscisse,ordonnee,i,rect=[max(S-15,0),0.8*C,min(S+15,200),1.2*C])
  end

    plot2d([0;200],[C;C],16,rect=[max(S-15,0),0.8*C,min(S+15,200),1.2*C])
endfunction
```

Fonction « Traceresults »

```
// La fonction 'traceresults' prend en entrée 4 tableaux de type Amon (1 pour chaque isotope
// radioactif) et 4 concentrations et ouvre une fenêtre comportant 4 sous-fenêtres : chacune
// contient un graphe avec toutes les courbes des  concentrations pour les différents rayons,
// ainsi que l'horizontale de la concentration à t0 pour chaque isotope.

function traceresults(tabBe,CBe,SBe,tabAl,CAl,SAl,tabCl,CCl,SCl,tabCa,CCa,SCa)

  // On se place dans le subplot en haut a gauche

  subplot(2,2,1)

  // On trace les courbes avec 'dessin'

  dessin(tabBe,CBe,SBe)

  // On met des titres

  xtitle('Comparaison des concentrations données par Amon avec celle trouvée pour le Béryllium
10','S','C')

  // Et une légende

  legends(['horizontale y=CBe'],[16],'ur')

  //On fait pareil pour les trois autres

   subplot(2,2,2)
  dessin(tabAl,CAl,SAl)
  xtitle('Comparaison des concentrations données par Amon avec celle trouvée pour
l''Aluminium 26','S','C')
  legends(['horizontale y=CAl'],[16],'ur')

  subplot(2,2,3)
  dessin(tabCl,CCl,SCl)
  xtitle('Comparaison des concentrations données par Amon avec celle trouvée pour le Chlore
36','S','C')
  legends(['horizontale y=CCl'],[16],'ur')

  subplot(2,2,4)
  dessin(tabCa,CCa,SCa)
  xtitle('Comparaison des concentrations données par Amon avec celle trouvée pour le Calcium
41','S','C')

  // La, on change la légende pour faire apparaitre toutes les courbe

  legends(['5cm';'10cm';'15cm';'25cm';'30cm';'32cm';'40cm';'50cm';'60cm';'65cm';'85cm';'
100cm';'120cm';'1000cm';'horizontale y=CCa'],[(1:14)';16],'ur')

endfunction
```

Fonction « dessingaz »

```
// La fonction 'dessingaz' prend en entrée un tableau de type gaz, une concentration C et un
// rapport R. Elle ne renvoie rien. Elle trace dans la fenêtre graphique courante l'ensemble des
// courbes représentant P(38Ar) en fonction du 4He/38Ar, l'horizontale y=C, la verticale x=R et
// est centrée au point (R,C)

function dessingaz(tableaugaz,rapp,C)
  decoupage = couper(tableaugaz);
  n = size(decoupage,2);
  decoupage = [decoupage,size(tableaugaz,1)+1];
  for i=1:n
    mini = decoupage(i);
    maxi = decoupage(i+1)-1;
    abscisse = tableaugaz(mini:maxi,2);
    ordonnee = tableaugaz(mini:maxi,3);
    plot2d(abscisse,ordonnee,i,rect=[max(rapp-15,40),0.8*C,min(rapp+15,140),1.2*C])
  end
  plot(rapp,C,'+')

  // On met un titre

  xtitle('Détermination du rayon avec les gaz rares','S','C')

  // et une légende pour faire apparaitre toutes les courbes

legends(['5cm';'10cm';'15cm';'25cm';'30cm';'32cm';'40cm';'50cm';'60cm';'65cm';'85cm';'100cm';'
120cm';'1000cm'],1:14,'ur')

endfunction
```

File “mindistance.sce”

Fonction « affine »

```
// 'affine' prend les coordonnées de deux points et un réel x et applique a x la fonction affine
//passant par ces deux points

function y = affine(x1,y1,x2,y2,x)
  y = (y2*(x-x1) + y1*(x2-x))/(x2-x1);
endfunction
```

Fonction « mindist »

```
// La fonction suivante prend en entrée les coordonnées du point (x0,y0),
// un tableau a deux colonnes et un entier i et minimise la fonction (x-x0)^2 + (f(x)-y0)^2
// où f est la fonction affine passant par (x(i),y(i)) et (x(i+1),y(i+1))
```

```
function [valeur,position] = mindist (x0,y0,tableau,i)

  // On vérifie que i n'est pas trop grand

  n = size(tableau,1);
  if i>n-1 then
    error('Indice trop grand')
  end

  gauche = tableau(i,1); droite = tableau(i+1,1);
  fgauche = tableau(i,2); fdroite = tableau(i+1,2);

  // Si les abscisses de gauche et droite sont égales alors, soit, c'est le même point (auquel cas,
  // on calcule la distance a ce point), soit ce sont deux points différents (auquel cas, on renvoie
  // un message d'erreur)

  if gauche == droite then
    if fgauche<>fdroite then
      error('Division par zero dans le calcul de distance')
    else
      position = gauche; valeur = (gauche-x0)^2 + (fgauche-y0)^2;
    end
  else
  // On calcule la dérivée de la distance qui vaut 2*(x-x0) + 2*(f(x)-y0)*f'(x)
  // et ce, en tableau(i,1) et tableau(i+1,1)
  // Rappel : f(gauche) vaut tableau(i,2) et f(droite) vaut tableau(i+1,2) et
  // Rappel : f' est constante et vaut (f(droite)-f(gauche))/(droite-gauche)

  deriveaffine = (fdroite - fgauche) / (droite-gauche);
  deriveegauche = 2*(gauche - x0) + 2*(fgauche-y0)*deriveaffine;
  deriveedroite = 2*(droite - x0) + 2*(fdroite-y0)*deriveaffine;

  // Si la derivee en droite est negative, on renvoie (distance(droite),droite)
  // De meme si la derivee en gauche est positive...

  if deriveegauche>=0 then
    position = gauche; valeur = (gauche-x0)^2 + (fgauche-y0)^2;
  else if deriveedroite<=0 then
      position = droite; valeur = (droite-x0)^2 + (fdroite-y0)^2;
    else

      // Sinon, cela veut dire que le minimum est atteint au milieu, au point d'annulation de la
      // dérivée

      obj = (fgauche*droite - fdroite*gauche)/(droite-gauche);
      position = (y0 - obj)*deriveaffine/(1+deriveaffine^2) + x0/(1+deriveaffine^2);
      valeur = (position-x0)^2 + (affine(gauche,fgauche,droite,fdroite,position)-y0)^2;
      end
    end
  end
endfunction
```

Fonction Distance

```
// La fonction suivante prend en entrée les coordonnées du point (x0,y0) et un tableau a deux
// colonnes et renvoie le minimum de la distance entre (x0,y0) et le graphe de la fonction affine
// par morceau associé au tableau.

function [valeur,position] = distance (x0,y0,tableau)
  n = size(tableau,1);

  //Le nombre de lignes du tableau.
  // Pour chaque tronçon, on va chercher la distance entre (x0,y0) et le tronçon.

  minima = zeros(n-1,0); pos = zeros(n-1,0)
  for i=1:n-1

    //On stocke les minima et les positions de chaque minimum dans les tableaux
    // définis ci-dessus

    [v,p] = mindist(x0,y0,tableau,i);
    minima(i) = v;
    pos(i) = p;
  end

  [valeur,indice] = min(minima);

  //On cherche le minimum des minima ainsi que sa place dans le tableau

  position = pos(indice)

  // L'indice nous donne la position du minimum absolu

endfunction
```

Fonction « choixdeRpardistance »

```
// Maintenant, il s'agit de prendre en entrée un tableau de type He4/Ar38 ainsi qu'un
// point de données, pour savoir à quel rayon correspondent les données

function  rayon = choixdeRpardistance (x0,y0,tableauAmon)

  // On decoupe le tableau de Amon suivant les differents rayons.
  // La fonction 'couper' a ete definie dans le fichier 'rayoncourbes.sce'

  tableaurayons = couper(tableauAmon)

  // ATTENTION : les tableaux de Amon ont 4 colonnes ! On ne travaille avec
  // les fonctions précédentes qu'avec des tableaux a deux colonnes

  n= size(tableaurayons,2) - 1;
```

```
  // Le nombre de courbes dont on calculera la distance avec le point (x0,y0)

  minimum = zeros(n,1);
  for i = 1:n
    coupure = tableaurayons(i):(tableaurayons(i+1)-1);
    tableau = tableauAmon(coupure,[2,3]),

    // On ne garde que les lignes qui nous intéressent

    [val,pos] = distance(x0,y0,tableau);
    minimum(i) = val;
  end

  [a,b] = min(minimum);

  // On recherche pour quel R la distance est minimale

  ligne = tableaurayons(b)
  rayon = tableauAmon(ligne,1);

endfunction
```

File “rayoncourbes.sce”

Fonction « couper »

```
// ---------- UNE DETERMINATION GRAPHIQUE DU RAYON -------------------------

// La fonction 'couper' prend en entrée un tableau du type Amon et renvoie le numéro des lignes
// correspondant aux séparations des différents rayons. Elle va servir dans la suite à séparer les
// différents graphes d'un tableau de type Amon

function tabsol = couper(tableauAmon)
  n = size(tableauAmon,1);
  tabsol = [1];
  for i=2:n
    if tableauAmon(i,1)<>tableauAmon(i-1,1) then
      tabsol = [tabsol,i];
    end
  end

  //On rajoute le dernier indice (+1!) de tableauAmon a la fin du tableau

  tabsol = [tabsol,n+1];
endfunction
```

Fonction « findshield »

```
// La fonction 'findshield' prend en entrée un tableau a deux colonnes représentant une fonction
// affine par morceaux f ainsi qu'une constante C et renvoie les abscisses des points
// d'intersection de la courbe représentative de f et de la droite d'équation y=C.

function solution = findshield(tableau,C)
  n = size(tableau,1)-1 ;

  // c'est le nombre de lignes du tableau moins 1 : le nombre de segments à traiter

  solution = [];
  for i=1:n

    // Pour chaque segment, on stocke les ordonnées des points a gauche et a droite

    gauche = tableau(i,1); droite = tableau(i+1,1);
    fgauche = tableau(i,2); fdroite = tableau(i+1,2);

    //Pour chaque segment, on va regarder s'il traverse l'horizontale.  cela, on regarde le signe de
    // (fgauche-C)(fdroite-C). Il existe une solution si et seulement si cette quantité est négative.

    if (fgauche-C)*(fdroite-C)<=0 then

      // S'il y a une solution, on la stocke dans le tableau des solutions

      D = (fdroite - fgauche) / (droite-gauche);
      obj = (fgauche*droite - fdroite*gauche)/(droite-gauche);
      solaux = (C - obj)/D; solution = [solution,solaux]
    end
  end
endfunction
```

Fonction findRandS

```
// La fonction suivante prend en entrée un tableau de type Amon ainsi qu'une
// concentration de matière C et renvoie la taille du plus petit rayon tel que
// la courbe associée soit en dessous de la droite d'équation y = C.
// ainsi que l'abscisse d'un point d'intersection entre la courbe et l'horizontale

function [rayon,shieldings] = findRandS(tableauAmon,C)
  tableaurayons = couper(tableauAmon);
  n = size(tableaurayons,2)-1;

  // Le nombre de courbes a tester

  pastrouve = %T; i=1;

  // Tant qu'on n'a pas trouvé de courbe dont le minimum est en dessous de l'horizontale y=C,
  // on continue

  while pastrouve & i<=n
```

```
    // On choisit le bout de tableau a garder

    lignes = tableaurayons(i):(tableaurayons(i+1)-1);
    tableau = tableauAmon(lignes,1:4);

    // On cherche le minimum de la fonction

    test = min(tableau(:,4));

    // Si ce min est plus petit que C, on s'arrête, sinon, on continue

    if test<C then
      pastrouve = %F;
      else i=i+1;
    end
  end

  // Le rayon recherché se trouve alors dans la première colonne de tableauAmon à la ligne
  // tableaurayons(i)

  rayon = tableauAmon(tableaurayons(i),1);

  // L'ensemble des shieldings possibles sera donne par le tableau donne en sortie de
  // 'findshield'.

  tableau = tableau(:,[2,4])
  shieldings = findshield(tableau,C);
endfunction
```

File “chondrites.sce”: ordinary chondrites, radionuclides only, Leya (2009).

```
// On commence par charger le fichier Excel dans le script.
// ATTENTION A CHANGER DE REPERTOIRE !

sheet = readxls('Donnees.xls')

// On charge également les autres fichiers Scilab dont on aura besoin, notamment pour chercher
// R et S :

exec('rayoncourbes.sce',-1)
exec('dessin.sce',-1)
exec('mindistance.sce',-1)

// La fonction suivante est une fonction auxiliaire qui prend un des tableau du
// type d'Amon, un rayon, un shielding min et max et envoie une quantité de matière
// associée

// La première colonne du tableau regroupe les différents rayons de météorite.
```

```
// La seconde, les shieldings minimaux associes aux rayons.
// La troisième, les shieldings maximaux associes aux rayons.
// La quatrième, les quantités de matières déduites du modèle de Amon

function solution = cherche(tableau,R,Smin,Smax)

  // On cherche tout d'abord la partie du tableau correspondant au rayon R

  r = find(tableau(:,1) == R);

  // Renvoie les numeros de lignes qui nous intéressent
  // Si r est vide, cela veut dire que le rayon n'est pas dans la tableau.
  // On renvoie un message d'erreur :

  if r==[] then
    error('Valeur du rayon non compatible avec les données')
  end

  // On garde le plus grand et le plus petit de ces indices en mémoire

  rmax = max(r); rmin = min(r);

  //On stocke la partie du tableau qui nous intéresse en enlevant la première colonne

  tabaux = tableau(rmin:rmax,2:4);

  // On fait de même pour le shielding minimal et maximal

  s1 = find(tabaux(:,1) >= Smin);

  //Regarde dans la colonne des shielding minimaux et prend les indices qui conviennent.

  s2 = find(tabaux(:,2) <= Smax);

  //Regarde dans la colonne des shielding maximaux et prend les indices qui conviennent.
  // On garde le plus petit indice de s1 et le plus grand de s2 pour ne garder que les
  // lignes qui nous intéressent

  smin = min(s1); smax = max(s2);

  // Si smin>smax, cela veut dire que l'intervalle de shielding est trop étroit
  // et tombe a cote des données du tableau.
  // Le probleme est qu'on ne veut pas renvoyer de message d'erreur, on fait donc
  // comprendre au programme qu'il ne doit pas finir

  continuer = smin<smax;

  // SI LA FONCTION EST AUTORISEE A CONTINUER :

  if continuer then
```

```
    //On stocke la partie du tableau qui nous intéresse en enlevant les colonnes de shielding

    tabaux = tabaux(smin:smax,$);

    // On fait la moyenne entre les valeurs extrêmes dans le tableau, ce qui nous donne la
solution

    solution = (max(tabaux) + min(tabaux)) / 2;
  else

    // Sinon, on renvoie une valeur impossible (négative) dans solution

    solution = -1;
  end

endfunction


function solution = modeleLeya(tableauRadioactif)

  // On extrait les différents tableaux des isotopes radioactifs

  tabBe = tableauRadioactif(1);
  tabAl = tableauRadioactif(2);
  tabCl = tableauRadioactif(3);
  tabCa = tableauRadioactif(4);

  // - tableauCl, ...Ca, etc... representent les donnees des tableaux de Amon

  mesures = tableauRadioactif(5);

  //Les différentes mesures nous sont données par le tableau 'mesures'. On va les stocker une à
  //une.

  Be10=mesures(3,2);      Al26=mesures(3,3);      Ar36=mesures(3,4);      Cl36=mesures(3,5);
  Ca41=mesures(3,6);

  //Tout comme les temps de demi-vie.

  L10=mesures(4,2); L26=mesures(4,4); L36=mesures(4,5); L41=mesures(4,6);

  // - He4 représente la quantité d'hélium 4 mesurée
  // - Ar38 représente la quantité d'argon 38 mesurée
  // - Cl36 représente la quantité de chlore 36 mesurée
  // - Ar36 représente la quantité d'argon 36 mesurée
  // - Be10 représente la quantité de béryllium 10 mesurée
  // - Ca41 représente la quantité de calcium 41 mesurée
  // - Al26 représente la quantité d'aluminium 26 mesurée
  // - L10,L26,L36,L41 représentent les constantes de décroissance radioactive resp. du
  // Béryllium, Aluminium, Chlore et Calcium
```

```
// On aura ici DEUX jeux de données : un qui sera donne par le rapport
// Béryllium/Chlore et l'autre par le rapport Chlore/Calcium

// On aura donc un âge terrestre Béryllium et un Calcium tout comme les rayon et shieldings

// On calcule Tterr a la première étape via le modèle de Lavielle avec le rapport
// Béryllium sur Chlore.
// On ne se servira plus de cette formule après.

auxBe10 = 6.01 - 0.28*Be10 - 0.009*Be10^2;
TterrBe10 = abs ((log(Cl36/Be10) - log(auxBe10)) / (L36 - L10));

// NB : On met des valeurs absolues, sinon c'est negative.
// On calcule une deuxième version de Tterr a la première étape via le modèle
// de Lavielle mais avec le rapport Calcium sur Chlore.

auxCa41 = 1.25 + 0.003*Cl36 - 0.0006*Cl36^2;
TterrCa41 = abs ((log(Cl36/Ca41) + log(auxCa41)) / (L36 - L41));

// On affiche les deux résultats

mprintf('L''estimation de l''âge terrestre de la météorite via le Béryllium est de %f milliers d''années. \n',TterrBe10*1000)
mprintf('L''estimation de l''âge terrestre de la météorite via le Calcium est de %f milliers d''années.\n',TterrCa41*1000)

// On ne calcule pas TCRE ! En effet, on a besoin de mesure d'Argon, impossible à fournir ici !!
// On n'a donc que deux âges terrestres
// Attention, les valeurs du Béryllium 10, du calcium 41 et du chlore 36 seront réajustées au
// fur et a mesure que l'on changera les âges de la météorite ! Il faut donc leur allouer
// une variable

Cl = Cl36; Ca = Ca41; Be = Be10;

// Là commence une boucle qui continue tant que l'utilisateur le demande

R= 0; Smin = 0; Smax = 0; continuer = %T;

// On initialise les valeurs de R (rayon) et S(shielding) et des erreurs terrestres et cosmiques
// On aura potentiellement besoin de ne pas afficher l'aluminium
// On introduit donc une variable test qui nous dit si on doit afficher l'alu

afficheralu = 1;

// Il est également possible de demander de fixer une variable par avance : l'âge ou l'un des
// rayon

fixerrayon = input('Voulez-vous fixer le rayon de la meteorite ? Taper 0 pour non, 1 pour oui : ')
if fixerrayon then
  R = input('Quelle valeur voulez-vous attribuer au rayon ? ')
```

```
  end
  fixerageterrestre = input('Voulez-vous fixer l''age terrestre de la meteorite ? Taper 0 pour non,
1 pour oui : ')
  if fixerageterrestre then
    Tterr = input('Quelle valeur voulez-vous attribuer à l''age terrestre ? (en milliers d''annees) :
')/1000
  end

  while continuer

    // On va chercher les valeurs de R et S. Pour cela, on va utiliser les tableaux
    // de type Amon pour le Chlore, le Calcium, etc...

    //-------------------------------------------------------------------------------------

    // ON COMMENCE PAR LES RESULTATS POUR LE BERYLIUM

    // De meme, chaque isotope radioactif va nous donner une valeur de R et de S
    // Pour chaque isotope, on calcule tout d'abord sa concentration au temps
    // d'entree sur terre.
    // Ensuite, on utilise la fonction 'findRandS' du fichier 'rayoncourbes.sce'

    CBe10ini = Be10*exp(L10*TterrBe10); [RBe10,SBe10] = findRandS(tabBe,CBe10ini);
    CAl26ini = Al26*exp(L26*TterrBe10); [RAl10,SAl10] = findRandS(tabAl,CAl26ini);
    CCl36ini = Cl36*exp(L36*TterrBe10); [RCl10,SCl10] = findRandS(tabCl,CCl36ini);
    CCa41ini = Ca41*exp(L41*TterrBe10); [RCa10,SCa10] = findRandS(tabCa,CCa41ini);

    // CAS 1 ON N'A PAS FIXE LE RAYON
    // On demande ensuite d'afficher les différents rayons proposes pour les différents isotopes
    // On distingue les cas suivant que l'aluminium est gardé ou pas :

    if ~fixerrayon then
      if afficheralu then
        disp('D''après les mesures des isotopes radioactifs pour l''âge terrestre au Béryllium, les
différents rayons sont respectivement : ')
        mprintf('Be10 : %i cm, Al26 : %i cm, Cl36 : %i cm, Ca41 : %i cm.
\n',RBe10,RAl10,RCl10,RCa10)
        else
        disp('D''après les mesures de isotopes radioactifs, les différents rayons sont
respectivement : ')
        mprintf('Be10 : %i cm, Cl36 : %i cm, Ca41 : %i cm. \n',RBe10,RCl10,RCa10)
        end
      end

      // CAS 2 : ON A DEMANDE DE FIXER LE RAYON : dans ce cas, il ne se passe rien.
      // Si pour un isotope donne, plusieurs shieldings sont possibles, on demande
      // à l'utilisateur d'en choisir 1.

      if size(SBe10,2)<>1 then
        disp('Attention ! Le Béryllium propose plusieurs valeurs de shielding : ')
        disp(SBe10)
```

```
    SBe10 = input('Laquelle choisissez-vous  parmi celles proposées ? ')
  end

  if size(SAl10,2)<>1 then
    disp('Attention ! L''Aluminium propose plusieurs valeurs de shielding : ')
    disp(SAl10)
    SAl10 = input('Laquelle choisissez-vous  parmi celles proposées ? ')
  end

  if size(SCl10,2)<>1 then
    disp('Attention ! Le Chlore propose plusieurs valeurs de shielding : ')
    disp(SCl10)
    SCl10 = input('Laquelle choisissez-vous  parmi celles proposées ? ')
  end

  if size(SCa10,2)<>1 then
    disp('Attention ! Le Calcium propose plusieurs valeurs de shielding : ')
    disp(SCa10)
    SCa10 = input('Laquelle choisissez-vous  parmi celles proposées ? ')
  end


  // On affiche ensuite les différents shieldings proposes pour les différents isotopes
  // On distingue les cas suivant que l'aluminium est gardé ou pas :

  if afficheralu then
    disp('Les different shieldings sont respectivement : ')
    mprintf('Be10 : %f cm, Al26 : %f cm, Cl36 : %f cm, Ca41 : %f cm.
\n',SBe10,SAl10,SCl10,SCa10)
  else
    disp('Les different shieldings sont respectivement : ')
    mprintf('Be10 : %f cm, Cl36 : %f cm, Ca41 : %f cm. \n',SBe10,SCl10,SCa10)
  end

  // On ouvre une autre fenêtre que l'on vide après chaque boucle.
  xset('window',2)
  clf()

  // Et on affiche un résultat graphique de la détermination de R et S pour les isotopes
  // radioactifs

traceresults(tabBe,CBe10ini,SBe10,tabAl,CAl26ini,SAl10,tabCl,CCl36ini,SCl10,tabCa,CCa41ini,SCa
10)

  //-------------------------------------------------------------------------------

  // ON COMMENCE PAR LES RESULTATS POUR LE BERYLIUM

  // De même, chaque isotope radioactif va nous donner une valeur de R et de S
  // Pour chaque isotope, on calcule tout d'abord sa concentration au temps
  // d'entrée sur terre.
```

```
// Ensuite, on utilise la fonction 'findRandS' du fichier 'rayoncourbes.sce'

CBe10ini = Be10*exp(L10*TterrCa41); [RBe41,SBe41] = findRandS(tabBe,CBe10ini);
CAl26ini = Al26*exp(L26*TterrCa41); [RAl41,SAl41] = findRandS(tabAl,CAl26ini);
CCl36ini = Cl36*exp(L36*TterrCa41); [RCl41,SCl41] = findRandS(tabCl,CCl36ini);
CCa41ini = Ca41*exp(L41*TterrCa41); [RCa41,SCa41] = findRandS(tabCa,CCa41ini);

// CAS 1 ON N'A PAS FIXE LE RAYON
// On demande ensuite d'afficher les différents rayons proposes pour les différents isotopes
// On distingue les cas suivant que l'aluminium est gardé ou pas :

if ~fixerrayon then
  if afficheralu then
    disp('D''après les mesures des isotopes radioactifs pour l''âge terrestre au Calcium, les différents rayons sont respectivement : ')
    mprintf('Be10 : %i cm, Al26 : %i cm, Cl36 : %i cm, Ca41 : %i cm. \n',RBe41,RAl41,RCl41,RCa41)
  else
    disp('D''apres les mesures de isotopes radioactifs, les différents rayons sont respectivement : ')
    mprintf('Be10 : %i cm, Cl36 : %i cm, Ca41 : %i cm. \n',RBe41,RCl41,RCa41)
  end
end

// CAS 2 : ON A DEMANDE DE FIXER LE RAYON : dans ce cas, il ne se passe rien.

// Si pour un isotope donne, plusieurs shieldings sont possibles, on demande à l'utilisateur
// d'en choisir 1.

if size(SBe41,2)<>1 then
  disp('Attention ! Le Béryllium propose plusieurs valeurs de shielding : ')
  disp(SBe41)
  SBe41 = input('Laquelle choisissez-vous  parmi celles proposées ? ')
end

if size(SAl41,2)<>1 then
  disp('Attention ! L''Aluminium propose plusieurs valeurs de shielding : ')
  disp(SAl41)
  SAl41 = input('Laquelle choisissez-vous  parmi celles proposées ? ')
end


if size(SCl41,2)<>1 then
  disp('Attention ! Le Chlore propose plusieurs valeurs de shielding : ')
  disp(SCl41)
  SCl41 = input('Laquelle choisissez-vous  parmi celles proposées ? ')
end

if size(SCa41,2)<>1 then
  disp('Attention ! Le Calcium propose plusieurs valeurs de shielding : ')
  disp(SCa41)
```

```
    SCa41 = input('Laquelle choisissez-vous  parmi celles proposées ? ')
  end

  // On affiche ensuite les différents shieldings proposes pour les différents isotopes
  // On distingue les cas suivant que l'aluminium est gardé ou pas :

  if afficheralu then
    disp('Les different shieldings sont respectivement : ')
    mprintf('Be10 : %f cm, Al26 : %f cm, Cl36 : %f cm, Ca41 : %f cm.
\n',SBe41,SAl41,SCl41,SCa41)
  else
    disp('Les different shieldings sont respectivement : ')
    mprintf('Be10 : %f cm, Cl36 : %f cm, Ca41 : %f cm. \n',SBe41,SCl41,SCa41)
  end

  // On ouvre une autre fenêtre que l'on vide après chaque boucle.

  xset('window',2)

  clf()

  // Et on affiche un résultat graphique de la détermination de R et S pour les isotopes
  // radioactifs.

traceresults(tabBe,CBe10ini,SBe41,tabAl,CAl26ini,SAl41,tabCl,CCl36ini,SCl41,tabCa,CCa41ini,SCa
41)

  //-------------------------------------------------------------------------------------

  // Et on demande à l'utilisateur de rentrer les valeurs du rayon et les bornes du shielding
  // voulues :


  if ~fixerrayon then
    R = input('Choisissez la valeur de R qui vous convient : ')
  end
  Smin = input('Choisissez la valeur de S minimale qui vous convient : ')
  Smax = input('Choisissez la valeur de S maximale qui vous convient : ')

  // À partir de là, 2 cas se présentent : soit les valeurs de S que l'on
  // a rentrées sont cohérentes, soit elles ne le sont pas (ce qui aura un
  // impact dans la fonction 'cherche')
  // On va donc entrer dans une boucle dans laquelle on ne pourra ressortir
  // que quand les valeurs de S seront cohérentes (i.e. lorsque Cl et Ca seront
  // positives)
  boucleShield = 1;

  while boucleShield

    // A partir de la, on peut rechercher dans les tableaux de Amon les quantités de calcium
    // et de chlore correspondant via la fonction auxiliaire 'cherche'
```

```
    // Cette quantité correspondra au modèle de Amon

    Be = cherche(tabBe,R,Smin,Smax);
    Cl = cherche(tabCl,R,Smin,Smax);
    Ca = cherche(tabCa,R,Smin,Smax);

    // On fait ensuite le test pour savoir si on reste dans la boucle. Si tel est le cas, il faudra
    // réaffecter des valeurs a Smin et Smax

    if Cl<0 then
      disp('Les valeurs du shielding ne sont pas cohérentes. Redéfinissez Smin et Smax')
      Smin = input('Choisissez la valeur de S minimale qui vous convient : ')
      Smax = input('Choisissez la valeur de S maximale qui vous convient : ')
    else
      boucleShield = 0;
    end

  end

  // On recalcule Tterr via la formule de Amon mais cette fois on recalcule 2 âges terrestres :
  // le Béryllium et le Calcium.

  TterrnewCa41 = abs ((log(Cl36/Ca41) - log(Cl/Ca)) / (L41 - L36));
  TterrnewBe10 = abs ((log(Cl36/Be10) - log(Cl/Be)) / (L10 - L36));

  // Là encore, il y a des valeurs absolues.
  // On affiche les deux résultats

  mprintf('L''estimation de l''âge terrestre de la météorite via le Béryllium est de %f milliers d''années. \n',TterrnewBe10*1000)
  mprintf('L''estimation de l''âge terrestre de la météorite via le Calcium est de %f milliers d''années. \n',TterrnewCa41*1000)

  // On calcule les erreurs commises entre les deux ages

  errterrBe10 = abs(TterrBe10 - TterrnewBe10)/TterrBe10;
  errterrCa41 = abs(TterrCa41 - TterrnewCa41)/TterrCa41;

  // On affiche les deux erreurs

  mprintf('L''erreur commise sur l''âge terrestre de la météorite avec la formule du Béryllium est de %i pour cent. \n',errterrBe10*100)
  mprintf('L''erreur commise sur l''âge terrestre de la météorite avec la formule du Calcium est de %i pour cent. \n',errterrCa41*100)

  disp(' ')

  // Et on réaffecte les nouveaux âges dans les anciennes variables
  // CAS 1 : ON N'A PAS DEMANDE DE FIXER L'AGE TERRESTRE
  // Dans ce cas, on remplace l'âge terrestre par le nouvel âge
```

```
    if ~fixerageterrestre then
      TterrBe10 = TterrnewBe10;
      TterrCa41 = TterrnewCa41
    end

    // CAS 2 : ON A DEMANDE DE FIXER L'AGE TERRESTRE : dans ce cas, il ne se passe rien.
    // On demande a l'utilisateur s'il veut continuer

    continuer = input('Voulez-vous recommencer une boucle ? Taper 0 pour non, 1 pour oui : ')

    // On lui demande s'il veut continuer a garder l'aluminium si c'était le cas dans la boucle
    //précédente

    if afficheralu then
      afficheralu = input('Voulez-vous continuer a prendre l''aluminium en compte ? Taper 0
pour non, 1 pour oui : ')
    end
  end

  // On renvoie la solution composée de Tterr, TCRE, R et Smin et Smax ou un message d'erreur
  // si l'utilisateur a arrêté manuellement le script.
  solution = [TterrBe10,TterrCa41,R,Smin,Smax];

endfunction
```

File “iron.sce” : iron meteorites, radionuclides and noble gaz, Ammon (2009).

```
// On commence par charger le fichier Excel dans le script.
// ATTENTION A CHANGER DE REPERTOIRE !

sheet = readxls('Donnees.xls')
sheet2 = readxls('testgaz.xls')

// On charge également les autres fichiers Scilab dont on aura besoin, notamment pour chercher
// R et S :

exec('rayoncourbes.sce',-1)
exec('dessin.sce',-1)
exec('mindistance.sce',-1)

// La fonction suivante est une fonction auxiliaire qui prend un des tableaux du type d'Amon, un
// rayon, un shielding min et max et envoie une quantité de matière associée

// La première colonne du tableau regroupe les différents rayons de météorite.
// La seconde, les shieldings minimaux associes aux rayons.
// La troisième, les shieldings maximaux associes aux rayons.
```

```
// La quatrième, les quantités de matières déduites du modèle de Amon

function solution = cherche(tableau,R,Smin,Smax)

  // On cherche tout d'abord la partie du tableau correspondant au rayon R

  r = find(tableau(:,1) == R); // Renvoie les numéros de lignes qui nous intéressent

  // Si r est vide, cela veut dire que le rayon n'est pas dans la tableau : On renvoie un message
  // d'erreur :

  if r==[] then
    error('Valeur du rayon non compatible avec les données')
  end

  // On garde le plus grand et le plus petit de ces indices en mémoire

  rmax = max(r); rmin = min(r);

  //On stocke la partie du tableau qui nous intéresse en enlevant la première colonne

  tabaux = tableau(rmin:rmax,2:4);


  // On fait de même pour le shielding minimal et maximal

  s1 = find(tabaux(:,1) >= Smin);

  //Regarde dans la colonne des shielding minimaux et prend les indices qui conviennent

  s2 = find(tabaux(:,2) <= Smax);

  //Regarde dans la colonne des shielding maximaux et prend les indices qui conviennent

  // On garde le plus petit indice de s1 et le plus grand de s2 pour ne garder que les
  // lignes qui nous intéressent

  smin = min(s1); smax = max(s2);

  // Si smin>smax, cela veut dire que l'intervalle de shielding est trop étroit
  // et tombe a cote des données du tableau. On renvoie donc un message d'erreur

  if smin>smax then
    error('Problème au niveau des valeurs de shielding')
  end

  //On stocke la partie du tableau qui nous intéresse en enlevant les colonnes de shielding

  tabaux = tabaux(smin:smax,$);

  // On fait la moyenne entre les valeurs extrêmes dans le tableau, ce qui nous donne la solution
```

```
  solution = (max(tabaux) + min(tabaux)) / 2;
endfunction

// La fonction qui va suivre va prendre en entrée plusieurs mesures et données connues  (cf. ci-
// dessous) et renvoyer l'âge terrestre de la météorite étudiée

function solution = modeleAmon(tableauRadioactif,tableauGaz)

  // On extrait les différents tableaux des isotopes radioactifs

  tabBe = tableauRadioactif(1);
  tabAl = tableauRadioactif(2);
  tabCl = tableauRadioactif(3);
  tabCa = tableauRadioactif(4);

  // On extrait le tableau du rapport 4He/38Ar

  tabNoblegas = tableauGaz(1);
  mesuresgaz = tableauGaz(2);

  // On stocke les différentes quantités mesurées

  He4 = mesuresgaz(3,2) ; Ar38 = mesuresgaz(3,3) ;

  // - tableauCl, ...Ca, etc... représentent les données des tableaux de Amon

  mesures = tableauRadioactif(5);

  //Les différentes mesures nous sont données par le tableau 'mesures'. On va les stocker une à
  //une.

  Be10=mesures(3,2);      Al26=mesures(3,3);      Ar36=mesures(3,4);      Cl36=mesures(3,5);
Ca41=mesures(3,6);

   //Tout comme les temps de demi-vie

  L10=mesures(4,2); L26=mesures(4,4); L36=mesures(4,5); L41=mesures(4,6);

  // - He4 représente la quantité d'hélium 4 mesurée
  // - Ar38 représente la quantité d'argon 38 mesurée
  // - Cl36 représente la quantité de chlore 36 mesurée
  // - Ar36 représente la quantité d'argon 36 mesurée
  // - Be10 représente la quantité de béryllium 10 mesurée
  // - Ca41 représente la quantité de calcium 41 mesurée
  // - Al26 représente la quantité d'aluminium 26 mesurée
  // - L10, L26, L36, L41 représentent les constantes de décroissance radioactive resp. du
  // Béryllium, Aluminium, Chlore et Calcium

  // On calcule Tterr à la première étape via le modèle de Lavielle
  // On ne se servira plus de cette formule après.
```

```
aux = 5.97 - 0.184*Be10 - 0.024*Be10^2;
Tterr = abs ((log(Cl36/Be10) - log(aux)) / (L36 - L10));

// NB : On met des valeurs absolues, sinon c'est négatif.

// On calcule TCRE à la première étape. On a besoin de l'âge terrestre précédent
// En effet, on a besoin de la quantité de Cl36 au moment de l'arrivée sur Terre et on n'a que la
// quantité au moment de la mesure

Cl36ini = Cl36 * exp(L36*Tterr);
TCRE = Ar36 / (2.296E-3 * Cl36ini);

// Attention, les valeurs du calcium 41 et du chlore 36 seront réajustées au
// fur et a mesure que l'on changera les âges de la météorite ! Il faut donc leur allouer une
// variable

Cl = Cl36; Ca = Ca41;

// On affiche les deux résultats

mprintf('L''estimation de l''âge terrestre de la météorite est de %f milliers d''années.
\n',Tterr*1000)
mprintf('L''estimation de l''âge cosmique de la météorite est de %f millions d''années.\n
',TCRE)

// Là commence une boucle qui continue tant que l'utilisateur le demande

R= 0; Smin = 0; Smax = 0; continuer = %T;

// On initialise les valeurs de R (rayon) et S(shielding) et des erreurs terrestres et cosmiques

while continuer

  // On va chercher les valeurs de R et S. Pour cela, on va utiliser les tableaux
  // de type Amon pour le Chlore, le Calcium, etc... ainsi que celui des gaz rares

  // On va tout d'abord utiliser les données de He4 et Ar38
  // On calcule d'une part le rapport He4/Ar38 et d'autre part la vitesse de création
  // d'Argon grâce a l'âge TCRE :

  rapport = He4/Ar38; PAr38 = Ar38/TCRE;

  // Puis on regarde a quel rayon ce point correspond le mieux

  Rgazrare = choixdeRpardistance(rapport,PAr38,tabNoblegas)

  // On affiche ensuite le rayon propose pour les gaz rares

  mprintf('D''après les mesures d''Hélium et d''Argon, le rayon serait de %i cm. \n',Rgazrare)
```

```
// On ouvre une fenêtre

xset('window',1)

// que l'on vide après chaque boucle.

clf()

// Et on affiche un résultat graphique pour la détermination du rayon par les gaz rares

dessingaz(tabNoblegas,rapport,PAr38)

// De même, chaque isotope radioactif va nous donner une valeur de R et de S
// Pour chaque isotope, on calcule tout d'abord sa concentration au temps d'entrée sur terre.
// Ensuite, on utilise la fonction 'findRandS' du fichier 'rayoncourbes.sce'

CBe10ini = Be10*exp(L10*Tterr); [RBe,SBe] = findRandS(tabBe,CBe10ini);
CAl26ini = Al26*exp(L26*Tterr); [RAl,SAl] = findRandS(tabAl,CAl26ini);
CCl36ini = Cl36*exp(L36*Tterr); [RCl,SCl] = findRandS(tabCl,CCl36ini);
CCa41ini = Ca41*exp(L41*Tterr); [RCa,SCa] = findRandS(tabCa,CCa41ini);

// On affiche ensuite les différents rayons proposes pour les différents isotopes

disp('D''après les mesures de isotopes radioactifs, les différents rayons sont respectivement:
')
mprintf('Be10 : %i cm, Al26 : %i cm, Cl36 : %i cm, Ca41 : %i cm. \n',RBe,RAl,RCl,RCa)

// Si pour un isotope donne, plusieurs shieldings sont possibles, on demande à l'utilisateur
// d'en choisir 1.

if size(SBe,2)<>1 then
  disp('Attention ! Le Béryllium propose plusieurs valeurs de shielding : ')
  disp(SBe)
  SBe = input('Laquelle choisissez-vous  parmi celles proposées ? ')
end

if size(SAl,2)<>1 then
  disp('Attention ! L''Aluminium propose plusieurs valeurs de shielding : ')
  disp(SAl)
  SAl = input('Laquelle choisissez-vous  parmi celles proposées ? ')
end

if size(SCl,2)<>1 then
  disp('Attention ! Le Chlore propose plusieurs valeurs de shielding : ')
  disp(SCl)
  SCl = input('Laquelle choisissez-vous  parmi celles proposées ? ')
end

if size(SCa,2)<>1 then
  disp('Attention ! Le Calcium propose plusieurs valeurs de shielding : ')
  disp(SCa)
```

```
  SCa = input('Laquelle choisissez-vous  parmi celles proposées ? ')
end

// On affiche ensuite les différents shieldings proposes pour les différents isotopes

disp('Les different shieldings sont respectivement : ')
mprintf('Be10 : %f cm, Al26 : %f cm, Cl36 : %f cm, Ca41 : %f cm. \n',SBe,SAl,SCl,SCa)

// On ouvre une autre fenêtre

 xset('window',2)

// que l'on vide après chaque boucle.

clf()

// Et on affiche un résultat graphique de la détermination de R et S pour les isotopes
// radioactifs

traceresults(tabBe,CBe10ini,SBe,tabAl,CAl26ini,SAl,tabCl,CCl36ini,SCl,tabCa,CCa41ini,SCa)

// Et on demande a l'utilisateur de rentrer les valeurs du rayon et les bornes du shielding
// voulues :

R = input('Choisissez la valeur de R qui vous convient : ')
Smin = input('Choisissez la valeur de S minimale qui vous convient : ')
Smax = input('Choisissez la valeur de S maximale qui vous convient : ')

// À partir de là, on peut rechercher dans les tableaux de Amon les quantités de calcium et de
// chlore correspondant via la fonction auxiliaire 'cherche'
// Cette quantité correspondra au modèle de Amon

Cl = cherche(tabCl,R,Smin,Smax);
Ca = cherche(tabCa,R,Smin,Smax);

// On recalcule Tterr via la formule de Amon

Tterrnew = abs ((log(Cl36/Ca41) - log(Cl/Ca)) / (L41 - L36));

// Là encore, il y a des valeurs absolues.
 // On remonte la décroissance pour arriver au temps d'arrivée sur Terre

Cl36ini = Cl36 * exp(L36*Tterrnew);

// On recalcule TCRE via la formule de Amon

TCREnew = Ar36 / (2.296E-3 * Cl36ini);

// On affiche les deux résultats
```

```
    mprintf('L''estimation de l''âge terrestre de la météorite est de %f milliers d''années.
\n',Tterrnew*1000)
    mprintf('L''estimation de l''âge cosmique de la météorite est de %f millions d''années.
\n',TCREnew)

    // On calcule les erreurs commises entre les deux ages

    errterr = abs(Tterr - Tterrnew)/Tterr;
    errcosm = abs(TCRE - TCREnew)/TCRE;

    // On affiche les deux erreurs

    mprintf('L''erreur commise sur l''âge terrestre de la météorite est de %i pour cent.
\n',errterr*100)
    mprintf('L''erreur commise sur l''âge cosmique de la météorite est de %i pour cent.
\n',errcosm*100)

    disp(' ')

    // Et on réaffecte les nouveaux âges dans les anciennes variables

    Tterr = Tterrnew; TCRE = TCREnew;

    continuer = input('Voulez-vous recommencer une boucle ? Taper 0 pour non, 1 pour oui : ')

  end

  // On renvoie la solution composée de Tterr, TCRE, R et Smin et Smax ou un message
  // d'erreur si l'utilisateur a arrêté manuellement le script.

  solution = [Tterr,TCRE,R,Smin,Smax];

endfunction
```

File "iron_no_gaz.sce": iron meteorites, radionuclides, Ammon (2009).

```
// On commence par charger le fichier Excel dans le script.
// ATTENTION A CHANGER DE REPERTOIRE !

sheet = readxls('Donnees.xls')
// On charge également les autres fichiers Scilab dont on aura besoin, notamment pour chercher
// R et S :

exec('rayoncourbes.sce',-1)
exec('dessin.sce',-1)
exec('mindistance.sce',-1)

// La fonction suivante est une fonction auxiliaire qui prend un des tableaux du
// type d'Amon, un rayon, un shielding min et max et envoie une quantité de matière
```

```
// associée

// La première colonne du tableau regroupe les différents rayons de météorite.
// La seconde, les shieldings minimaux associes aux rayons.
// La troisième, les shieldings maximaux associes aux rayons.
// La quatrième, les quantités de matières déduites du modèle de Amon

function solution = cherche(tableau,R,Smin,Smax)

  // On cherche tout d'abord la partie du tableau correspondant au rayon R

  r = find(tableau(:,1) == R); // Renvoie les numéros de lignes qui nous intéressent

  // Si r est vide, cela veut dire que le rayon n'est pas dans la tableau.
  // On renvoie un message d'erreur :

  if r==[] then
    error('Valeur du rayon non compatible avec les données')
  end

  // On garde le plus grand et le plus petit de ces indices en mémoire

  rmax = max(r); rmin = min(r);

  //On stocke la partie du tableau qui nous intéresse en enlevant la première colonne

  tabaux = tableau(rmin:rmax,2:4);

  // On fait de même pour le shielding minimal et maximal

  s1 = find(tabaux(:,1) >= Smin);

  //Regarde dans la colonne des shielding minimaux et prend les indices qui conviennent

  s2 = find(tabaux(:,2) <= Smax);

  //Regarde dans la colonne des shielding maximaux et prend les indices qui conviennent
  // On garde le plus petit indice de s1 et le plus grand de s2 pour ne garder que les lignes qui
  // nous intéressent

  smin = min(s1); smax = max(s2);

  // Si smin>smax, cela veut dire que l'intervalle de shielding est trop étroit et tombe a cote des
  // données du tableau. On renvoie donc un message d'erreur

  if smin>smax then
    error('Problème au niveau des valeurs de shielding')
  end

  //On stocke la partie du tableau qui nous interresse en enlevant les colonnes de shielding
```

```
  tabaux = tabaux(smin:smax,$);

  // On fait la moyenne entre les valeurs extrêmes dans le tableau, ce qui nous donne la solution

  solution = (max(tabaux) + min(tabaux)) / 2;
endfunction

// La fonction qui va suivre va prendre en entrée plusieurs mesures et données connues (cf. ci-
// dessous) et renvoyer l'âge terrestre de la météorite étudiée

function solution = modeleAmonbis(tableauRadioactif)

  // On extrait les différents tableaux des isotopes radioactifs

  tabBe = tableauRadioactif(1);
  tabAl = tableauRadioactif(2);
  tabCl = tableauRadioactif(3);
  tabCa = tableauRadioactif(4);

  // - tableauCl, ...Ca, etc... représentent les données des tableaux de Amon

  mesures = tableauRadioactif(5);

  //Les différentes mesures nous sont données par le tableau 'mesures'. On va les stocker une a
  // une

  Be10=mesures(3,2);      Al26=mesures(3,3);      Ar36=mesures(3,4);      Cl36=mesures(3,5);
  Ca41=mesures(3,6);

  //Tout comme les temps de demi-vie

  L10=mesures(4,2); L26=mesures(4,4); L36=mesures(4,5); L41=mesures(4,6);

  // - He4 représente la quantité d'hélium 4 mesurée
  // - Ar38 représente la quantité d'argon 38 mesurée
  // - Cl36 représente la quantité de chlore 36 mesurée
  // - Ar36 représente la quantité d'argon 36 mesurée
  // - Be10 représente la quantité de béryllium 10 mesurée
  // - Ca41 représente la quantité de calcium 41 mesurée
  // - Al26 représente la quantité d'aluminium 26 mesurée
  // - L10,L26,L36,L41 représentent les constantes de décroissance radioactive resp. du
  // Béryllium, Aluminium, Chlore et Calcium

  // On calcule Tterr à la première étape via le modèle de Lavielle
  // On ne se servira plus de cette formule après.

  aux = 5.97 - 0.184*Be10 - 0.024*Be10^2;
  Tterr = abs ((log(Cl36/Be10) - log(aux)) / (L36 - L10));

  // NB : On met des valeurs absolues, sinon c'est négatif.
```

```
// On ne calcule pas TCRE vu qu'on n'a pas de données sur l'argon

// Attention, les valeurs du calcium 41 et du chlore 36 seront réajustées au fur et à mesure que
// l'on changera les âges de la météorite ! Il faut donc leur allouer une variable.

Cl = Cl36; Ca = Ca41;

// On affiche les deux résultats.

mprintf('L''estimation de l''âge terrestre de la météorite est de %f milliers d''années.
\n',Tterr*1000)

// Là commence une boucle qui continue tant que l'utilisateur le demande.

R= 0; Smin = 0; Smax = 0; continuer = %T;

// On initialise les valeurs de R (rayon) et S(shielding) et des erreurs terrestres et cosmiques.

while continuer

  // On va chercher les valeurs de R et S. Pour cela, on va utiliser les tableaux de type Amon
  // pour le Chlore, le Calcium, etc... ainsi que celui des gaz rares.

  // De même, chaque isotope radioactif va nous donner une valeur de R et de S.
  // Pour chaque isotope, on calcule tout d'abord sa concentration au temps d'entrée sur terre.

  // Ensuite, on utilise la fonction 'findRandS' du fichier 'rayoncourbes.sce'.

  CBe10ini = Be10*exp(L10*Tterr); [RBe,SBe] = findRandS(tabBe,CBe10ini);
  CAl26ini = Al26*exp(L26*Tterr); [RAl,SAl] = findRandS(tabAl,CAl26ini);
  CCl36ini = Cl36*exp(L36*Tterr); [RCl,SCl] = findRandS(tabCl,CCl36ini);
  CCa41ini = Ca41*exp(L41*Tterr); [RCa,SCa] = findRandS(tabCa,CCa41ini);

  // On affiche ensuite les différents rayons proposes pour les différents isotopes.

  disp('D''après les mesures de isotopes radioactifs, les différents rayons sont respectivement :
')
  mprintf('Be10 : %i cm, Al26 : %i cm, Cl36 : %i cm, Ca41 : %i cm. \n',RBe,RAl,RCl,RCa)

  // Si pour un isotope donne, plusieurs shieldings sont possibles, on demande à l'utilisateur
  // d'en choisir 1.

  if size(SBe,2)<>1 then
    disp('Attention ! Le Béryllium propose plusieurs valeurs de shielding : ')
    disp(SBe)
    SBe = input('Laquelle choisissez-vous  parmi celles proposées ? ')
  end

  if size(SAl,2)<>1 then
    disp('Attention ! L''Aluminium propose plusieurs valeurs de shielding : ')
```

```
  disp(SAl)
  SAl = input('Laquelle choisissez-vous  parmi celles proposées ? ')
end

if size(SCl,2)<>1 then
  disp('Attention ! Le Chlore propose plusieurs valeurs de shielding : ')
  disp(SCl)
  SCl = input('Laquelle choisissez-vous  parmi celles proposées ? ')
end

if size(SCa,2)<>1 then
  disp('Attention ! Le Calcium propose plusieurs valeurs de shielding : ')
  disp(SCa)
  SCa = input('Laquelle choisissez-vous  parmi celles proposées ? ')
end

// On affiche ensuite les différents shieldings proposes pour les différents isotopes.

disp('Les differents shieldings sont respectivement : ')
mprintf('Be10 : %f cm, Al26 : %f cm, Cl36 : %f cm, Ca41 : %f cm. \n',SBe,SAl,SCl,SCa)

// On ouvre une autre fenêtre

xset('window',2)

// que l'on vide après chaque boucle.

clf()

// Et on affiche un résultat graphique de la détermination de R et S pour les isotopes
// radioactifs.

traceresults(tabBe,CBe10ini,SBe,tabAl,CAl26ini,SAl,tabCl,CCl36ini,SCl,tabCa,CCa41ini,SCa)

// Et on demande a l'utilisateur de rentrer les valeurs du rayon et les bornes du shielding
// voulues :

R = input('Choisissez la valeur de R qui vous convient : ')
Smin = input('Choisissez la valeur de S minimale qui vous convient : ')
Smax = input('Choisissez la valeur de S maximale qui vous convient : ')

 // À partir de là, on peut rechercher dans les tableaux de Amon les quantités de calcium et
// de chlore correspondant via la fonction auxiliaire 'cherche'.
// Cette quantité correspondra au modèle de Amon.

Cl = cherche(tabCl,R,Smin,Smax);
Ca = cherche(tabCa,R,Smin,Smax);

// On recalcule Tterr via la formule de Amon.

Tterrnew = abs ((log(Cl36/Ca41) - log(Cl/Ca)) / (L41 - L36));
```

```
    // Là encore, il y a des valeurs absolues.

    // On affiche les deux résultats.
    mprintf('L''estimation de l''âge terrestre de la météorite est de %f milliers d''années.
\n',Tterrnew*1000)

    // On calcule les erreurs commises entre les deux ages.

    errterr = abs(Tterr - Tterrnew)/Tterr;

    // On affiche les deux erreurs.

    mprintf('L''erreur commise sur l''âge terrestre de la météorite est de %i pour cent.
\n',errterr*100)

    disp(' ')

    // Et on réaffecte les nouveaux âges dans les anciennes variables.

    Tterr = Tterrnew;

    continuer = input('Voulez-vous recommencer une boucle ? Taper 0 pour non, 1 pour oui : ')

  end

  // On renvoie la solution composée de Tterr, TCRE, R et Smin et Smax ou un message d'erreur
  // si l'utilisateur a arrête manuellement le script.

  solution = [Tterr,R,Smin,Smax];

endfunction
```

Donnees.xls and testgaz.xls must follow the model shown in fig. C-1 and fig. C-2.

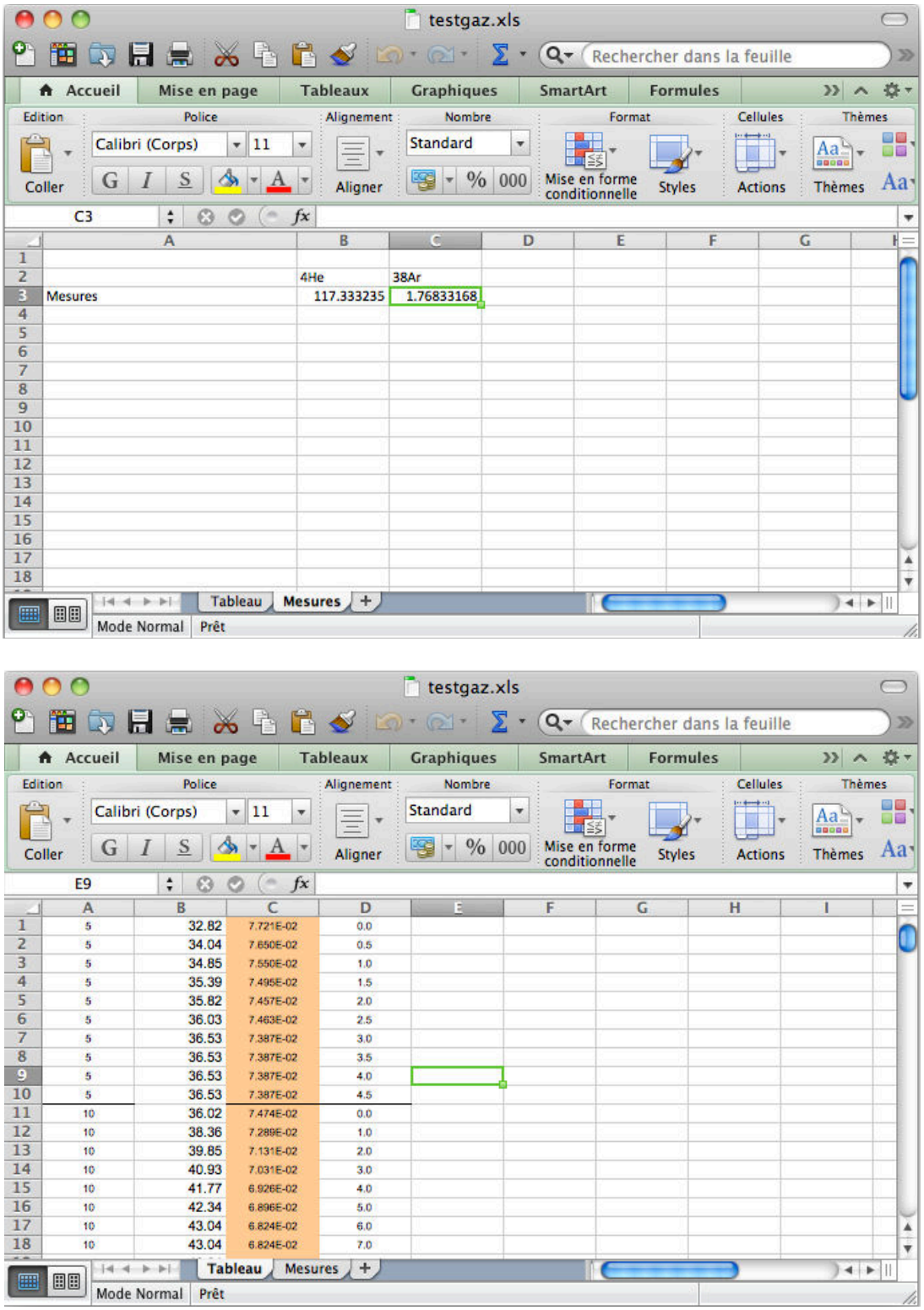

Figure C-1: testgaz.xls

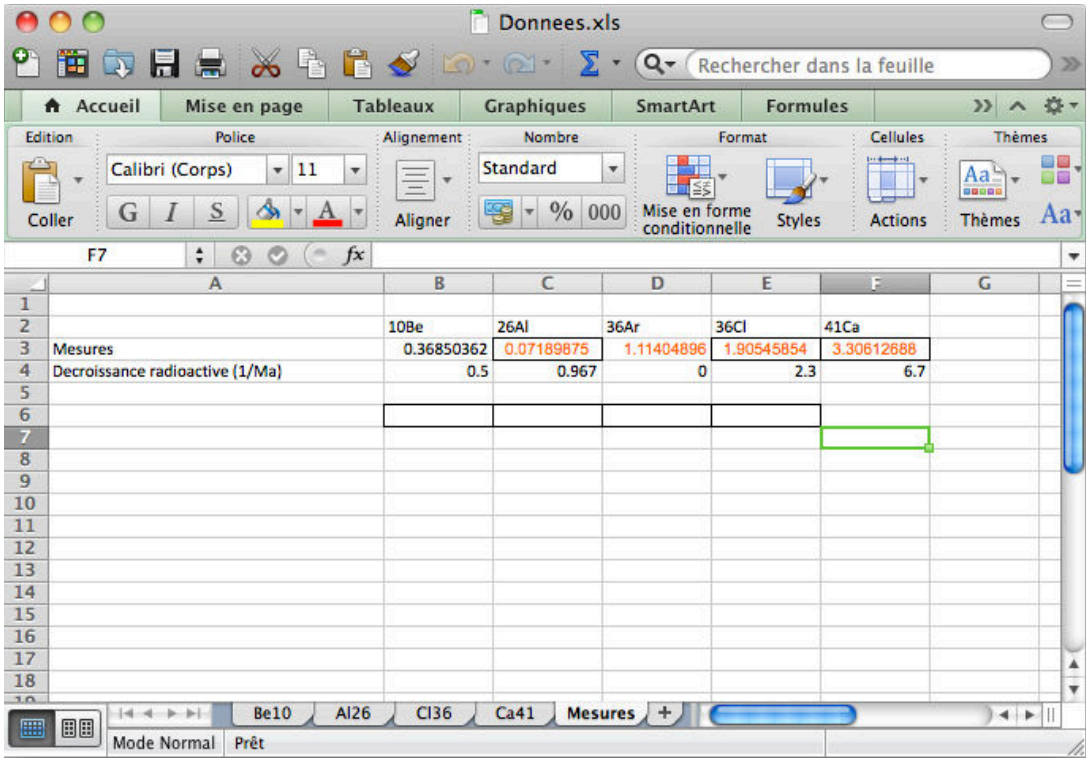

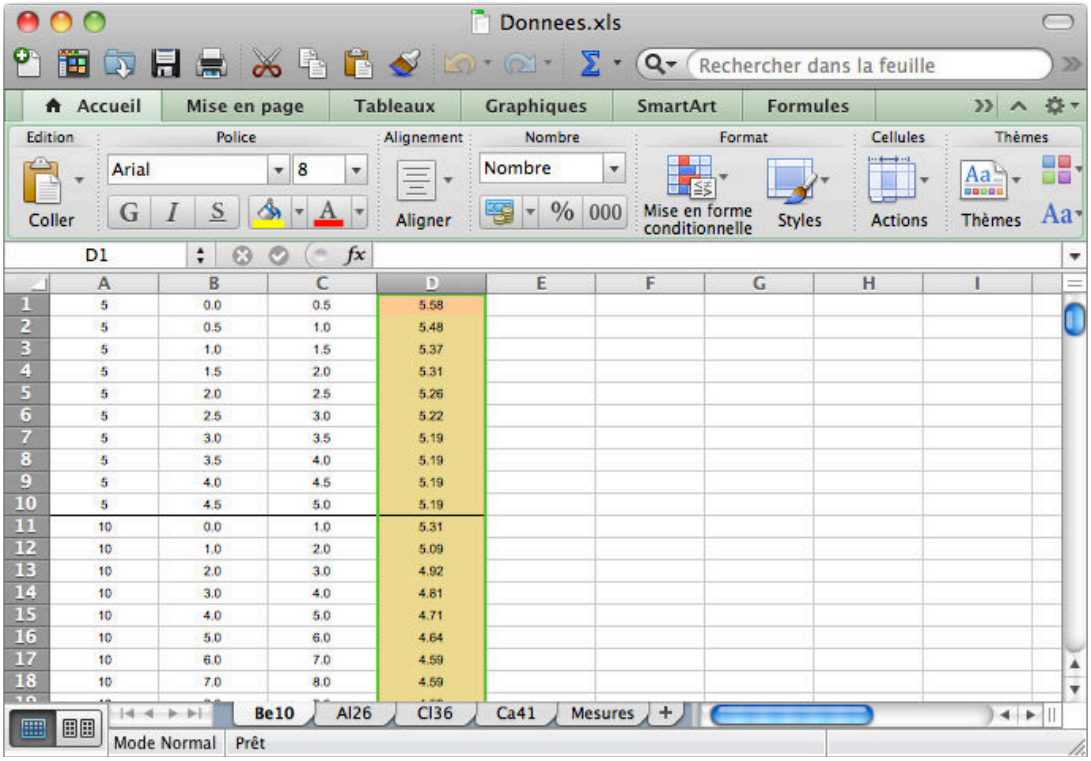

Figure C-2: donnees.xls

APPENDIX D: El Médano collection meteorites: a selection.

ElM 100. (left) 11mmx13mm. (right) 7mmx10mm

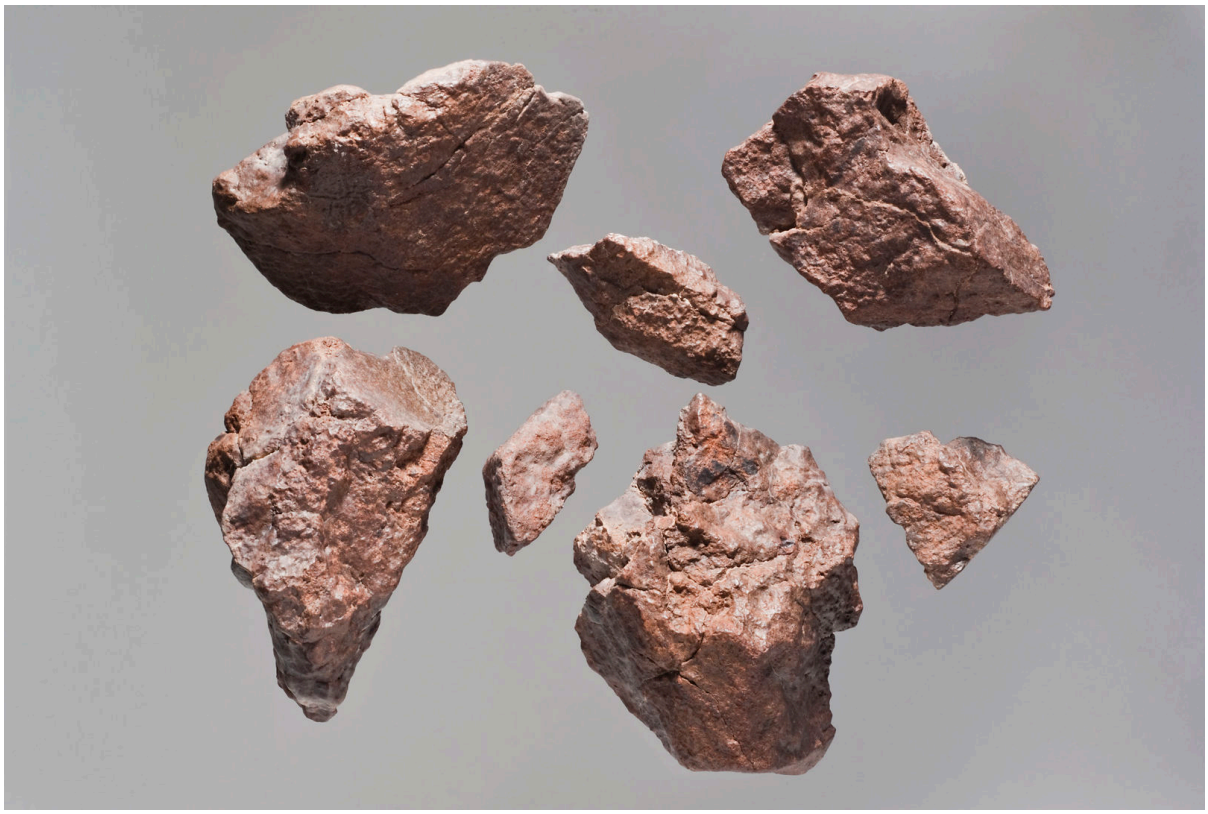

ElM 190. (bottom left) 58mmx116mm

ElM 141. (top) 82mmx88mm.

ElM 128. 69mmx78mm.

ElM 195. 14mmx20mm.